NTNU – Trondheim
Norwegian University of
Science and Technology

Borehole image log analysis for sedimentary environment and clay volume interpretation

Atefeh Shahinpour

Petroleum Geosciences
Submission date: September 2013
Supervisor: Helge Langeland, IPT

Norwegian University of Science and Technology
Department of Petroleum Engineering and Applied Geophysics

Preface

This thesis completes my petroleum geoscience degree at the Norwegian University of Science and Technology. The project has been performed at the Department of Petroleum Engineering and Applied Geophysics.

VNG Norge AS has provided me with all data for this study from an exploration well drilled in 2009. FMI run in 8.5 inch section of the well, petrophysical well logs, final well report and core photos are the available data for this study.

Primarily I studied the Fullbore Formation MicroImager (FMI) log of a case well to interpret the sedimentary environment of the reservoir rock. Secondly the focus was to highlight information potential of the image logs by quantitative analysis of log data for net to gross calculation of a thinly laminated reservoir. The FMI tool includes 192 electrodes which measure the formation microresistivity and the log is displayed as an image of the borehole. In this study independent FMI interpretation is integrated with conventional log interpretation to analyze the reservoir facies and sedimentary environment. First, the petrophysical interpretation of the logs is carried out and the image log interpretation is integrated afterward to interpret the sedimentary environment. The FMI imaged section is divided into four different sections for the interpretation. The quantitative analysis of the FMI log is then carried out to demonstrate the capability of this log in shale volume and net to gross calculation of thinly laminated reservoirs where the other logs may not be able to distinguish shale and sands properly.

I want to thank Helge Langeland for his good advice and motivation and also for his companionship and patient because I was located in Oslo when writing the thesis. My special thanks also go to VNG Norge AS for providing me with well data for this study.

Finally, I would like to thank my family for support and encouragement during the whole study at NTNU.

Abstract

This project focuses on measurements from the electrical image tool, Fullbore Formation MicroImager (FMI). Firstly, borehole imaging technology is discussed and some of the available imaging tools from the three main service providers are presented. The focus later is on the interpretation of the FMI log from an exploration well in the North Sea operated by VNG Norge AS. Necessary preparations including log data processing and corrections on the FMI log were carried out before doing the log interpretation. All corrections are used to enhance the log quality, locate the image data in the correct depth position and match the image log with the conventional logs and cores.

Image log interpretation is then carried out in the main reservoir section. The lithofacies and possible depositional environment have been interpreted first based on the core description made by an external source. The result is then used for identification of the sedimentary bedding features, depositional settings and structural elements in the image log. This correlation was later extended to the rest of the FMI logged interval, i.e. over the non-cored formation.

The sedimentary interpretation from the FMI images has been focused mainly on energy level of the depositional system. The lithofacies and sedimentological descriptions of the cores helped in better understanding of the turbidite depositional environment and sediment origin in this reservoir. The main depositional environment defined as submarine fan deposits with deposition of the sediments mainly by turbidity flow. Bioturbational features were spotted both in the cores and image log in few intervals of the well. The reservoir column is then classified into four intervals with defined sedimentary environment in the submarine fan from low energy distal basin fan into a high energy channelized turbidity environment.

In addition to the qualitative analysis, quantitative analysis of image logs with focus on clay volume and net to gross calculation is carried out afterward. Clay volume in a thinly bedded interval was estimated based on the gamma ray log and one FMI trace (out of 192 traces). The gamma ray log data resolution is considerably lower than the FMI log to reflect accurate lithology changes in thinly bedded reservoirs. After some calibrations and corrections on the FMI resistivity log, the new processed log is used for clay volume and net to gross calculation of the reservoir, indicating the potential of this log for analysis of thin beds.

Sammendrag

Dette prosjektet fokuserer på malinger fra den elektriske bildeloggen som blir kalt Fullbore Formation MicroImager (FMI). I det første delen av prosjektet, blir bildeloggens teknologi diskutert og noen av de tilgjengelige bildebehandlings verktøy fra de tre viktigste service selskaper blir presentert. Fokuset er senere på bildeloggens tolkning fra en letebrønn i Nordsjøen drives av VNG Norge Oljeselskap. Nødvendige forberedelser som data prosessering og korreksjoner av FMI-loggen utføres før tolkningen. Alle korreksjoner benyttes til å forbedre kvaliteten til loggen, å sette bildeloggen i riktig dybde posisjon og korrelere bildeloggen ved de konvensjonelle logger og kjerner.

Bildelogg tolkning deretter blir utført i hovedreservoaret. Lithofacies og mulig avsetningsmiljøet har blitt tolket først basert på kjernebeskrivelse fra en ekstern kilde. Resultater har blitt brukt for identifisering av de sedimentære stukturer, deposisjonelle miljøer og strukturelle elementer i bildeloggen. Denne korrelasjon ble deretter utvidet til resten av FMI-log intervallen, dvs. over den ikke-kjernete formasjon.

Sedimentære tolkning fra den FMI-loggen har hovedsakelig fokus på energi nivå av avsetningsmiljø systemet. Lithofacies og sedimentologiske beskrivelser av kjernene bidratt til bedre forståelse av turbiditet avsetningsmiljøet og sediment opprinnelse i dette reservoaret. Det viktigste avsetningsmiljøet blir definert som undersjøiske vifte avsetting med deponering av sedimentene hovedsakelig av turbiditet strømmen. Bioturbiditiske strukturer blir oppdaget både i kjernene og bildeloggen i noen intervaller av brønnen. De reservoarseksjoner blir deretter klassifisert i intervaller med definert sedimentære avsetningsmiljøer i undersjøiske vifte fra lav-energi distal bassenget vifte til i en høy-energi kanalisert turbiditet-miljø.

I tillegg til det kvalitativ analyse, utføres en kvantitativ analyse av bildeloggen med hensyn til leirvolum og netto til brutto beregningen. Leirvolumet i et tynt intervallet ble estimert av gammaloggen og en FMI kurve. Den gammaloggen har betydelig lavere oppløsningen enn bildeloggen for å reflektere nøyaktige litologi endringer i tynnere reservoarer. Derfor etter noen kalibreringer og korreksjoner på FMI bildeloggen, brukes den nye behandlet loggen til leirvolum og netto til brutto beregning av reservoaret, som indikerer det potensialet i denne loggen for analyse tynne lag.

Table of Contents

Table of Figures

1. Introduction

Sedimentary environments are depositional settings that may have a large variability in the number of layers and sedimentary structures. Sedimentary depositional environment describes the combination of physical, chemical and biological processes associated with the deposition of a particular type of sediment and, therefore, the rock types that will be formed after sediment lithification (Slatt, 2006). A routine way to model the reservoir rock deposition system and sedimentary environment is to core the reservoir rock and study the cores in combination with the other geological information. However, coring may not be possible throughout the whole reservoir and non-reservoir parts due to some obligations, among them, the cost of coring and the time of rig. An appropriate and cost/time saving tool, borehole imaging, has been developed in the oil industry to combine with limited core information to analyze the reservoir sedimentary environment. Borehole image logs provide important sedimentological and structural data for use in reservoir evaluation. The log contains specific information in relation to bedding style (bedding dip and azimuth), orientation of faults, fractures, structural regimes, unconformities together with recognition of palaeo-slopes and palaeo-currents and etc. The best source of information which can be used to strength the image log evaluation is to integrate them with core data where available.

Primary techniques for acquiring borehole image data are electrical (microresistivity) and acoustic measurements. Significant improvements have recently been made in the quality of borehole imaging measurements, which have led to growing applications of this technology (Felder, 1994). History of dipmeter and borehole imaging tools began in 1941 with a 3-arm dipmeter tool with mechanical inclinometry measurements. In the late 1950s, the technology started to develop (Lagraba et al. 2010). In 1986, the latest dipmeter tool was developed by Schlumberger, called the Formation MicroScanner (FMS). Later versions of this tool were called Fullbore Formation Microimager (FMI). There is now similar services available from other suppliers for borehole imaging. Today there are more than 30 tool types to choose from depending on the detail of the investigation required, type of mud system, expected formation response, and expected borehole conditions (Lagraba et al. 2010). Most of these imaging tool measurements are based on microresistivity or acoustic wave velocity principals.

Borehole image logs play a major role in reservoir description since they provide very detailed information about the reservoir rocks. Most of the imaging tools sampling intervals are about 2.5 mm while standard logs are sampled every 15 cm (Rider and Kennedy, 2011). The log data is presented as an image, and most of the time the interpretation of image logs is

usually qualitative. In this project the electrical image logs and conventional logs together with core photos were studied. The purpose of this work is to interpret the reservoir sedimentary environment using an integrated study between the image logs and core data. In addition a quantitative analysis of sedimentary features like bedding, fault and fracture dip angle and azimuths were studied. The well data and the electrical image log data (FMI) were acquired from one of VNG Norge operated wells in the North Sea. In the petrophysical software program, "Interactive Petrophysics" (IP), formation evaluation were done and fluid saturation and lithology were estimated. Image logs were then loaded, edited and processed before interpretation. Available sedimentary interpretation of the limited cores from the reservoir used to pick the relevant facies and environments in the image logs. Image log interpretation showed turbidity channel sands and submarine fans as the dominant deposition model for this reservoir. Depositional settings from high energy proximal point to the low energy basin sediments of submarine fans were recognized from the image log interpretation and core analysis. The results showed that the dominant sedimentation process is turbidity flow in the submarine fan deposits.

Subsequently, quantitative analysis of the image log was carried out to analyze the reservoir shale volume and net to gross ratio. Although the main purpose of acquiring borehole image logs is qualitative interpretation of the sedimentary environment and structural interpretation of reservoir, the log contains a lot more information than what is normally used at the present time. This log can play a major role in today's reservoir description, because the log provides very high resolution information about the reservoir where conventional logs are not able to the same extent. Image logs are generally sampled every 2.5mm where conventional logs sample every 15 cm (150mm), with 60 times less resolution than the image logs (Rider and Kennedy, 2011). So far few quantitative analyses of the image logs have been conducted to characterize thin beds, rock permeabilities, fractures and sedimentary environments. The main challenge in quantitative analysis of the image logs is the huge volume of data that has to be formulated in a proper mathematical manner to extract potential information from the log. In this project a mathematical approach is implemented to find a better estimation of the reservoir shale volume and net to gross ratio in thinly bedded reservoirs. The main purpose is to investigate the information potential in the image logs that is normally under-used by the log operators.

2. Borehole imaging technology

Borehole imaging tools are characterized in the three main wireline tools of Borehole Televiewer (BHTV), Electrical Resistivity and Ultrasonic tools. A wide range of imaging tools are also available with LWD imaging tools becoming increasingly important compared to the 'traditional' wireline tools. Commonly the datasets from these tools are underutilized due to a lack of awareness. Among the others, Electrical Imaging and Azimuthal Density-Neutron-Gamma Ray logs are important LWD image logs. Based on variations in rock properties these tools can produce detailed images of the wellbore wall.

Wireline log data are normally acquired after a particular section of well was drilled and all drilling strings pooled out of the hole (POOH). The time to POOH and rig up the wireline tools is quite long and therefore causes long exposure of reservoir formation to borehole fluids and subsequently filtrate invasion. Quite number of methods have been developed to solve the filtrate invasion effect on the measured reservoir properties however, no particular solution has been developed to fully model the invasion effect on every particular log.

LWD logging technology, among the others, was developed to minimize the borehole environmental effects, in particular filtrate invasion, on the measured formation properties. The main idea is to lower the formation exposure time to borehole fluids and decrease the mud/mud-filtrate invasion and, therefore, its impact on the measured formation properties. It should be noted that despite LWD refers to logging while drilling, it takes some time from when a formation is drilled until it is logged by an LWD tool behind the drill bit. An LWD run includes a number of measuring tools (e.g., Gammaray, Neutron/Density, etc) mounted on the measuring string each of which with particular distance from drill bit. The time exposure of the reservoir to the borehole fluids depends on the distance between the bit and measuring point as well as drilling speed. The time may also increase considerably if the reservoir is cored. The time exposure may vary from seconds to minutes for tools mounted just behind the bit to minutes/hours for the tools mounted in a longer distance to the drill bit and maybe days for the runs after coring.

The Resistivity at Bit tool is one of the LWD tools that can provide azimuthal-oriented images of the formation resistivity. These types of tools can provide resistivity images in individual azimuths of interests. Except for cored intervals, LWD data are acquired in a short time after a formation is drilled, limiting the extent of hydrate dissociation on the measured properties. This helps in better understanding of the original spatial distribution of formation

fluids in the reservoir. LWD imaging technology is developing quite fast nowadays because of the low service cost, saving rig time, and low environmental impacts. However, the resolution of the LWD logs is still not as good as the wireline imaging. FMI log for example measures the microresistivity of the formation rock with 2.5mm vertical resolution while the LWD imaging resolutions are quite far from this resolution.

Acoustic image logs are also a replacement for resistivity image logs for assessing structure and stratigraphy of reservoir rocks and for identification of fracture intensity and fracture porosity. Tool design has improved considerably since its introduction. The tool works in liquid filled open holes. In cased hole, the same tool is used as cement and pipe integrity tool, but it does not provide any reservoir property information. This imaging log, also known as acoustic televiewer or ultrasonic borehole imaging tool. Fractures and breakout can be easily detected by acoustic imaging. Usually the image quality can be stretched or squeezed to enhanced particular features.

Borehole image logs (e.g. resistivity or acoustic based images) are used to visualize sedimentary features to define important reservoir geometries and petrophysical reservoir parameters. The interpretation of image-derived sedimentary information including the bedding dip angle, dip azimuth, structural elements like faults, fractures, helps to better understand the sedimentary deposition and depositional structure. Borehole imaging is the preferred approach for determining net pay in the thinly laminated sediments of fluvial and turbidite depositional environments and for stochastically modeling the sand-shale distribution (Schlumberger).

Image logs are also used for accurate locating of the formation tester probes during the formation pressure measurement and reservoir fluid sampling. Correct placement of the pressure probes against the target zones are very critical when the reservoir rock is a thinly bedded shale and sand.

Resistivity imaging devices are widely used in the oil industry and particularly effective at separating geological features because of their inherent high-resolution capability and the wide dynamic range of the formation properties being measured. These tools have different borehole coverage (e.g., 30% to 80%) depending upon the number of pads and borehole size. Resistivity imaging devices send alternating current radially from one or more electrodes of limited azimuthal and vertical extent into the formation. The current returns via the mud

column to the metallic housing of the tool. This technique necessitates a current path through the drilling fluid and filter cake present between the electrodes and the borehole wall. Consequently, the use of resistivity tools for borehole imaging has been historically restricted to water-based drilling fluids.

In water-based muds (WBM), the resistivities of the fluid, filter-cake and filtrate are low because of the naturally high conductivity of water, and, to a greater extent, saline solutions. Because high conductivity provides relatively unrestricted current flow from a logging tool, signal response from the formation is generally of the highest quality when using WBM. Conversely, conventional oil-based and synthetic-based invert-emulsion fluids are designed to provide oil-wet or synthetic-wet surfaces and water-free filtrates. These fluids consist of an internal brine phase that is strongly emulsified into a non-polar oil or synthetic phase. Thus, the fluid, filter cake, and filtrate are non-conductive, thereby blocking the flow of electrical current. Consequently, responses from resistivity logging tools are poor or non-existent.

Wireline resistivity image tools are pad tools that measure the formation microresistivity directly through an array of resistivity buttons mounted on pads pressed against the borehole wall. Such tools normally provide the high-resolution borehole images in conductive (water-based) muds. Figure 1a shows an FMI image log produced in a synthetic rock filled with conductive brine. The quality of the image is similar to that achieved by typical FMI in water based mud with real rocks. The layers with different resistivities are clearly delineated in the figure. The middle light layer corresponds to the resistive cement, the lower dark layer is the medium resistivity cement, and the upper dark layer is the low resistivity cement. There are two boundaries across the middle and lower cement layers - the first is somewhat faint, but the second is clearly marked. These are cracks resulting from each cement layer having been poured in two separate operations. According to the resistivity of the infill fluid relative to that of the layer, these boundaries can appear light, dark, or even invisible. Figure 1b shows the FMI log in an oil based mud (OBM). The only visible feature is the highly diffused variation in contrast from top to bottom of the image. No usable information could be extracted from this image.

Figure 1c shows the FMI log produced in the conductive oil based mud (COBM). The imaging of the layer boundaries and pebbles is as clear as that achieved in brine. As expected, the cracks are now light, because the conductive mud is more resistive than the cement layers. Moreover, the cracks are clearly visible because of the very strong contrast between these

resistivities. The signal amplitude (button current) in the conductive mud was about twice that measured in brine. This suggests that in the new COBM, which is more resistive than the formation (cement in this case), practically all the current passed through the formation. Conversely, in less-restrictive brine, most of the current passed through the brine which acted as a near short-circuit (Tehrani et al., 2001).

Ultrasonic imaging logs deliver a high-resolution acoustic image of the 360 degree borehole wall. These images cover 100% of the borehole wall because the tool sends an ultrasonic wave out into the wellbore and the reflection of the wave from the entire borehole wall is recorded in the receiver. Use of this type of log, however, is limited to low solids fluids and mud densities less than 1.45 sg (11 lb/gal), because of attenuation of the sonic waves. These logs are slower than conventional electric logs and generate poorer image quality, (Figure 2). A resistivity image log has about 10 times the spatial resolution of an acoustic image log and 500 times the amplitude resolution, due to the difference in contrast between the resistivity and acoustic impedance ranges measured by the respective tools.

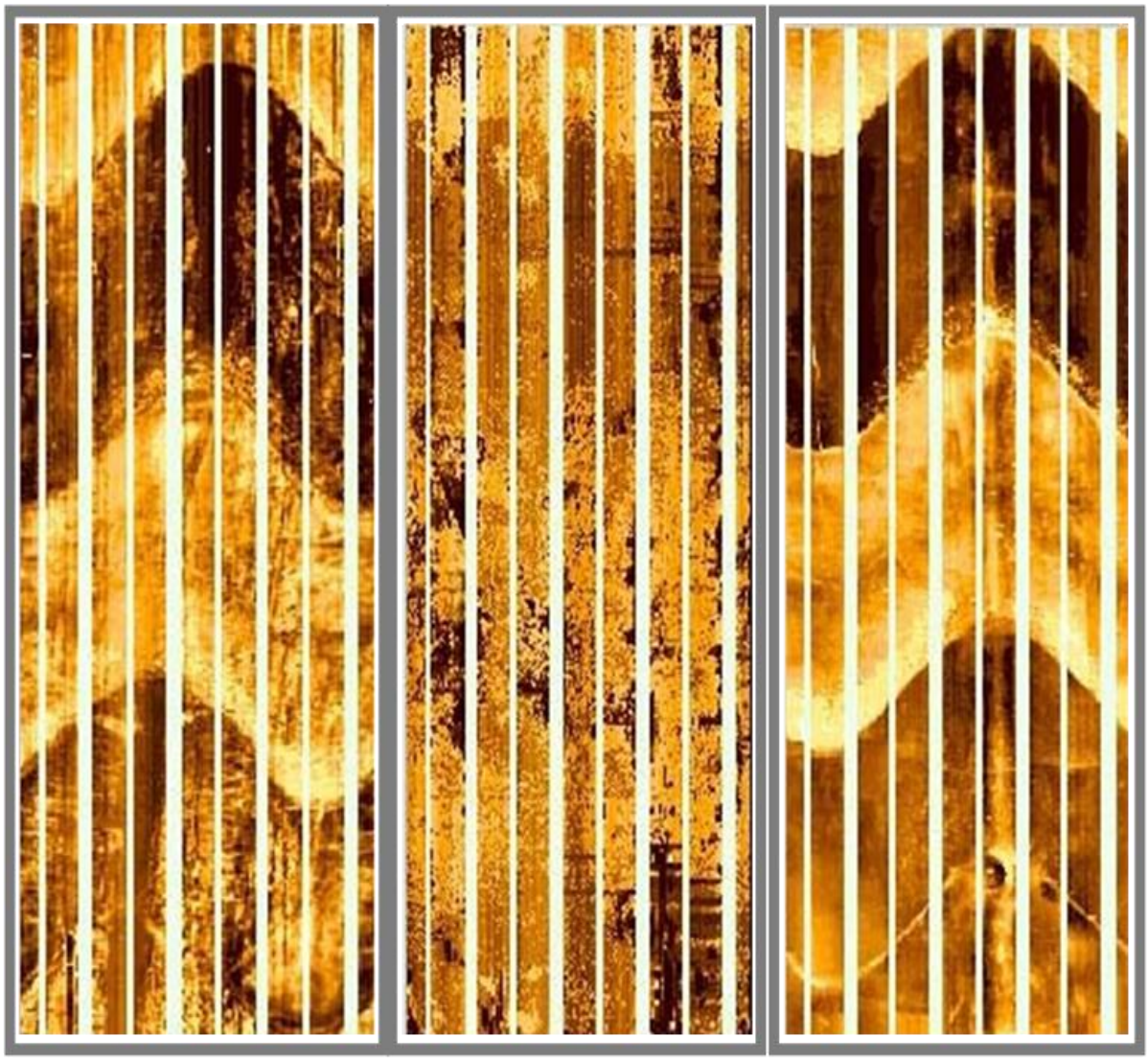

Figure 1. FMI image log comparison in (a) water based mud, (b) oil based mud, and (c) conductive oil based mud (Tehrani et al., 2001).

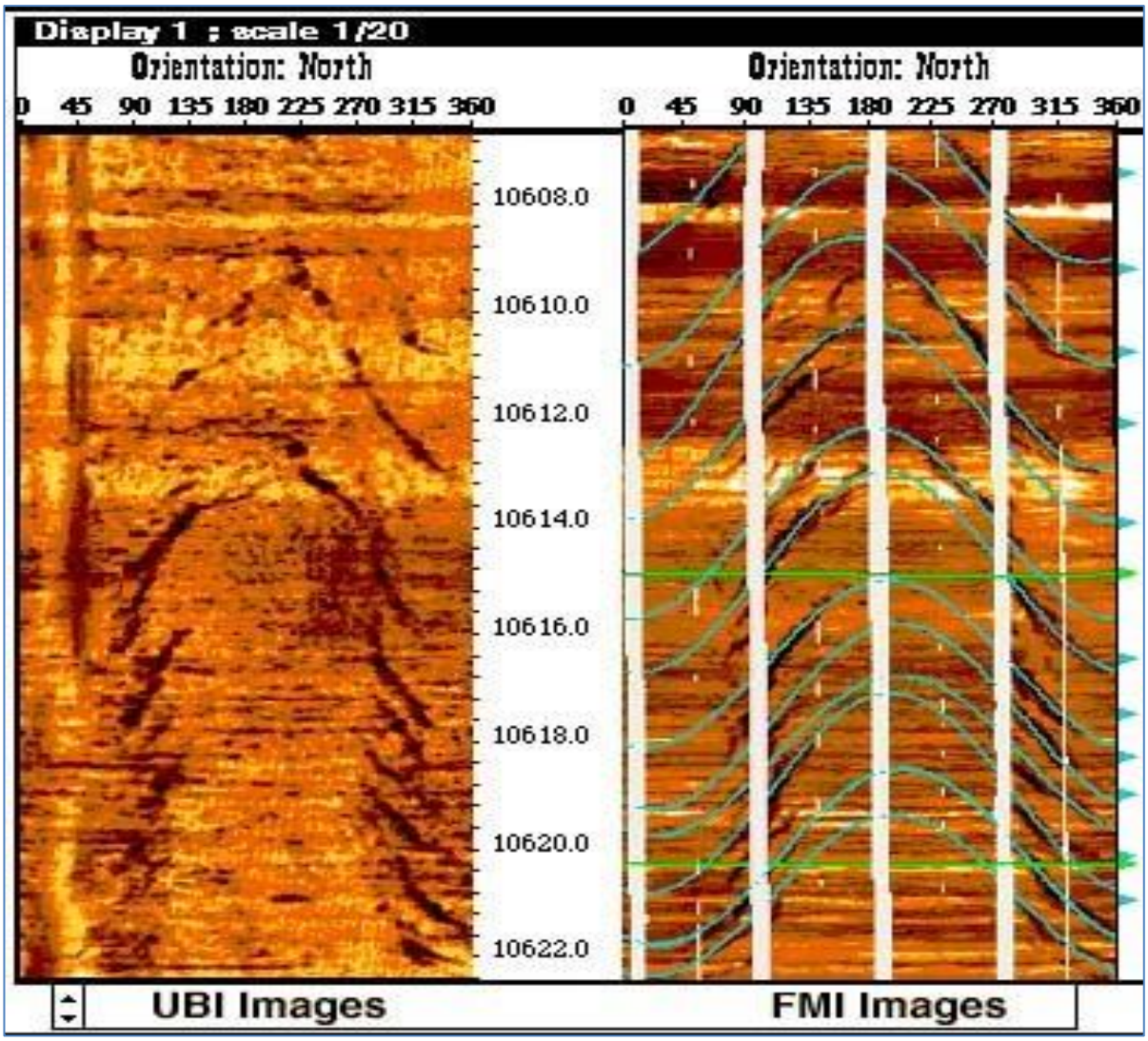

Figure 2. Comparison between ultrasonic and electrical imaging logs, showing the significantly greater detail with electrical imaging.

2.1 Imaging tools from different service companies

Various borehole imaging tools from different service companies are now available in the oil industry, each of which has its own characteristics proper for particular well/reservoir condition. Image logging can now be measured either by wireline or LWD tools. It is not intended here to list all these tools and logs but a summary of the most popular wireline imaging tools from the three service companies (Baker Hughes, Schlumberger and Halliburton) at present-day use are given below. All information for the presented tools has been taken from the companies product information. The pictures of the presented imaging tools are given at the end of the report in the Appendix.

Table 1. Baker Hughes imaging tools summaries

Service Company	Tools	Mud in Borehole	Tools characteristics and capabilities
Baker Hughes	**STAR Imager** Service	conductive /water based mud	Pads with 24 sensors mounted on each of the six articulated arms, giving a total of 144 microresistivity measurements with a vertical and azimuthal resolution of 0.2 in (~5 mm). Operates alone or in combination with the Baker Hughes CBIL imaging. Able to log images in vertical, horizontal, highly deviated, and rugose wells.
	Earth Imager Service	Non-conductive /oil based mud	Allows simultaneous acquisition of high-resolution microresistivity and acoustic borehole image data. Has an articulated six-arm carrier. Ability to log images in vertical, horizontal, highly deviated, and rugose wells.
	Circumferential Borehole Imaging Log (CBIL)	All type of muds	High-resolution borehole acoustic images in difficult conditions, including high-porosity, unconsolidated formations. Suitable for fracture and fault analysis. Can be used for interpretation of the near-wellbore stress field from borehole breakouts and drilling-induced fractures. 250-kHz operating frequency enables good performance in larger holes and heavier muds. Full 360-deg. borehole imaging tool operating in the pulse-echo mode. Generates sharp images and boundary delineation. Its small size of 3.625 in. (92 mm) allows for operation in slim holes as well as large-diameter holes.
	Ultrasonic Xplorer Imaging Service	All type of muds	High-resolution borehole acoustic images in difficult wellbore conditions, including OBM and large boreholes. Attains full 360° image coverage providing sharp images and boundary delineation. The lower operating frequency (250 kHz), along with downhole digital signal processing (DSP), allows for better performance in larger boreholes and in highly attenuating muds. Quite effective in horizontal wells. Its small size 3.625 in. (92 mm) allows for operation in slim holes, as well as large-diameter holes up to 16 in. (406 mm). Provides an acoustic amplitude image and a travel-time image. By calibrating the travel-time image, it is possible to provide a high-resolution borehole shape.

Baker Hughes	**GeoXplorer Imaging** Service	Non-conductive /oil based mud	Provides high-resolution formation microresistivity imaging in low-resistivity formations drilled with nonconductive mud systems. The high-resolution images allow for near-wellbore geological and petrophysical reservoir evaluation. 10 sensors mounted on six articulated arms to provide 60 microresistivity measurements, with a vertical resolution of 0.8 in (20 mm), and 79% borehole coverage in an 8.0" borehole. Operates in highly deviated boreholes. Determines an accurate net-pay even in thinly bedded intervals. Allows accurate positioning of fluid sampling or sidewall coring tools. The simultaneous acquisition of GeoXplorer and UltrasonicXplorer provides a more complete picture for accurate fracture evaluation, particularly in shale gas or fractured basement evaluation.

Table 2. Schlumberger imaging tools summaries

Service Company	Tools	Mud in Borehole	Tools characteristics and capabilities
Schlumberger	**FMI Fullbore Formation MicroImager**	conductive /water based mud	Provides real-time microresistivity formation images and dip with 80% borehole coverage in 8-in boreholes and 0.2-in image resolution in the vertical and azimuthal directions. Used for determining net pay in laminated sediments of fluvial and turbidite depositional environments, visualize sedimentary features to understand structure specially in not cored intervals, provide high quality of bedding dip data in highly deviated wells which improves the structural interpretation of seismic sections and computation of the true stratigraphic thickness. Improve modeling outputs, by supporting stochastic modeling of the sand-shale distribution. Define channel heights in amalgamated units, and others such as the channel width and channel sinuosity, can be estimated using geological analogs, based on detailed sedimentological analysis of FMI image data. Improve mechanical earth models for optimizing well planning. Better understanding of borehole stability.

Schlumberger	**Ultrasonic Borehole Imager (UBI)**	All type of muds	Analyze fractures, drilling-induced fractures and the stress regime and conduct borehole stability studies, with 100% borehole coverage, and structural interpretations. Two operating frequencies (measure both amplitude and transit time) modes of image resolution are available; standard and the higher resolution which deliver an accurate borehole cross section for deriving borehole stability and breakout information. The UBI processing technique avoids cycle skips and reduces echo losses. Image resolution is selected to correspond to the logging environment, such as mud type and density. The higher frequency yields higher image resolution. The lower standard frequency gives a robust measurement in highly dispersive muds. UBI tool measures attributes of ultrasonic waves reflected at the borehole wall and the rugosity of the borehole wall can dominate the reflection amplitude. UBI images are strongly sensitive to surface variations in the borehole wall but not to variations in lithology. Formation changes are normally seen on UBI images only if corresponding borehole surface effects, such as changes in rugosity or hole diameter, are present.
	Oil-Base MicroImager (OBMI)	Non-conductive /oil based mud	OBMI microresistivity imaging tool with four pads acquires five potential difference measurements that are used to quantitatively determine the resistivity of the invaded zone., see structural, stratigraphic, and anisotropic features as small as 0.4 in [1 cm], giving high-resolution azimuthal information. The sensitivity of the OBMI measurement delivers computed dips that are highly accurate even in formations with little resistivity contrast.

Table 3. Halliburton imaging tools summaries

Service Company	Tools	Mud in Borehole	Tools characteristics and capabilities
Halliburton	**Electrical Micro Imaging Service (EMI^{SM})**	Conductive/ water based mud	Six independent, articulating arms, each outfitted with 25 small electrodes on pad. Maintains optimum pad contact with a minimum of pad pressure, even in rugose, washed-out, or non-circular bore holes. An electrical current flows from the pads into the rock then upward in the wellbore to return at the top of the tool. Microresistivity contrast in the rock layers sampled 120 times per foot. Images are used to examine bed thicknesses ranging from a fraction of an inch to several feet; and accurately calculate sand thickness counts. Image enhancement techniques help further identify the precise characteristics of the formation reservoir. Identifies individual fault event and orientation. Detailed images of sedimentary features allow descriptions of bed boundaries, internal bed characteristics, textural changes, and laminated sand/shale sequences. Images can be presented in 2D and 3D formats.
	Oil-Based Micro-Imager Tool (OMRI^{SM})	Non-conductive/oil based mud	Six resistivity measurements per pad, each with a vertical resolution of 1 in. depth of investigation of about 3 in, data of 120 samples per foot with a proprietary signal acquisition scheme optimized for rugose hole conditions. The pads are mounted on six independent caliper arms. The sensor pads are mounted on the caliper arms with unique two-axis of articulation to improve pad contact in less ideal hole conditions which shows widest possible range of logging conditions. Used to analyze thin bed pay, structural and stratigraphic dips, sedimentary geometry and texture, borehole stresses, lithologic unit thickness, permeability barriers, sand attributes, clasts, vugs.
	X-Tended Range Micro Imager Tool (XRMI™)	Conductive/ water based mud	Coverage is 67% in 8.5 in. hole with 120 samples/ft. Good quality images even in high Rt:Rm environments. Has 32 bit digital signal acquisition architecture. S/N ratio by a factor of up to five, and the dynamic range expanded by a factor of up to three. The resulting images offer good reliability even in highly resistive formations (Rt > 2000 ohmm) or relatively salty borehole fluids (Rm < 0.1 ohmm). Pads mounted on six independently articulated arms help to maintain pad contact in rugose, washed-out, elliptical, or highly deviated boreholes.

Halliburton	**Circumferential Acoustic Scanning Tool-Visualization (CAST-V™)**	All type of muds	A high-frequency acoustic transducer to provide a full hole image. A second acoustic transducer is mounted in the scanner housing to measure characteristics of the borehole fluid. A directional sub is provided to orient images. Run primarily in open hole, 200 points horizontally by 40 samples/ft vertically. It is designed to operate in conjunction with other sonic tools but must be run centralized in fluid filled boreholes. Provides structural, stratigraphic, and sedimentological analyses for optimized offset well placement, completion design, and hydrocarbon depletion efficiency, thin bed delineation and improved net pay estimations, 2D and 3D borehole geometry and breakout presentations.

3. Image log analysis

Borehole imaging services provide microresistivity and acoustic images of the formation in both water based and oil based muds. Borehole imaging is the preferred approach for determining net pay in the laminated sediments of fluvial and turbidite depositional environments (SLB). Visualizing sedimentary features lets one to define important reservoir geometries and petrophysical reservoir parameters, and the interpretation of image-derived sedimentary dip data helps to better understand sedimentary structures. Geomechanical applications of image logs include fracture identification and differentiation of closed and open fractures along with stress analysis and borehole stability determination. Image logs also assist in porosity determination, presence of vugs, cemented nodules, induced fractures and etc.

3.1 Introduction

Borehole image logs span the scale gap between core and seismic observations and although do not replace core, provide key sedimentological and sub-seismic structural information, allow quantification of subsurface fracture networks and are inputs to geomechanical and petrophysical studies. These images are typically used to obtain the structural dip of the

formation penetrated by well, identify thinly bedded reservoirs, and analyze fractures and faults, particularly those of small scale below the seismic resolution.

In this study first some of the borehole image features are discussed with examples and then an image log case study is carried out to interpret the reservoir sedimentary environment. Examples of the geological features from a single well in the Ventura basin, California, contain excellent models of sedimentary features such as groove casts, lenticular bedding, scours graded beds, and rip-up clasts (Amer et. al., 2011). These features enable us to interpret depositional facies such as debris flows, channels, and amalgamated and layered turbidities to better understand the position of the well within the depositional system (**Figure 3**). We are also able to identify and verify overturned beds and repeat stratigraphic sections in the well because the image logs enable us to document the presence of reverse faults (**Figure 4**) (Amer et. al., 2011).

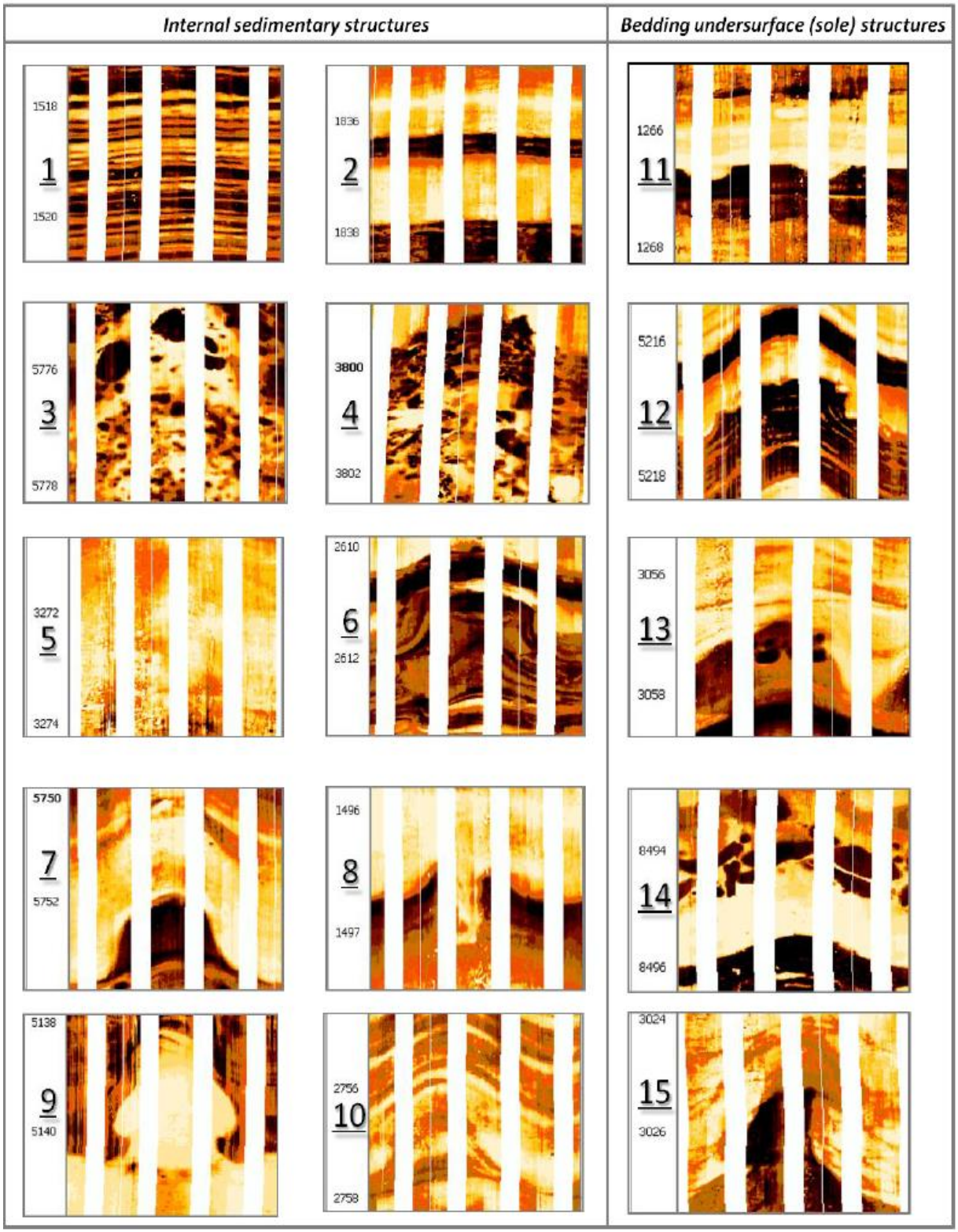

Figure 3. Sedimentary structures observed on the high-resolution borehole image logs. (depth in feet): 1,lamination ; 2,bedding; 3, inverse/reverse grading; 4, conglomerates; 5,massive bed; 6, convolute bedding (slump); 7, sediment deformation ; 8, water escape structure; 9, sand injection; 10, cross-bedding; 11,groove cast; 12 load cast; 13, small-scale scour surface; 14, erosional channel base with lag ;15 ,flame structure (Amer et. al., 2011).

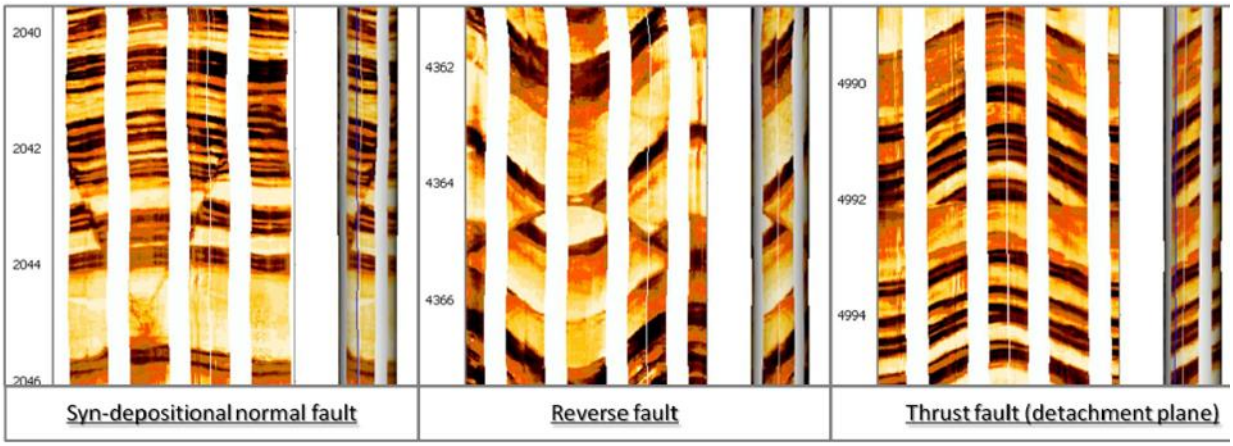

Figure 4. Normal, reverse and thrust faults as observed on high-resolution image logs (Amer et. al., 2011).

Generally, following work flow is used for the sedimentary interpretation from the use of borehole image logs in combination with the other logs and core data:

- Data processing and quality control
- Depth matching with the other logs
- Core facies tying with image data
- Interactive dip-picking of various features
- Dip vector plot (walkout plot) analysis
- Structural analysis from dip and image data
- Structural dip removal
- Image log facies analysis and,
- Sedimentary environment interpretation

Image logs, although, are widely used for formation dipping and sedimentary environment interpretation, they are being used for various objectives. Among the others, these logs are used for optimizing the pressure point location for wireline formation testers, interpret paleo-current direction and compute the cumulative sand thickness for accurate sand/reservoir pay calculation. In this study the step by step data processing and interpretation is conducted to define the sedimentary environment for the reservoir sands using the image logs. Available facies study from core analysis is used to complete the interpretation. Image logs are first analyzed and interpreted in the cored intervals and extended to the un-cored sections afterward.

3.2 Image log processing, correction and presentation

To display an image log of a cylindrical borehole, the well geometries and orientations has to be provided beside the image data. During the drilling a well, the three important logs of borehole deviation (DEV or DEVI), borehole azimuth (AZI or HAZI) and Relative Bearing (RB) are always measured by the service companies. These two first logs are needed for well trajectory, wellpath, iso-core and vertical depth calculations. By relative bearing (RB), the imaging tool rotation during the logging and its exact position inside the borehole is defined and measured at every point. The angle between the borehole azimuth and reference pad azimuth i.e. P1AZ is recorded at every data points as RB log. In general, these three logs are needed for accurate plotting of the image logs in correct depth position. Figure 5 shows an illustration of a deviated well with defined parameters including, borehole azimuth, borehole deviation, borehole high side, borehole axis, vertical axis, and horizontal plan with geometrical directions.

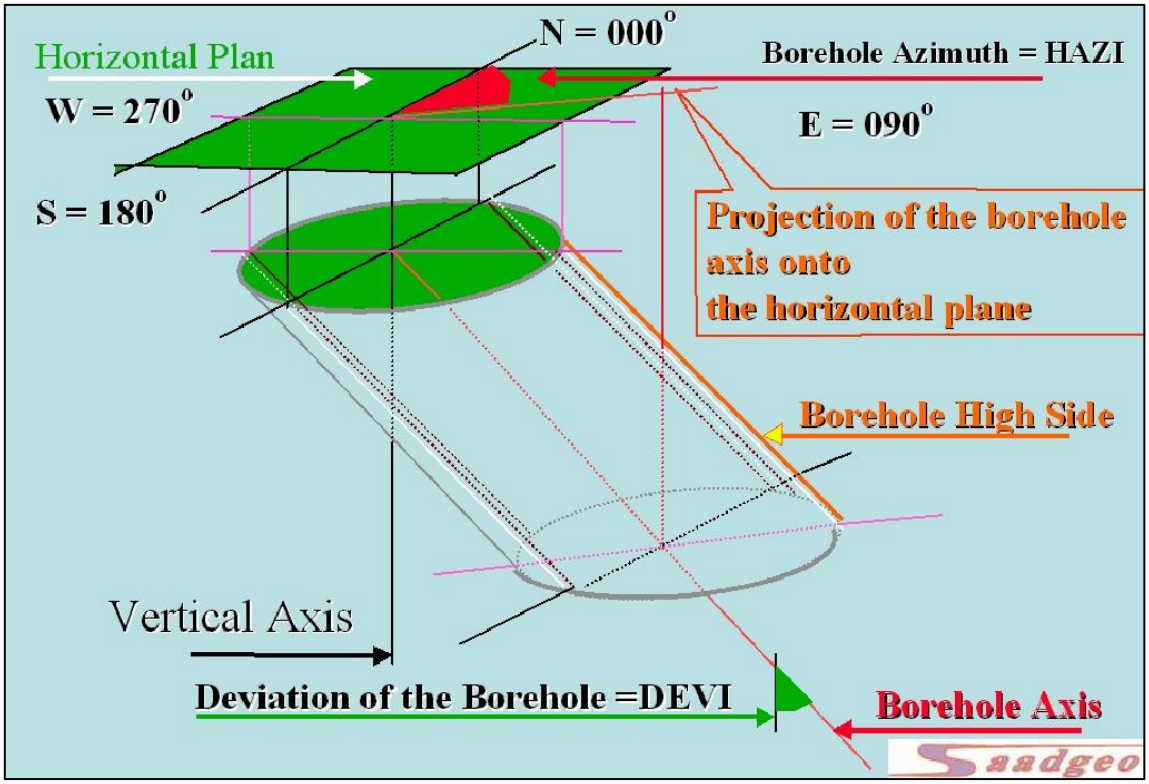

Figure 5. Orientation of borehole and defined borehole deviation and azimuth (Saadgallah).

Image logs depending on the service company and the tool type have certain number of pads, with defined number of electrical buttons on each pad. In this study an FMI log from an exploration well in the North Sea was provided by VNG Norge AS together with the other conventional logs to study the sedimentary environment of the reservoir. Principally, FMI resistivity tool does not measure the true resistivity like standard resistivity tools but reflects resistivity contrasts in the formation. The FMI curves are normally affected by changes in the formation properties in a similar way as the resistivity logs. This indicates that the FMI log can also be used numerically to describe the reservoir facies and thin layers due to a very high resolution of the log.

To be able to plot the image log data in the correct position, an understanding of the geometry of the tool, tool orientation, wellbore orientation, and borehole size is required. One of the pads in the FMI tool string has to be defined as a reference pad herein PAD1 azimuth (P1AZ) in FMI log which has a 0 to 360 degree values starting from North direction. Image log data are usually plotted from North orientation reference and ends to 360 degree at the same point again. So the orientation order of log plot is North-East-South-West-North.

Figure 6 shows an FMI image log with 8 pads presented from North, although the other directions can also be selected. In this figure two dipping layer/boundary markers are also highlighted. The principle of the image log presentation is shown in Figure 7. The figure shows that how a dipping layer in the well appears as a sinusoid curve on the unrolled flat view. Sine curves can be traced over different features in the image log. From these identified features in the image, one can calculate feature depth, dip angle and dip azimuth to analyze sedimentological and structural system of the rock. Figure 7 shows that if the distance between the sine curve top and bottom (Δz) is increased, the dip angle of the feature is also increased and vice versa. The upper sinusoid marker in Figure 6 has higher dip than the lower marker. According to **Figure 7**, the dip angle of every dipping feature is calculated as:

$$Tan(\alpha) = \frac{\Delta z}{BS} \qquad \text{Equ. 1}$$

α: dipping angle (degree)
Δz: sinusoid curve amplitude (cm)
BS: bit size (cm)

Figure 6. FMI image log orientation and presentation from North

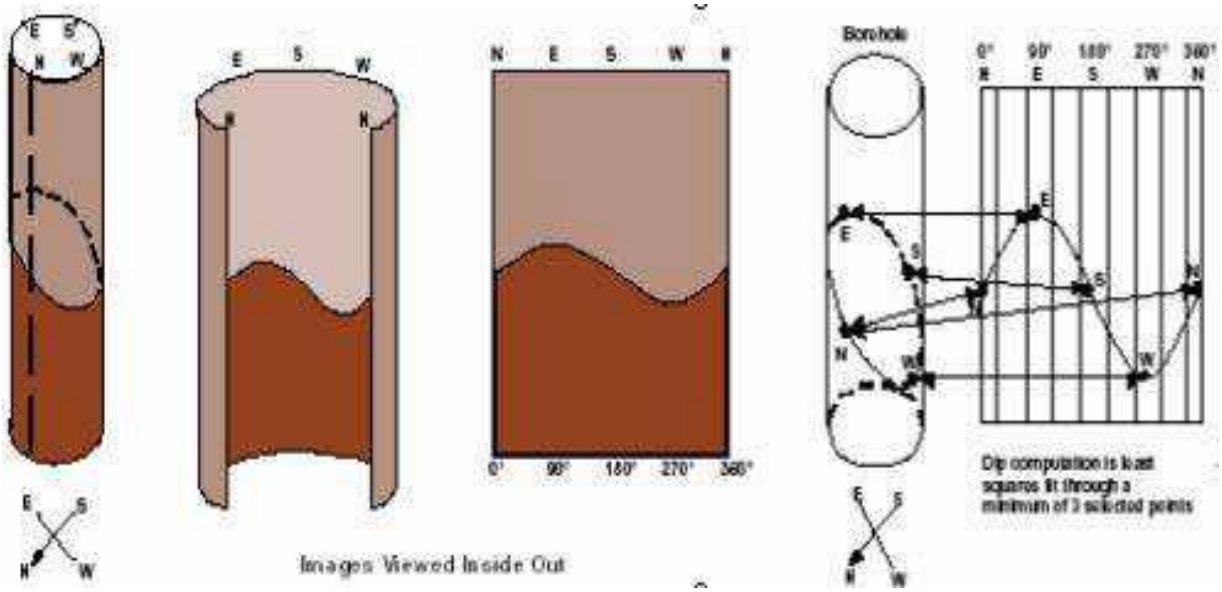

Figure 7. A dipping layer illustration of FMI image from borehole to log plot. Dipping layer appears as a sinusoid curve when the image opens in a 2D plan. (Schlumberger)

In FMI tool, formation microresistivity values are measured at vertical resolution of 2.5 mm. During the measurement, high frequency current is emitted from each buttons which creates an equipotential surface parallel to the borehole wall. The tool focuses the current a short distance into the formation. Differences of potential are measured between each buttons and the upper tool cartridge housing (tool upper electrode). **Figure 8** illustrates the tool upper electrode and microresistivity buttons equipped on the pads.

Image log data are formation microresistivity measurements by the imaging tool. The FMI tool has 24 micro buttons on every pad and 192 buttons in total, measuring 192 microresistivity values for one logging run at each depth increment. The raw data presentation would be a massive number of resistivity curves plotted in the log plot (**Figure 9**). In the image log processing, usually the color coding/normalization is done on the raw data to make the logs readable and easy for interpretation. The log visualization is consequently appeared to be such a resistivity image of the borehole wall. To visualize the image logs, two different types of color normalization are done on the data; Static and Dynamic normalization.

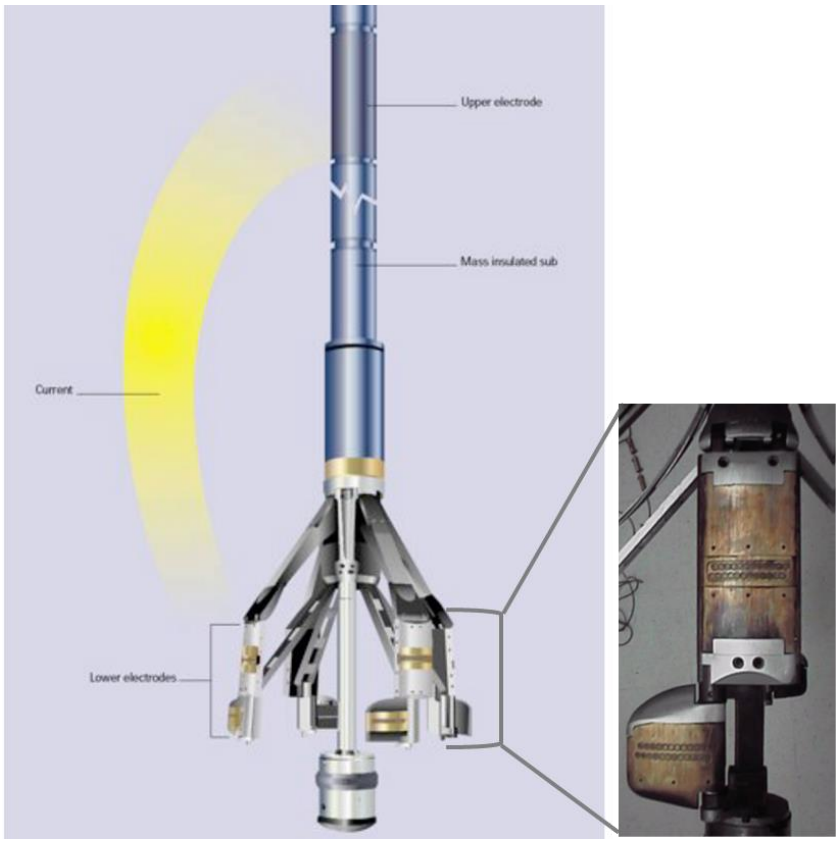

Figure 8. FMI Fullbore Formation Micro-imaging, Schlumberger

Static normalized images have the same color scaling over the entire logged interval and thus show large-scale resistivity variations related to lithology changes and structural events (faults, fractures unconformities, etc…). Dynamic normalized images are color scaled on a 2-ft-sliding window, thus maximizing rock fabric detail (texture) and bedding information. Figure 9 represents the FMI image data from being raw resistivity logs to the more readable images of the borehole wall.

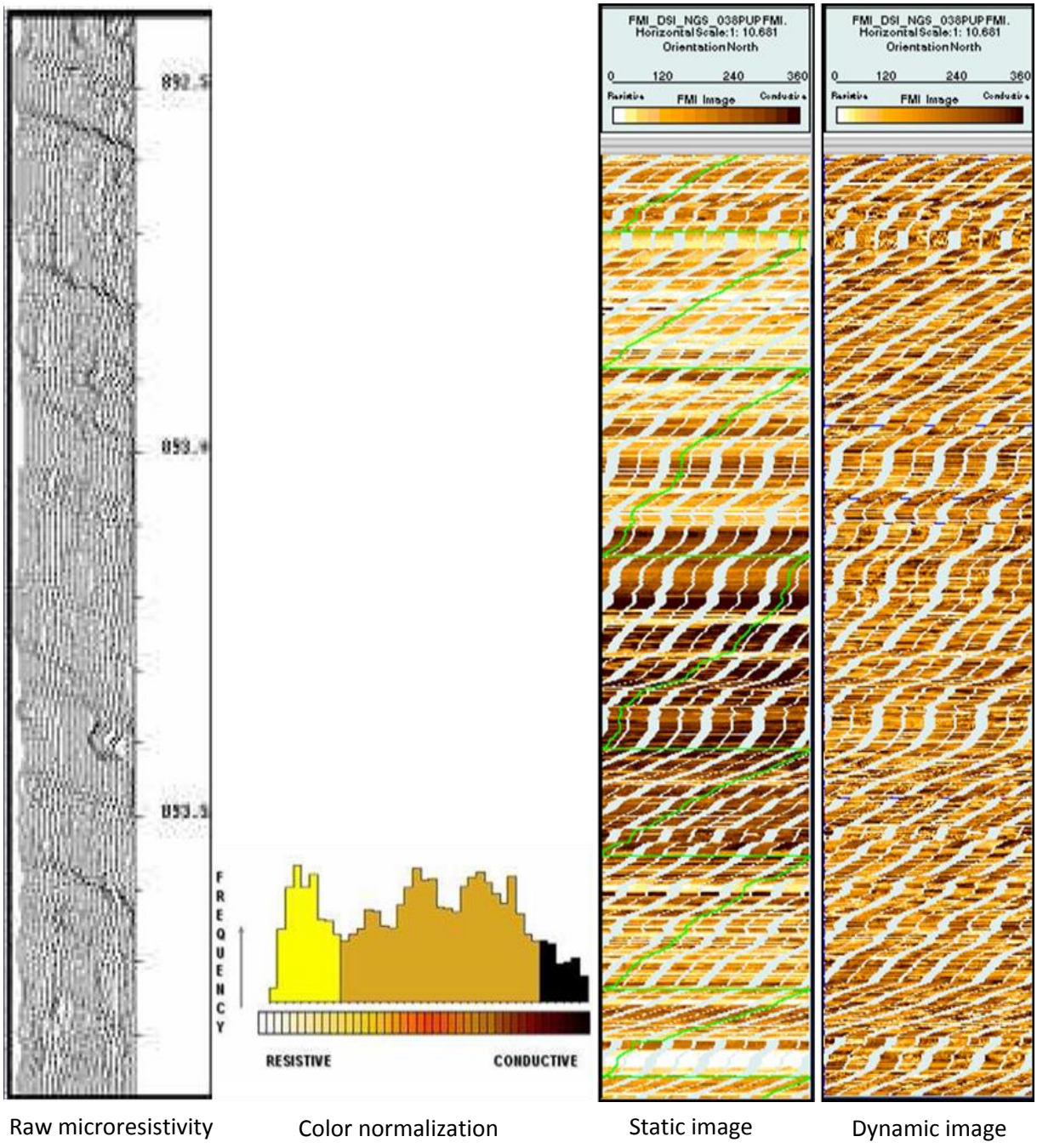

Figure 9. FMI log data from raw to static and dynamic normalized images, (Schlumberger)

In the static color normalization procedure, the resistivity values are color coded from highest resistivity values as white to the lowest resistivities as black in 32 color ranges. In dynamic normalization, a special range of resistivities are used to plot the data in a high resolution. Dynamic normalization allows a detailed resistivity image data visualization. Dips are observed on both image, but picked preferentially on dynamic images.

To perform the geological interpretation of the image logs, raw resistivity measurements recorded by electrode tool need to be processed. Speed correction, magnetic declination correction, and depth shifting offset are the main processing steps to generate the image logs for interpretation. Speed correction is to correct for irregular tool motion and to convert the time-based recorded data into a depth-based data. Magnetic declination correction is applied to inclinometry measurements recorded by the tool relative to the magnetic North to convert them into geographic North. Depth shift offset correction is done to match the image log and the other logs in depth using the GR log correlation from these runs. These corrections are partly done by the service companies and they deliver magnetic declination corrected and depth-based image data. However, a number of processing functions are applied to the image data by the interpreter to enhance the image accuracy and quality.

The irregular motion of the tool during the logging (due to sticking, variable tool friction, rig-heave, and cable stretch) is corrected by using accelerometer-based speed correction. This correction returns the miss-positioned data to the correct depth point. Depth matching of the logs between image logs and the other wireline logs are sometimes not adjusted by the service companies and has to be done before interpretation. Usually The GR log from both runs is used for this correlation. Additional minor processing may be applied to the data to remove saw tooth artifacts, malfunctions of buttons, misalignment of pad/pads, filling small gaps on data, and removing dead buttons. In all these corrections, filters can be applied to enhance the log quality and increase the geological and structural features resolution.

3.3 Borehole image log interpretation, wellbore Case-A

Image log interpretation is carried out after running the corrections and enhancements on the measured data. Since the image logs are going to be integrated with the conventional logs, necessary depth matching between the runs is carried out. Fewer corrections are usually implemented on the image logs since often service companies do necessary corrections on the logs before delivery. Completed corrections on the image log for this study is summarized below.

3.3.1 Depth matching

Depth matching is done between the FMI log run and the PEX run. PEX run includes the main porosity logs and the GR log. Figure 10 shows the two GR logs one from the PEX-run (comp:GR) and another from image log run (FMI_Base:GR_EDTC). The PEX run is assumed as the reference run in the well and all the other logs depth matched with this run. According to the plot, there is a need for +0.3m shift to the FMI run GR to match the composite log GR. The amount of the shift, however, is not the same in the whole well interval and changes from zero to about +0.7 meter. It should be noted that the amount of the depth matching shift between the LWD logs versus wireline logs (here we assumed PEX run) is most of the time different values. This is because the LWD tools are conveyed in the drilling strings while the wireline tools are hanged from wireline cable. Tension in cable and drill pipe is different; therefore the amount of shifting is different.

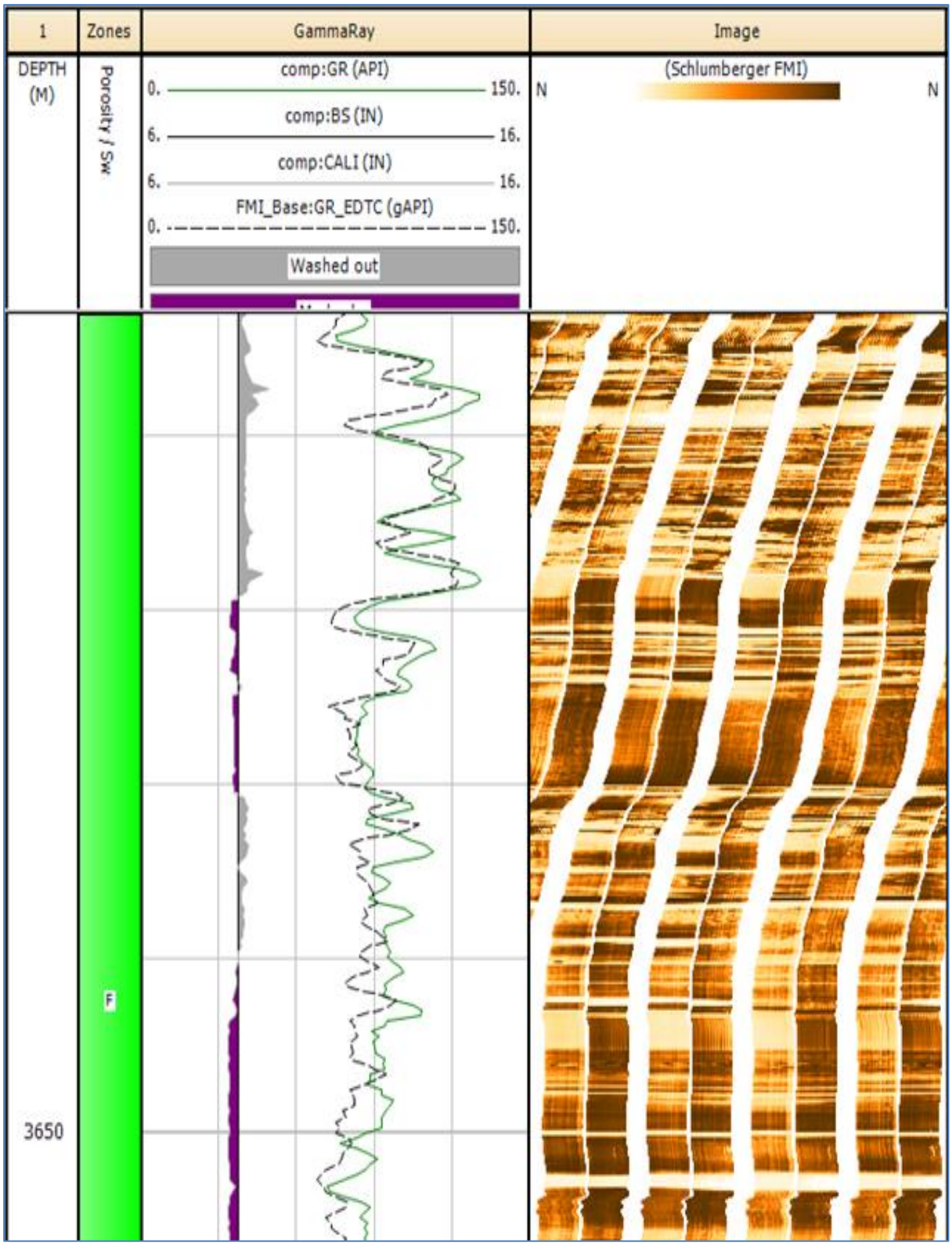

Figure 10. Comparison between the PEX-GR (comp:GR) and FMI-GR (FMI_Base:GR_EDTC) logs to check for the logging runs correlation and depth match. FMI logs positively depth shifted for 0.3 m down to match the composite logs. (Scale 1/20)

3.3.2 Image log processing and corrections

Image logs contain very high resolution recorded resistivity/acoustic measurements that creates a larger volume of data files compared to conventional low resolution logs. Image logs are usually stored as an array data since a number of data is recorded for every particular depth while in the conventional logs, there is only one record per sample point. These high resolution image data are generally provided by service companies in DLIS or LIS format due to their large volume. Once the image data has been coupled to a defined image log provider, FMI tool from Schlumberger in this case, the data can be corrected to enhance the log quality and reverse some of the environmental effects. As it is already mentioned above, some of the corrections are normally done by the service company during the logging acquisition. However, some of them have to be carried out by the operator.

The image logs are normally measured in the time scale and converted to the depth scale by Service Company. The conversion of the logs to depth scale is sometimes not accurate due to tool stuck and release, unreliable tool friction, rig heave, cable tension and so on. All these effects can cause a real feature like a bed boundary, fault or fracture to appear inconsistent from different pads. Figure 11 shows an interval of the Case-A well with raw image data (track-4) and the corrected one (track-5). Before the main correction (accelerometer correction) can be applied a depth shift curve must be created from the accelerometer data. Tool acceleration, elapsed time and surface velocities are used to create the depth shift curve for use in acceleration correction.

The corrections that have been applied to the raw log are then as follow:

- EMEX correction which is used to regulate the tool voltage by removing the effects of variable voltage on the raw current measurements to improve the tool resolution to generate better formation resistivity.
- Accelerometer correction that corrects the tool speed effects including rumbling, rebounding, sticks , etc, using the accelerometer readings and pre calculated depth shift curve.
- Streak correction that reduces vertical streaking by equalizing pad and button values and also corrects dead buttons.

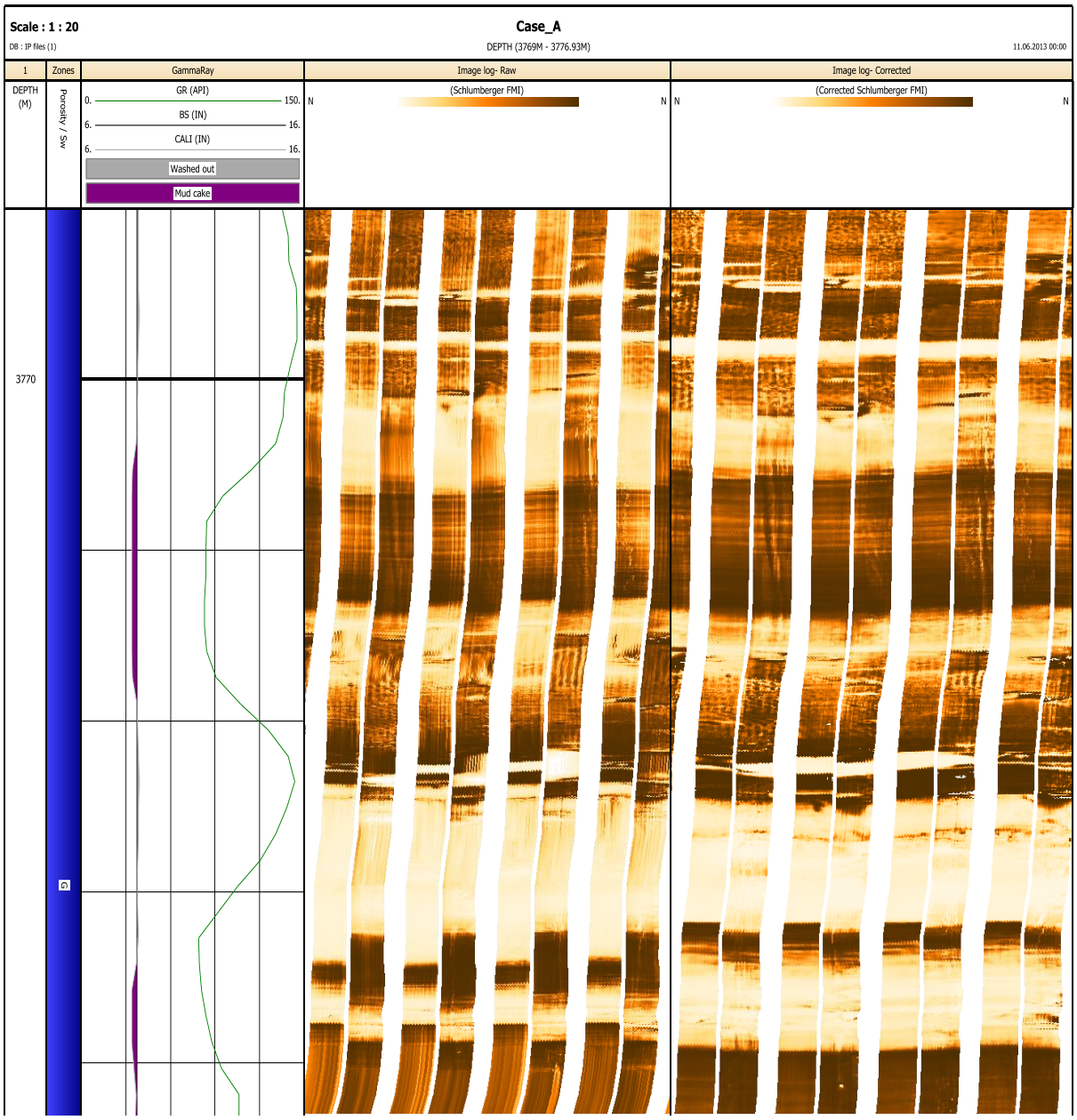

Figure 11. Comparison between the raw FMI data (track-4) versus corrected FMI data (track-5). (Scale 1/20)

All these corrections were done for the Case-A wellbore image log (FMI log). It should be noted that some of the un-even features are not possible to accuratly correct due to bad hole data quality.

Following the image corrections, image enhancements can be applied to the image log to enhance the log quality and resolution. Subsequent enhancements to apply in IP software:

Horizontal sobel to enhance horizontal edges, vertical sobel to enhance vertical edges, emboss to enhance all edges, Guassian blur to blur the image using Guassian function and adaptive smooth to remove noise with preserving the edges. In this well, the last enhancing module ‘’adaptive smooth’’ is used for FMI enhancement. Figure 12 shows the comparison between the raw image log (track-4) and the corrected and enhanced image log (track-5). After the log processing and corrections, sedimentary features will be picked to inter

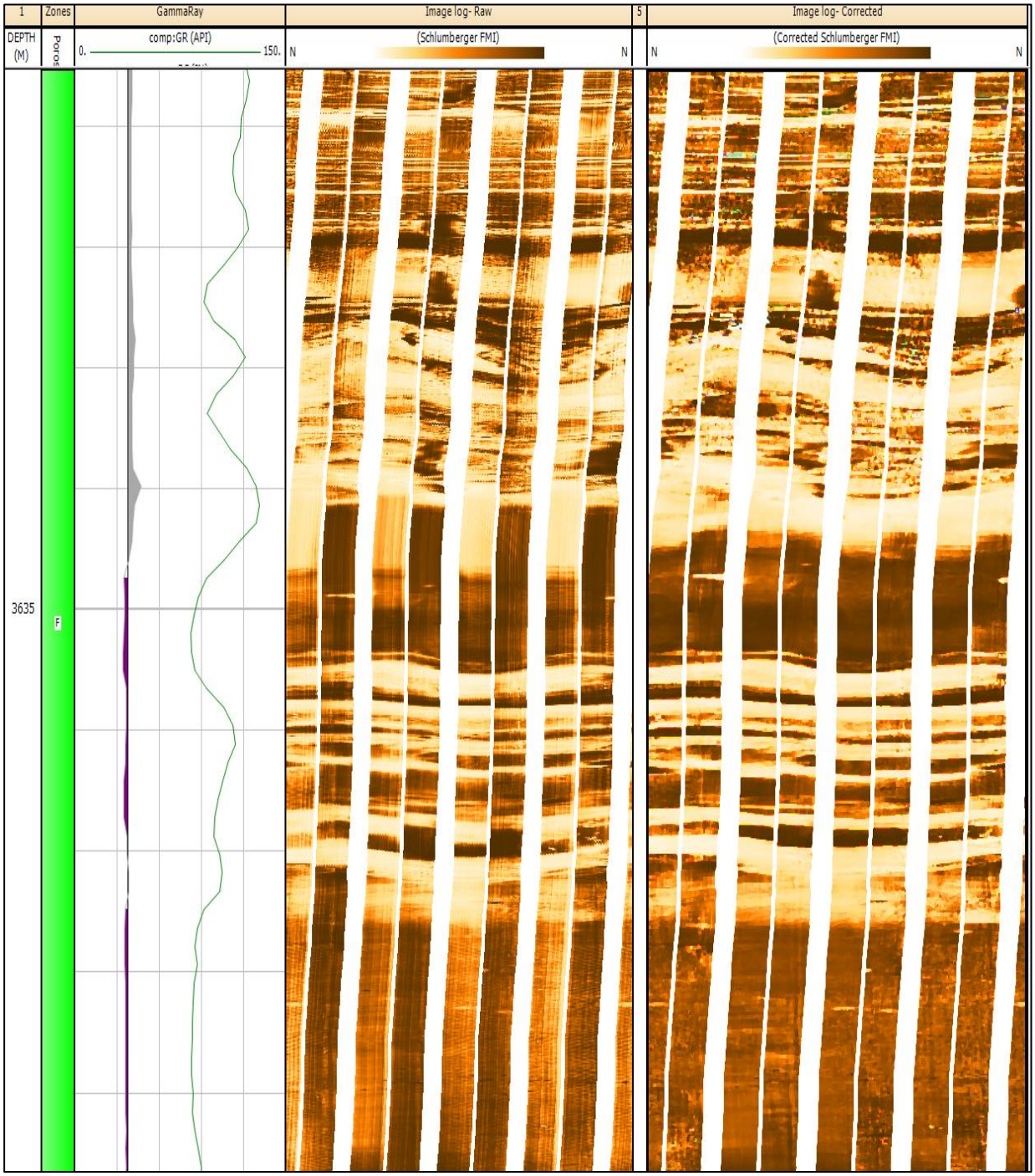

Figure 12. Comparison between the raw FMI data (track-4) versus corrected and enhanced FMI data (track-5). (Scale 1/20)

3.3.3 Dip picking and sedimentary features

The dips seen on the borehole image logs are as they appear on the surface of a conventional core. The trace of a plane dipping bed forms a sinusoidal curve when the image of the borehole wall is unwrapped and laid flat, as we see in Figure 6. Most of the picking tools generate a pick which can produce a meaningful dip representing the feature identified. A dip is composed of three elements, a depth, an angle, and an azimuth. Plotting a dip alongside the other dips with appropriate display allows trends, boundaries and patterns to be identified. Bed boundaries, beds, slump features, faults and fractures are easily seen in the image logs. To pick the dipping traces in the image logs, the logs were already enhanced by log processing. Dips on this case study image log are picked and classified manually. Different dipping features were identified and picked for sedimentary and structural interpretation. Identified dips are sedimentological and low angle features including, shale and sand bed boundaries, erosion surfaces, unconformities, high angle structural features such as faults, fractures and drilling induced fractures and some other features like nodules, lenticular features and deformations.

Figure 13 illustrates a four meter of the well interval with defined dipping layers. Two sandy beds; one at 3629m depth with 0.6 meter thickness and another at 3631.6m depth with 0.5 meter thickness. Track four shows the tadpole plot of the dips which display the sinusoid planes on the picked features as the dip angle and dip azimuth. This track shows the dip angle of the picks and the direction of the tadpole tail shows dip azimuth from the North. Accordingly, the azimuth of the thin shaly layers is about 180degree from the North with the dip angle of 5 to 10 degree. However, the sandy layer at the top has slightly higher dip angle of about 13 degree with similar dipping azimuth as shales beneath that sand toward the South.

The sandy layer at the bottom, however, has different dip angle and azimuth. The dip angle of the layer is 25 degree toward the 270 degree from North. The cemented shaly sand layers below the bottom sands show even more dipping layers of about 50 degree toward 270 degree north. In addition to the sedimentological beds and bed boundaries, two drilling induced fractures are seen in the image. These fractures are visible over the shaly and sandy layers indicating that the drilling mud pressure was considerably higher than the formation pressure.

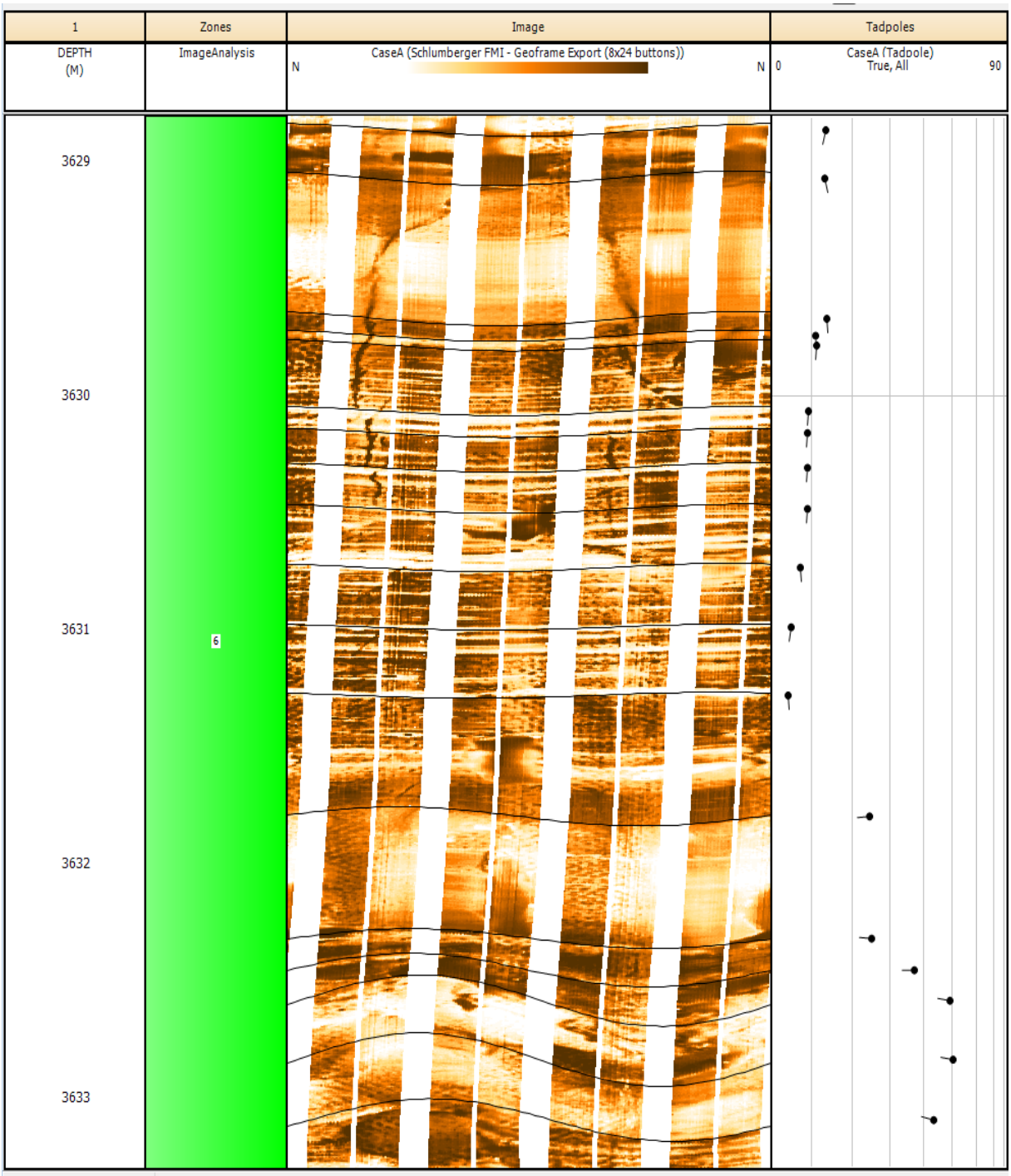

Figure 13. FMI image log with identified features including two sand bed boundaries at the top and bottom of plot, a number of low angles (5-10 degree) thin shale beds in between sandy layers. (Scale 1/20)

Logging quality for picking the sedimentary bedding features and structural analysis is also important factor. After logging quality control and acceleration correction to enhance the log quality, there are still some intervals that the image log is not interpretable due to tool stuck and distorted micro resistivity image values. **Figure 14** shows a three meter interval with not interpretable image data. Overall, the image quality in the case well is good but there are some intervals with bad quality images.

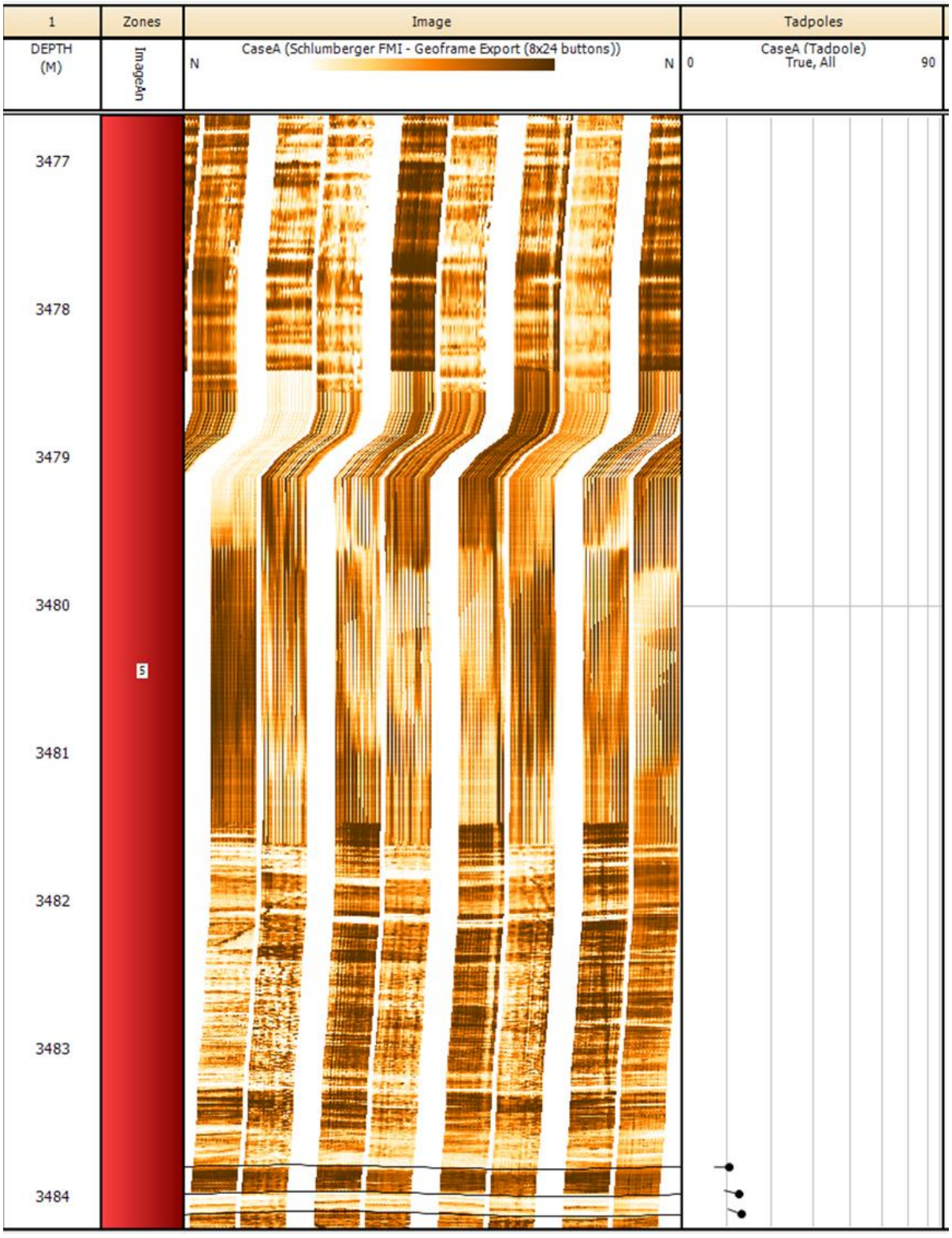

Figure 14. Bad hole image data due to tool stuck and release over the 3 meter interval. (Scale 1/20)

3.3.4 Convolute bedding (Slump)

Soft sediment deformation structures result from movement of sediment after deposition but prior to cementation. Sometimes this deformation is because of the application of some kind

of external load (e.g. faulting or tectonic force) but is usually due to density instability between different sediments layers. The most common are load structures, irregular bulbous features formed when a denser material has sunk into a less dense material. In some cases, denser material pinches off to form pseudo nodules (e.g. ball and pillow structures). This type of deformation can result in convolute bedding or slump if the structure experience intense structural deformation as illustrated in Figure 15.

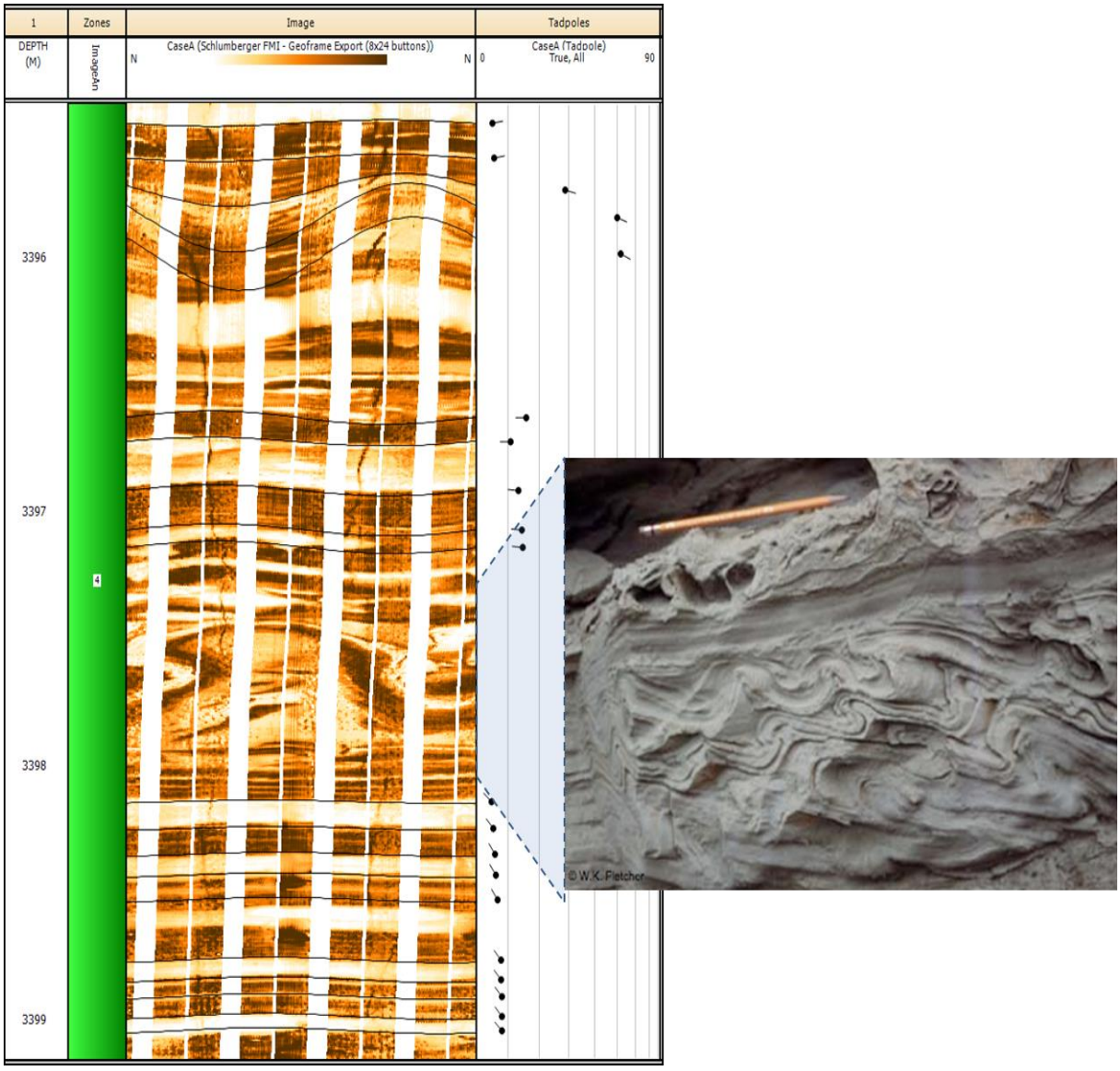

Figure 15. Deformation of soft sediment leading to convolute bedding (slump), suggesting intense structural deformation of the turbidity flow deposits. (Slump photo from GEOL342: Sedimentation and Stratigraphy Spring 2013). (Image log scale 1/20)

4. Sedimentary environment interpretation

According to the sedimentological interpretation of the limited cores in the upper part of the reservoir implemented by an external source, the reservoir depositional environment is a deep

marine sedimentary environment formed by submarine fan system. Submarine fans and related turbidite systems comprise deposits of mass movements, including slides, slumps, turbidity currents, and debris flows (Middleton & Hampton 1973) (Figure 16).

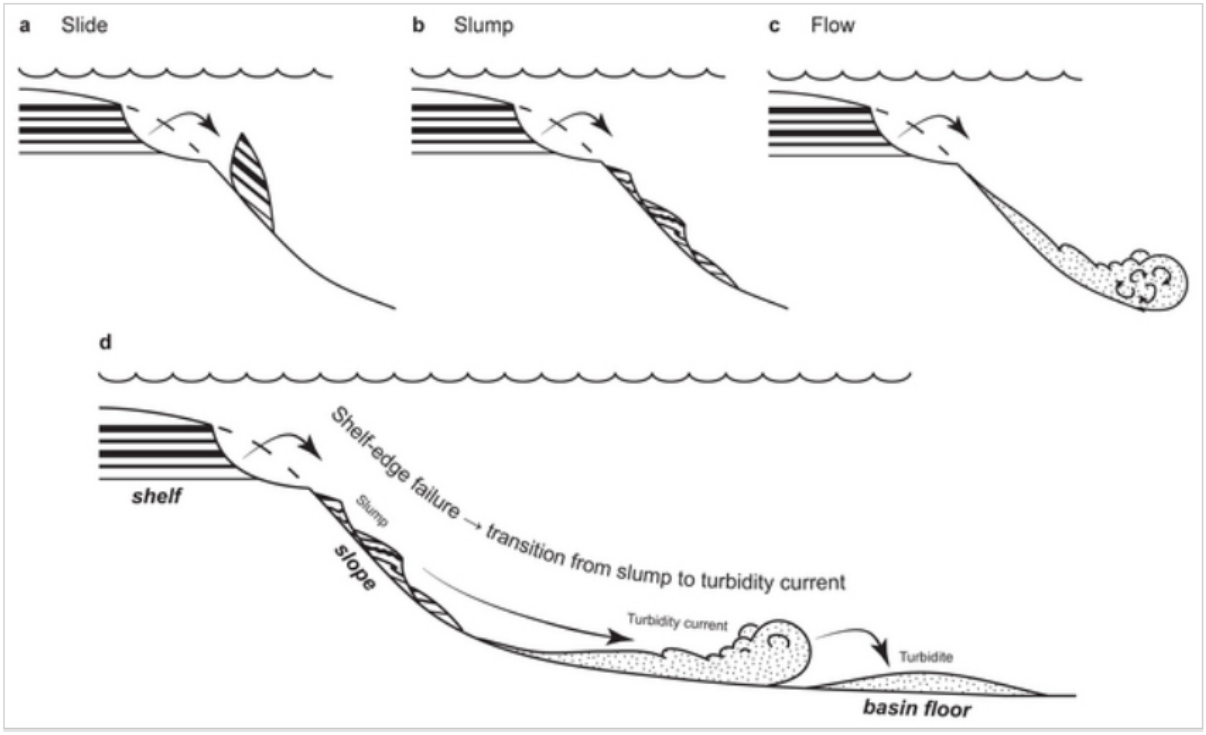

Figure 16. (a-c) Types of submarine mass movements, which generally are distinguished based on degree of internal deformation. (d) Initiation of a submarine mass movement as a result of shelf-edge sediment failure, followed by transformation from slumping to turbidity-current processes.

Slides and slumps are distinguished from debris flows and turbidity currents, which are types of sediment gravity flows, according to the degree of internal deformation: slides and slumps are characterized by less internal deformation, sediment gravity flows are characterized by more deformation (Middleton & Hampton 1973). Perhaps the most widely recognized deposit in submarine fans and related turbidite systems is a turbidite, the deposit of a turbidity current (Bouma *et al.* 1985). In this chapter the reservoir section is divided into different sections and discussed more in detail both structurally and sedimentologically using the borehole image logs and core data. The attempt is to correlate between the core recognized turbidity features in the image log and extend it to the un-cored sections.

The general trend of the bedding dip angles and azimuths are discussed and different sedimentary features are highlighted to recognize the sedimentary environment. Existing faults and fractures has been picked and explained in the interval description. The

interpretation is carried out from the cored reservoir interval of the image log toward the bottom of the well (e.g. younger deposits toward older sediments). The cored interval is chosen as the first step in the interpretation to correlate the core facies and image logs for sedimentary interpretation. Thereafter, the identified features and the recognized sedimentary environments are used in the interpretation of the un-cored sections. For every section a composite log plot including the FMI image log together with other conventional logs are presented. The conventional logs include caliper, bit size, gamma ray, neutron, density, photoelectric effect (PEF), deep and micro resistivity and sonic logs.

In addition to all these logs, two other log tracks including tadpole track and stick view track are included in the plot. Tadpole track shows all traced dips over the defined sinusoid curves in the image log as dip angle and azimuth. The horizontal scale of this track is in degree from zero to 90deg representing the dip angle of the feature. The direction of tail, on the other hand, shows the azimuth of the dip referencing from the north. In this plot the north direction is parallel to the vertical depth toward the top of the plot.

4.1 Depth interval 3610m to 3661m

This interval composed of an alternation of sand and shale layers. The main reservoir section of the well is this zone but due to the Microporous sand layers, the water saturation in the gas bearing sands are too high. The fluid sampling from the modular dynamic fluid sampling tool confirmed gas as main flowing phase of the reservoir. But at the same time, most of the sampling fluids were highly contaminated with mud filtrate. One possibility for having more contamination may be due to high filtrate invasion into the formation due to overbalanced drilling of the reservoir section. The well was drilled with more than 100 bar overpressure than the pore pressure and this may result in higher filtration and rock failure (induced drilling fractures seen in the image log). The petrophysical interpretation of the reservoir section is seen in Figure 17 together with FMI log and tadpole plot.

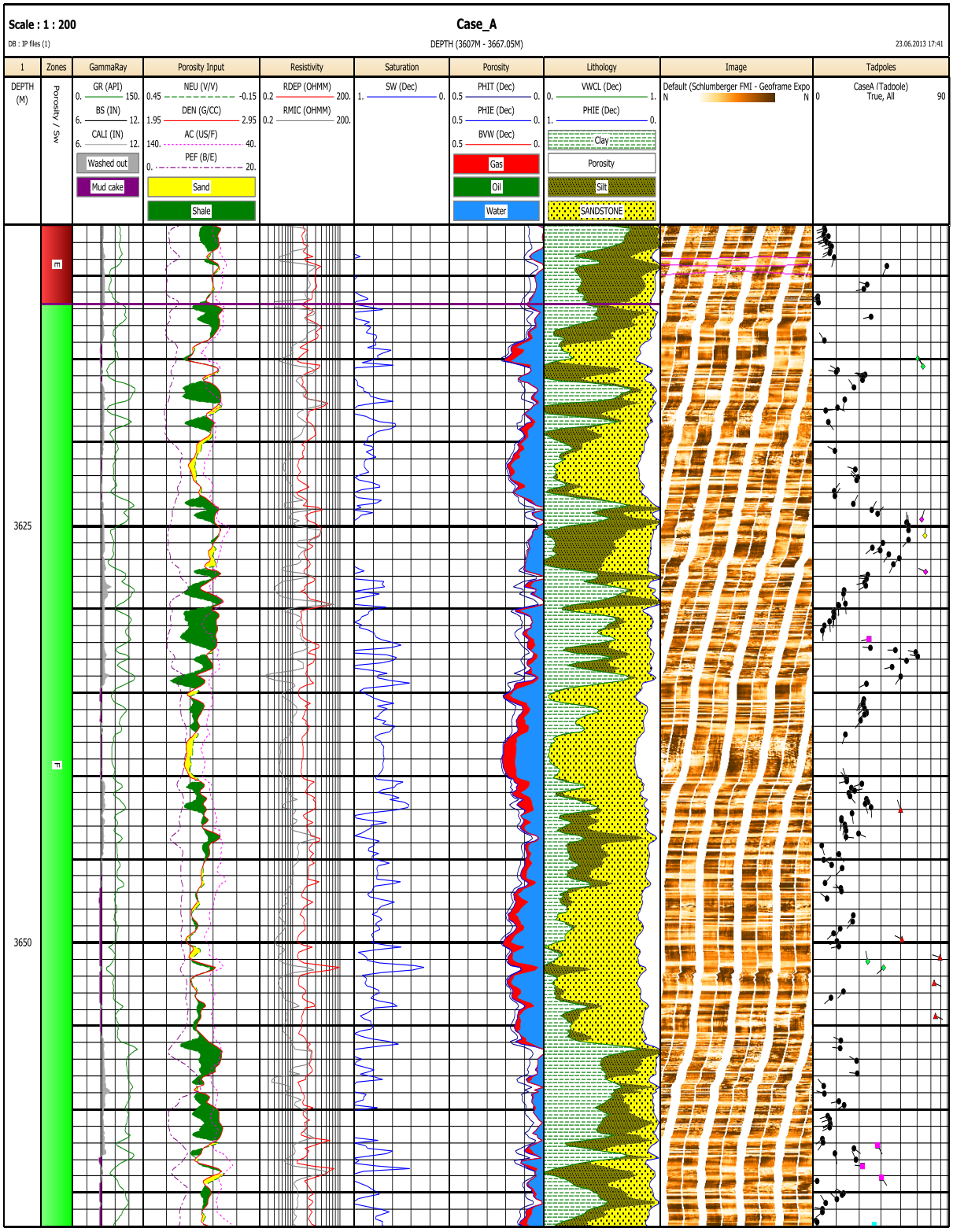

Figure 17. Petrophysical interpretation of the hydrocarbon bearing section of the reservoir. (Scale 1/200)

Core facies studies of this well conducted by an external company and the results are used together with FMI image log to define the sedimentary environment. The image log correlation with core facies is used for the interpretation of the rest of the well. Most of this

interval (3620m-3668m) has been cored and characterized in detail. Thus this interval has been used as reference for the FMI facies description and sedimentary environmental interpretation. The top of this section at 3608.8m is capped by an unconformable surface with average dip angle and azimuth of 5deg and N260deg respectively. Few intervals in this zone show clear continuous and consistent un-deformed beddings.

Some of the bedding and structural features in the image logs are compared with the core photos at the following section to understand the reservoir rock facies and structure.

Figure 18 shows two faulted layers in the image log one at 3624.7m and another at 3625.7m.

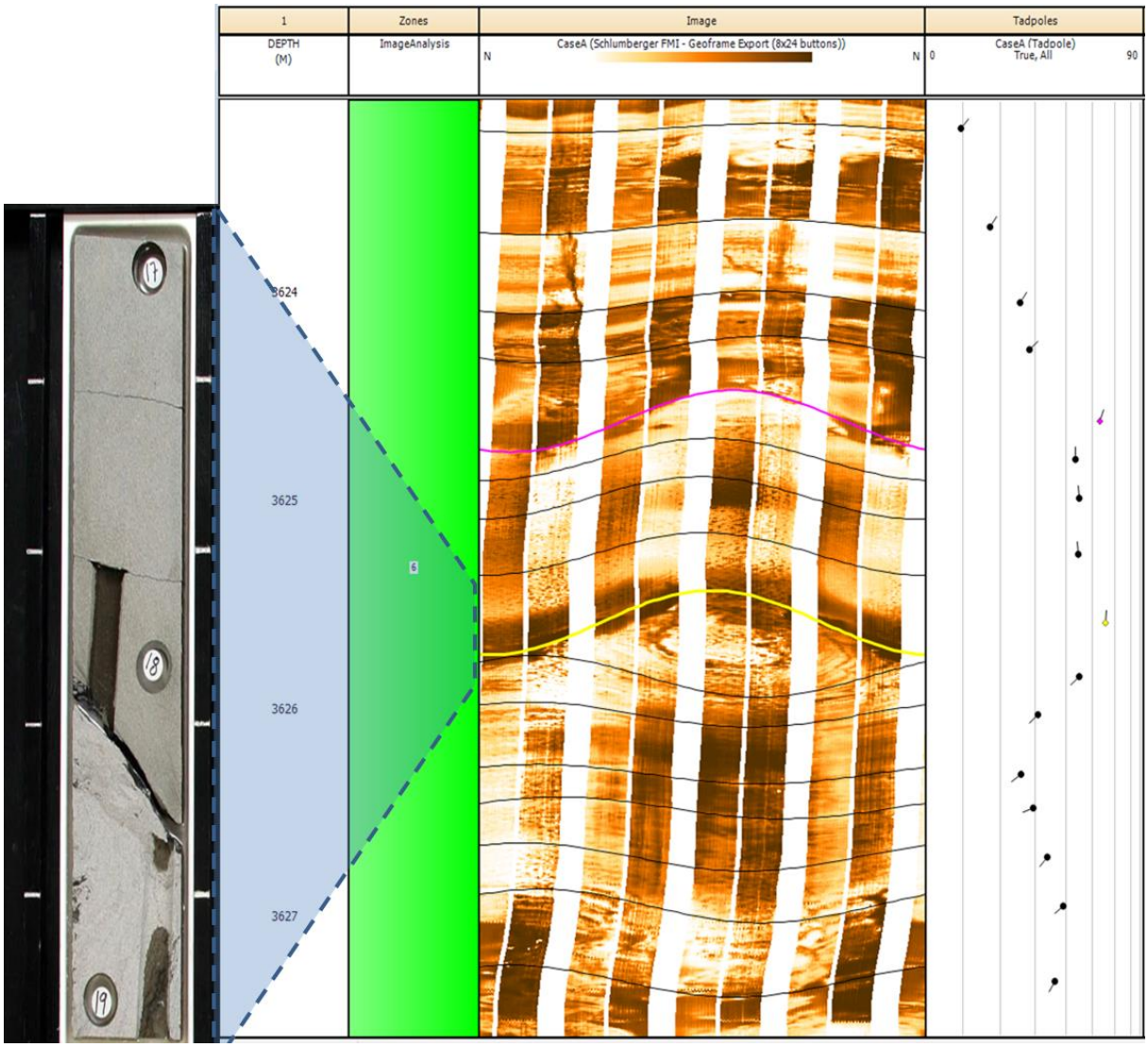

Figure 18. FMI image log with defined fault zone (yellow marked) together with core photo of the zone. Relative azimuthal direction of the hanging wall and foot wall indicate a trust fault movement type at this interval. (Core photo unit is 10cm and image log scale 1/20)

Faults can be recognized by the sharp change in the bedding dip angle and azimuth on the image log. In this figure, shaly beds at the top show gradual dip angle increase by depth until the upper fault (pink colored). Shale layers as is seen in the plot have been partly deformed. Dip angle of the fault is 53deg with an azimuth of N40deg. There is one meter thick sandy layer with dip angle and azimuth of 45deg and N0 (zero) deg beneath this fault. Another fault (yellow labeled) below the sand layer separates the upper and lower sands quite markedly (Figure 18).

The sands below this fault lie with somewhat in opposite direction to the fault with gradual change in dip angle. Relative azimuthal direction of the hanging wall and footwall beds and footwall lamination bending upward below the fault zone illustrate a trust fault movement at this interval. Note that the sands below the trust fault are moderately calcite cemented sandstone. Two small scale induced fractures can also be observed in the shaly section at the top of the plot.

Figure 19 illustrates four meter sandy interval of the reservoir zone that shows relatively consistent dip angle of 10deg but variable dip azimuths. Zones of sands with more calcite cement appear as lighter color in the image and cleaner sands appear as dark brown color as they flushed with more saline mud filtrate. A well sorted, highly rounded and elongated calcite cement nodule is detected in the image log and can be easily correlated to the core photo of the nodule. It should be noted that the vertical thickness of the nodule is approximately 30cm. A possible bioturbation feature is also seen in the lowermost part of the image log which is not possible to recognize in the core photo.

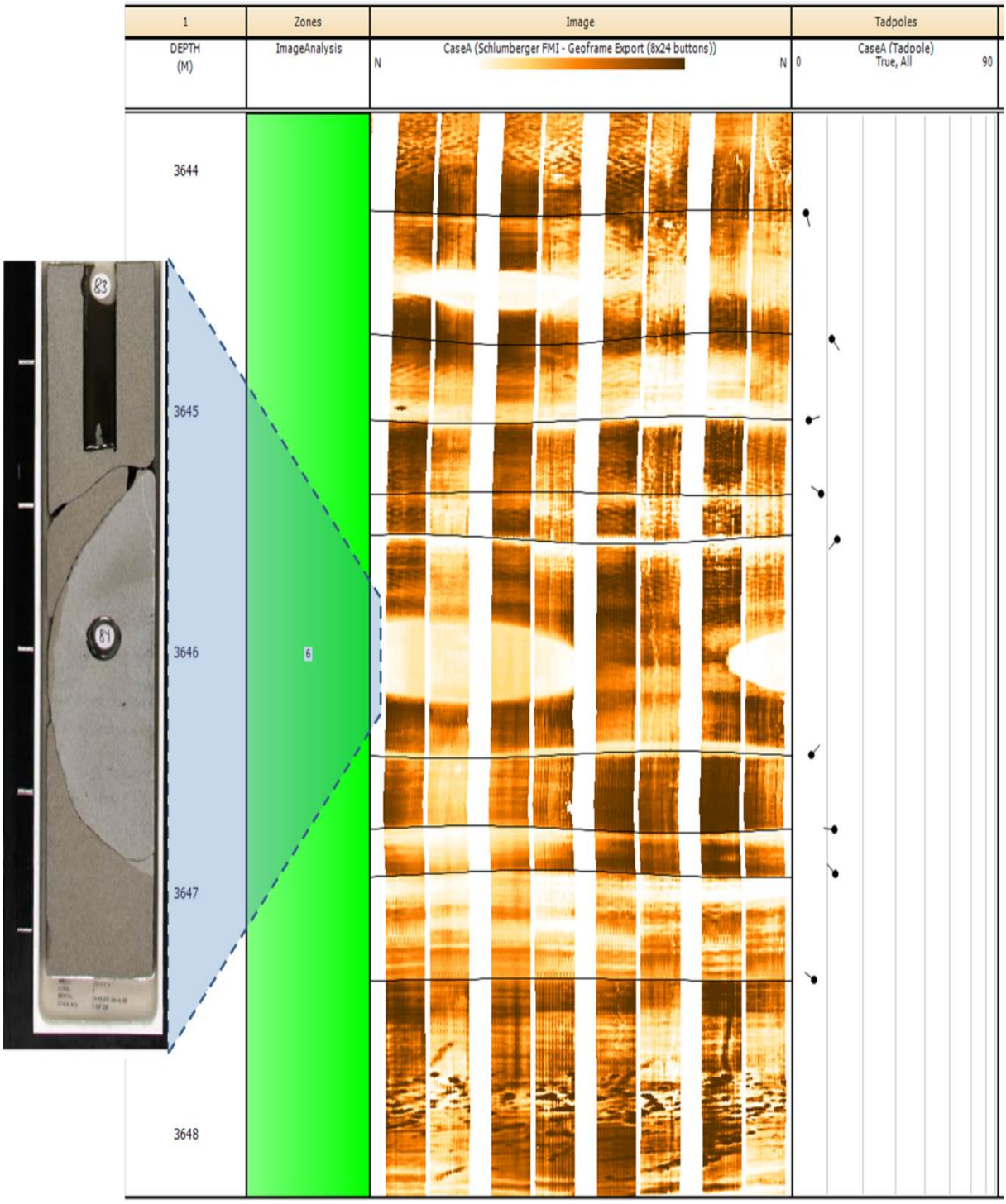

Figure 19. FMI image log with calcite cemented nodule. Image log shows that the nodule has not been detected by all image tool pads as can also be seen in the core photo. Note the possible bioturbation pattern in the bottom of the image log. (Core photo unit is 10cm and image log scale 1/20)

Figure 20 illustrates four meter of sandy interval with three conductive fractures and two cemented layers. Sand bed dipping angle is about 10deg with consistent azimuth of N220deg. Fractures are shown as red sinusoids on the image and they have higher dip angle of 40deg, 70deg, and 63deg toward N300deg, N290deg, and N100deg respectively. One particular

calcite cemented bed is bounded by two green color sinusoids in the image log which show different dip angle and azimuth. The boundary of this cement zone appears as diffusive to the sand zones above and below. These types of diffusive cements are seen in some intervals of the well and are interpreted as the compaction effect and possibly deformation of cemented nodules.

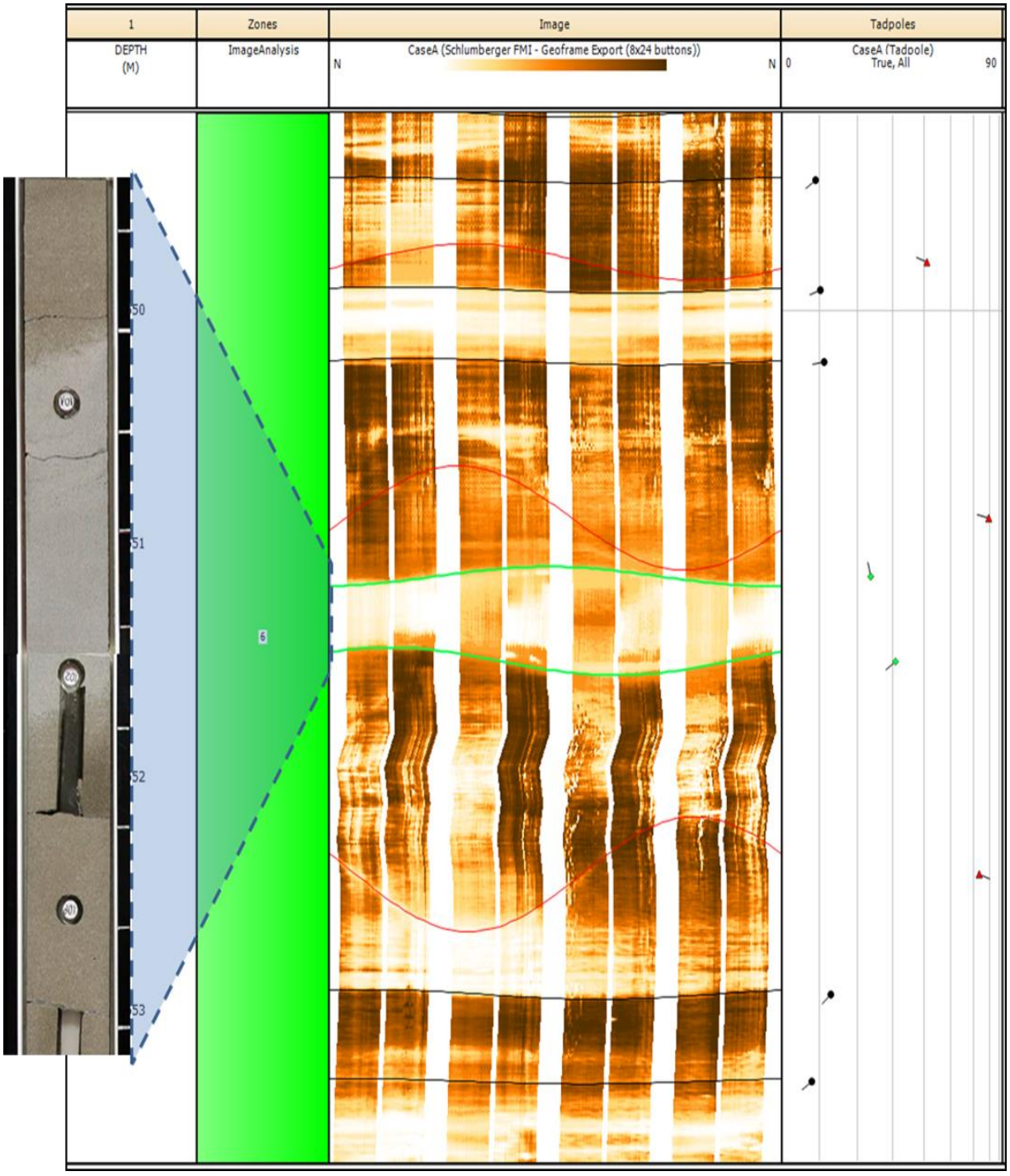

Figure 20. FMI image log with three conductive fractures and one diffusive calcite cemented zone. (Core photo unit is 10cm and image log scale 1/20)

Figure 21 shows three meter of homogeneous sand bed without structural lamination. Two thin shale beds at the top and bottom of the image/core can be seen in the figure. The sand bed is well sorted, clean, fine grained sandstone lacking the sedimentary structures. Lack of visible fluid escape features is probably due to the clean nature of the deposits. This sand bed is in the main gas bearing interval of the reservoir with 21% effective porosity. The darker color of the image log indicates the mud filtration into the sands during the drilling.

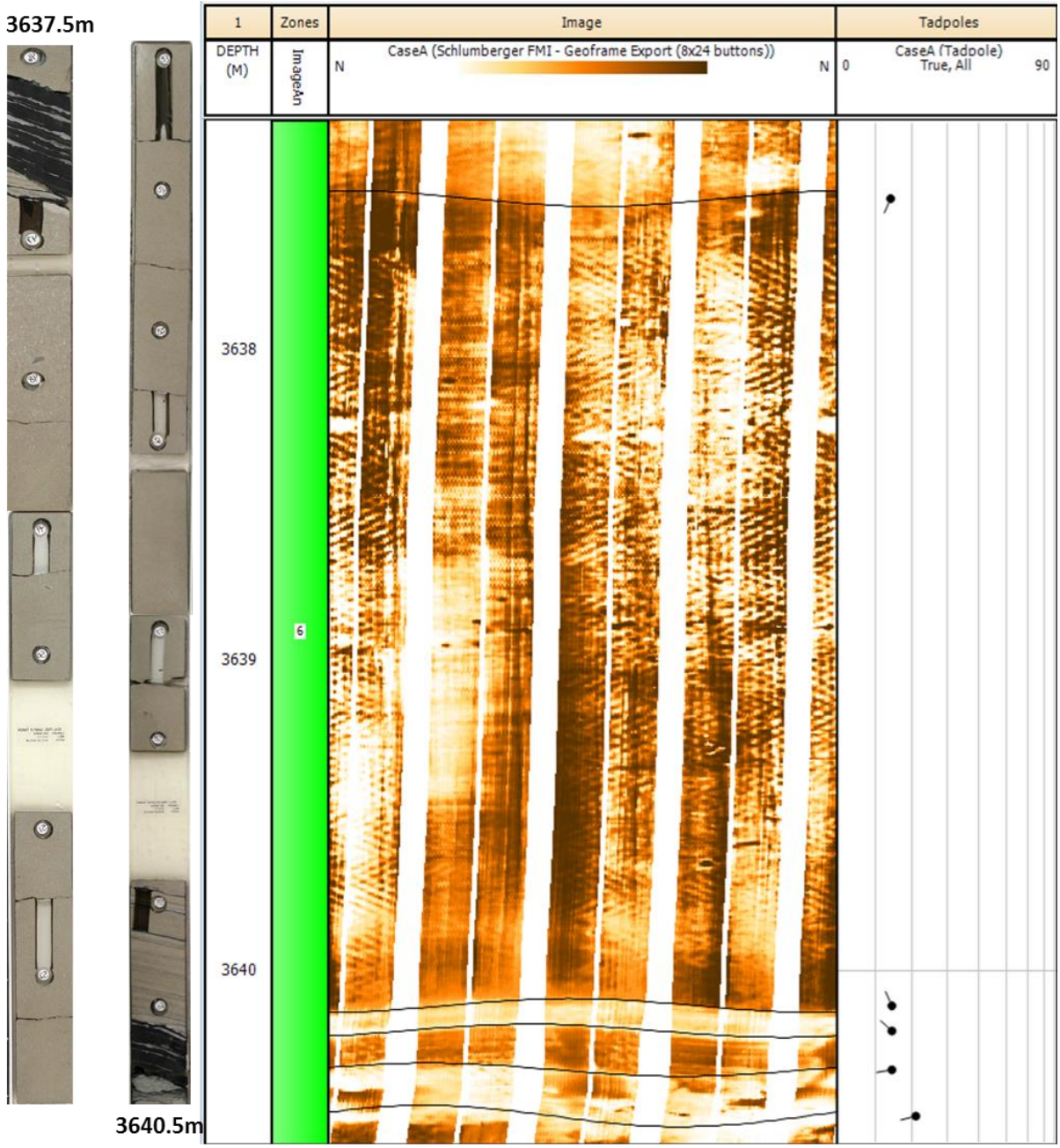

Figure 21. FMI image of 2.5m thick homogeneous sandstone layer without identifiable dip angle/azimuth in the sand. Few resistive mixtures of tight shales and calcite cement are identified at the top and bottom of the interval. (Every core column is 1.5m and image log scale is 1/20)

Figure 22 shows four meter of shaly interval within the reservoir section. Dipping angle of the layers is increased to the bottom of the interval but the dipping direction is approximately constant.

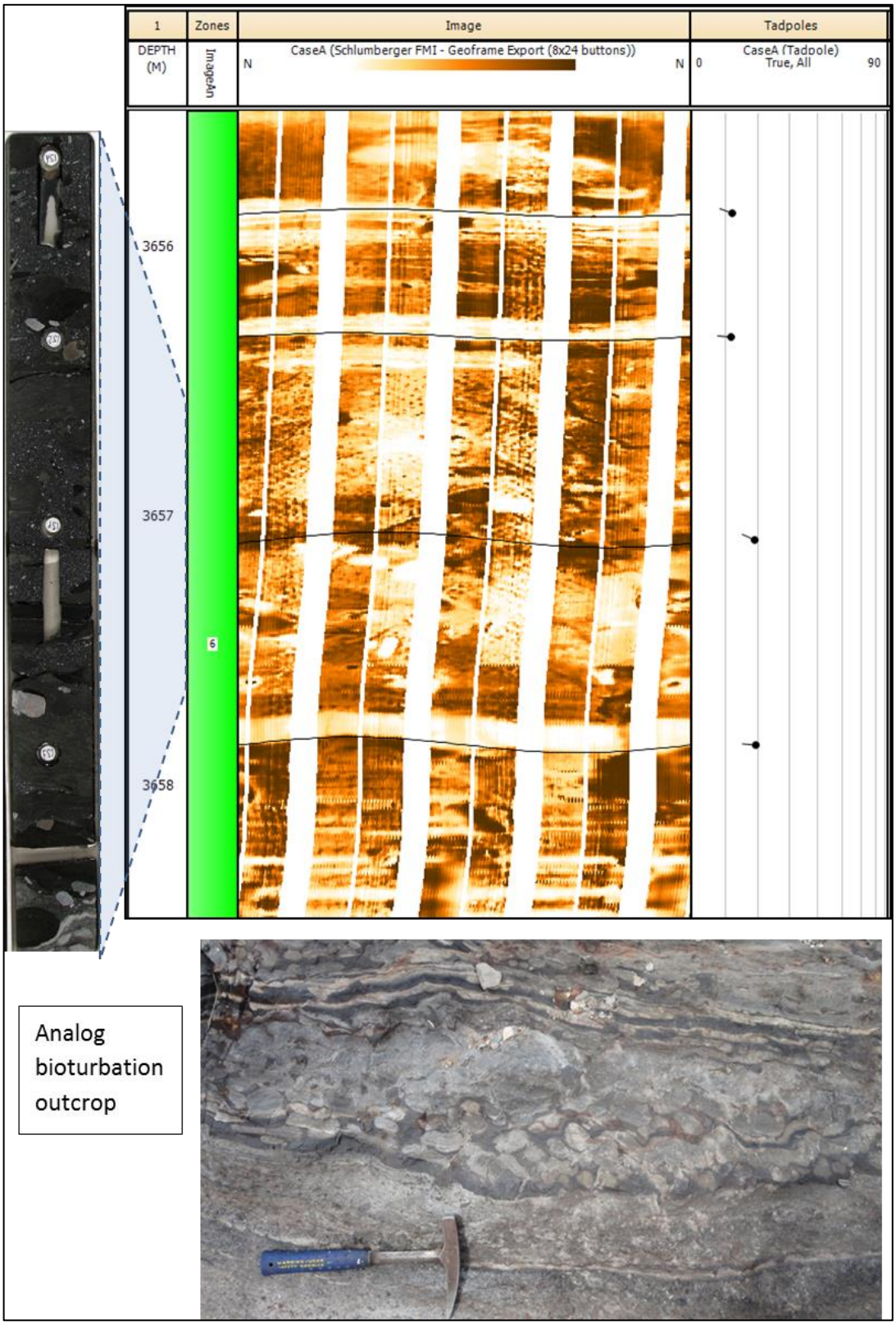

Figure 22. FMI image log of bioturbated zone with core photo of the zone. An analog outcrop of bioturbation is shown below the figure. (Core scale is 1m and image log scale is 1/20)

Cemented sand beds are visible in the image log. The middle part of the image shows possible bioturbation of the sediments which can also be spotted in the core photo. The outcrop analog for this type of sediments is shown at the bottom of the figure for comparison. Tight pseudo-nodules of cemented sands are common in the bioturbated environment.

Figure 23 shows the main gas bearing zone image log together with other conventional logs. There are many deformed beds in this zone between sand layers. The orientation of dips appears relatively scattered and the mean value may not be very representative. The different trends in the image log probably correspond to different deformed shale beds. Both resistive and conductive fractures are present in this section. As it is mentioned above (Figure 18) there is fault zone at 3625m which is most probably a trust fault. The stereonet, rose diagram and scatter plot of the beddings in this zone is shown in Figure 24. The bedding are shown as black dotted points in the plots. Both the plots show the scatter of the bedding dip angle and azimuths.

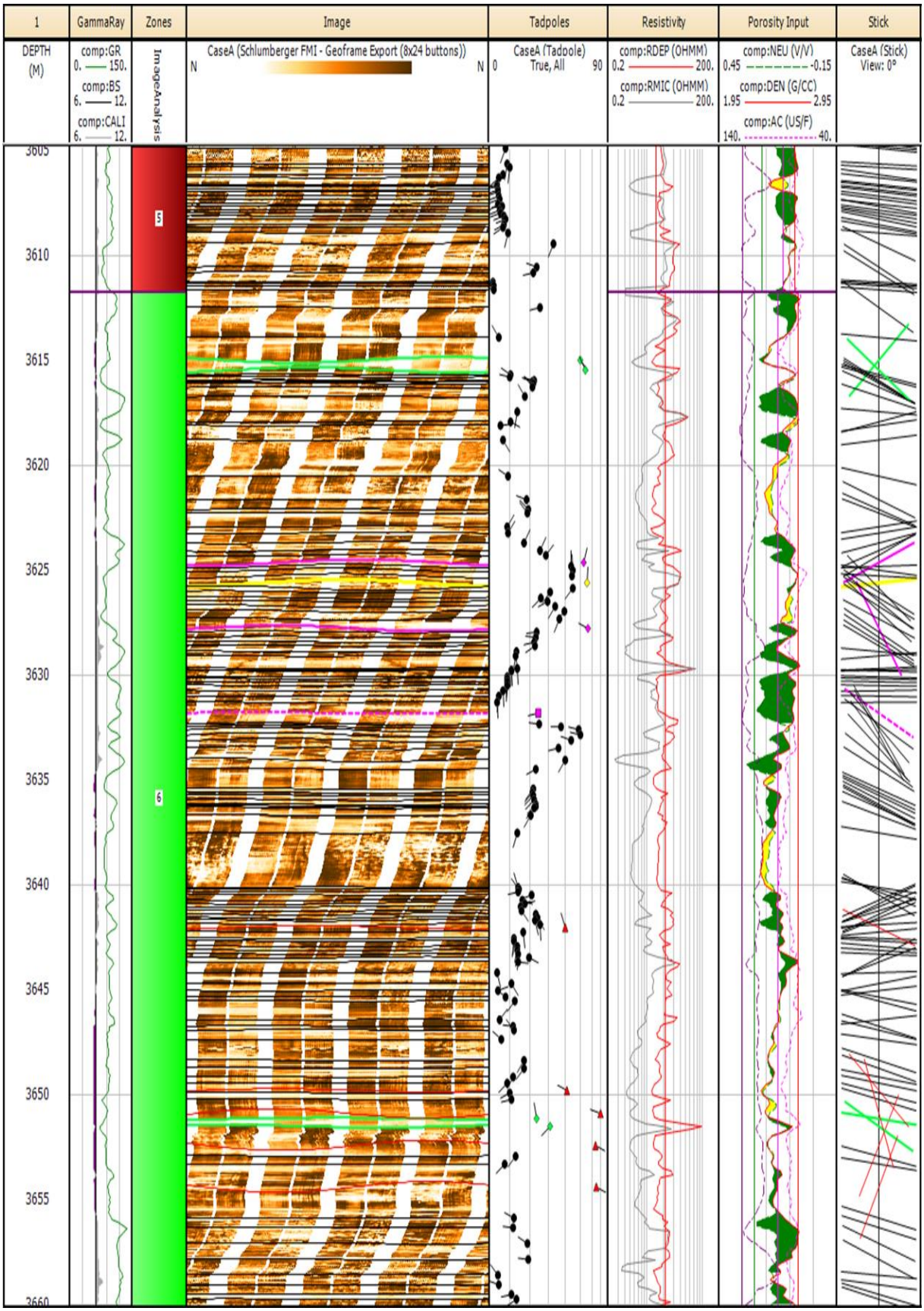

Figure 23. FMI image log of the sand and shale beds above the main sand package. Sequences of different dipping layers are observed in the image log. (Scale 1/150)

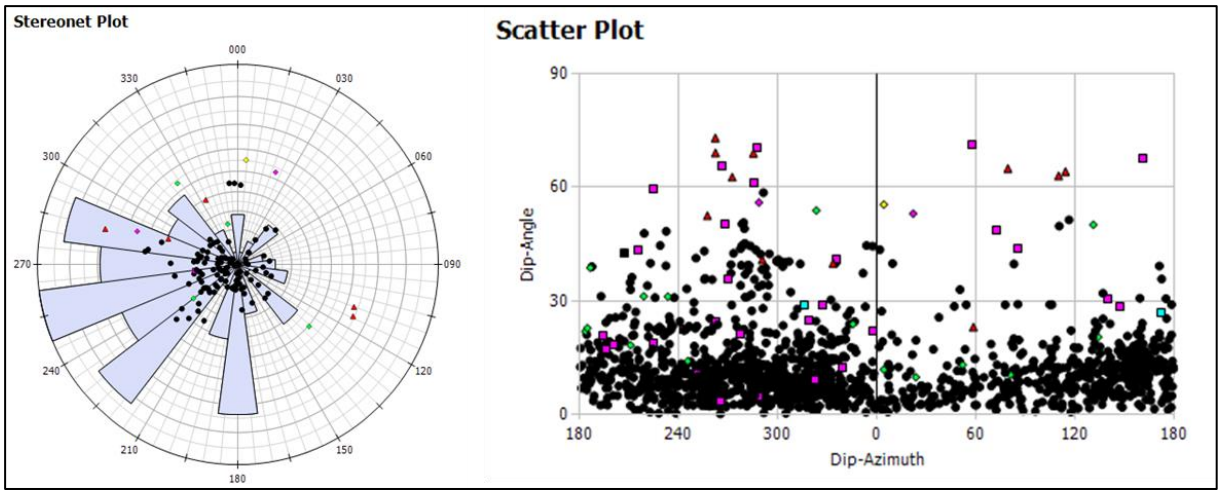

Figure 24. Stereonet, rose diagram and scatter plot of the bedding dip angles and azimuths in the main reservoir section.

In general, sand beds are normally separated by unconformable surfaces and shale beds and sometimes deformed shale beds. There are few shaly layers in this section. Bioturbation feature is not dominant in this interval except one example which was shown in Figure 22.Bed boundaries don't show a very clear orientation. Dip pattern is generally constant sequence, but their orientation is changing from one sand sequence to another. Both decreasing and increasing upward dip patterns are visible, but most of them have constant dip direction over each single sand set, separated by unconformable surfaces. The interval has been interpreted as turbiditic channels and sheets by core interpreter Figure 25. From the overall dip direction of the beddings, probable palaeo-flow direction is toward the North-North West. The channelization of the turbidite is less clear in the image log.

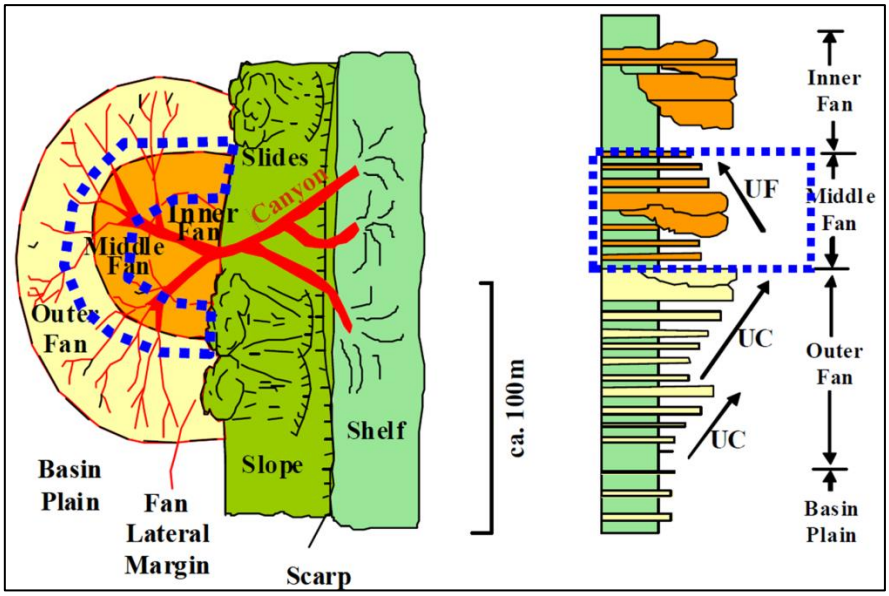

Figure 25. Sedimentary environment interpretation from core analysis. The middle fan and turbiditic channel (dashed blue area) is possible interpretation for the sediment deposition is the submarine fan system sedimentation. (modified from Pickering 1982 and Lucchi 1972)

4.2 Depth interval 3661m to 3738m

This interval is the thickest sand layer in the well. The fluid saturation from petrophysical interpretation is water with small residual gas saturation (Figure 26). This sand package has two deformed shale layers in between visible in both petrophysical interpretation plot (Figure 26) and the image logs. These shale beds due to deformation cannot be used for structural indication of this interval. There is a clear change of dip magnitude at 3698m (Figure 27) which indicates possible faults and fractures at this depth, easily visible in image plot Figure 28. This indicates that the fault may cross over this formation and may act as fluid flow barrier through the reservoir column. Meanwhile the pressure measurement from formation modular dynamic (MDT) tool indicates consistent water gradient throughout the whole sand bedding. This indicates that the fault is most probably is not acting as a fluid barrier in this interval.

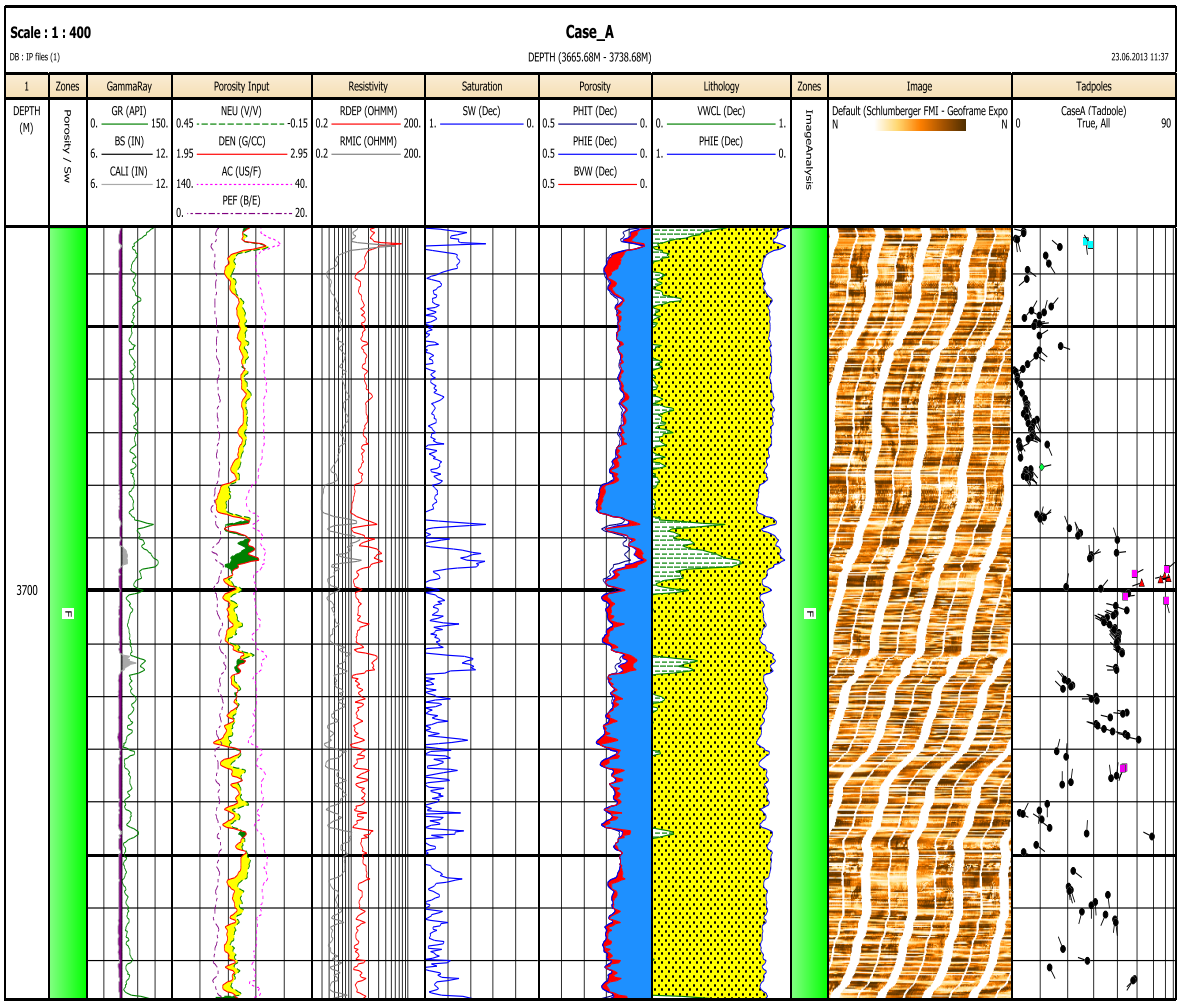

Figure 26. Petrophysical interpretation of the well in the thickest sand bedding. The reservoir is water bearing with tiny amount of gas saturation except the uppermost part of the sand with higher gas volume. Pressure measurements confirms a water gradient in this formation. (Scale 1/400)

The top of these sands is capped by an un-deformed and almost horizontal (5deg) shale bed with azimuthal direction to SW. The fault zone in the middle of the thick sand body divides the sands into two different bedding types. Sands at shallower depths to the fault zone show some high resistivity contrasts and thick sand bedding but the sands deeper to the fault seems to be more thinly laminated. Thus the sedimentary interpretation over this zone has been split into 2 parts, shallower and deeper zones to the fault.

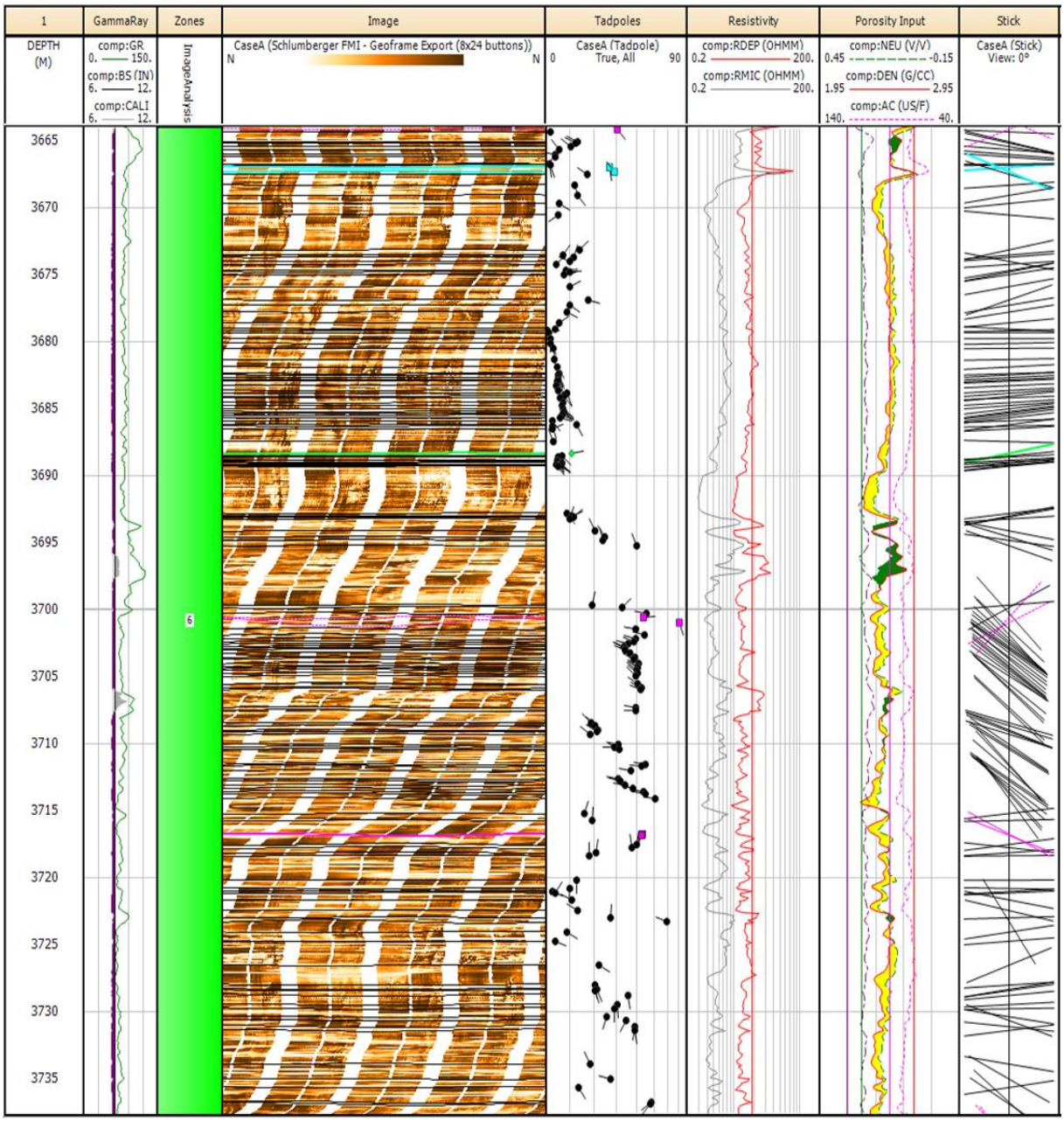

Figure 27. FMI image log showing heterogeneous dip angle magnitude and dip azimuth throughout the thick sandy body. Some fault and fracture plans are also visible in the image log. Two shaly zones one in the middle and one at the top is visible from the plot. (Scale 1/200)

As we can see from the shale layers within the sands, they are affected by compaction and deformed and therefore no orientation can be determined for structural dipping within these shale. A micro-fault is also visible below the main fault zone at 3700.5m.

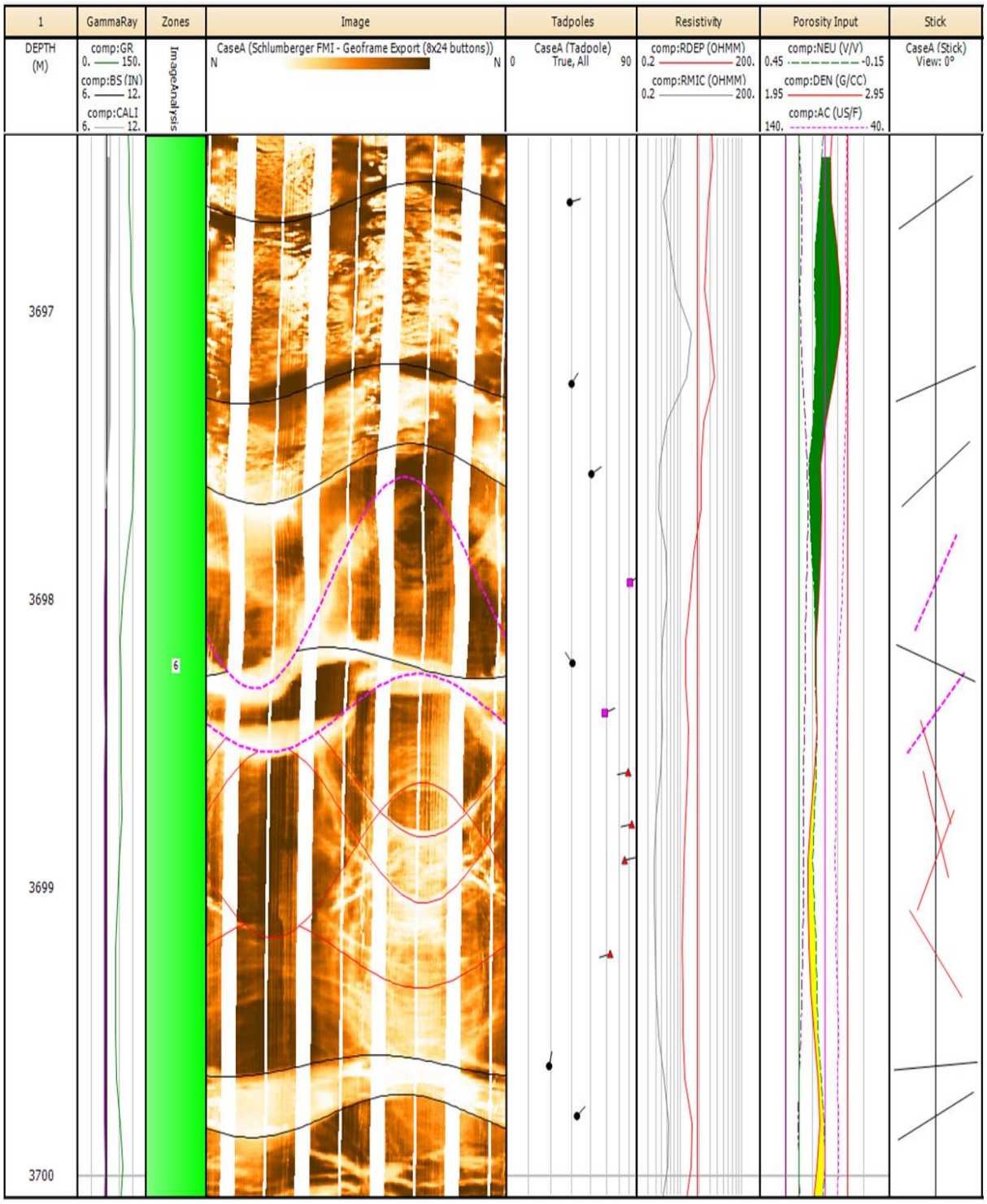

Figure 28. FMI image log showing two fault plans (dashed pink) and four closed fractures (solid red). Top of the image is deformed shale bed. (Scale 1/20)

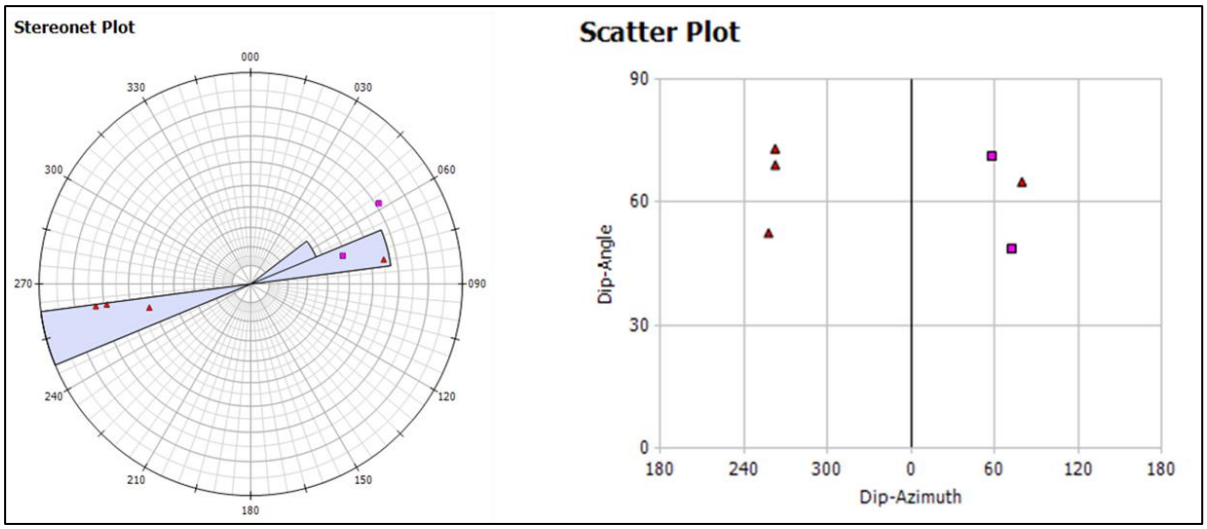

Figure 29. Stereonet plot, rose diagram and scatter plot of the faults (pink diamond) and fractures (red triangle) visible in the image log seen in Figure 28.

Deeper sands below the fault zone shows clean thinly laminated thick sand (Figure 30) with no massive shale and no clear indication of bioturbation. Most of the sand bed boundaries are dipping toward the North. This can be assumed as a good indication for a palaeo-flow direction toward N. The relatively high dip magnitude and the consistency would be an argument in favor of a channelized turbidite. This is different than what is seen in distal fan lobes that show lower dip angle with wide range of dipping directions. There is a secondary dipping trend toward the NNW in these sands as well. Both decreasing and increasing upward dip sequences has been observed.

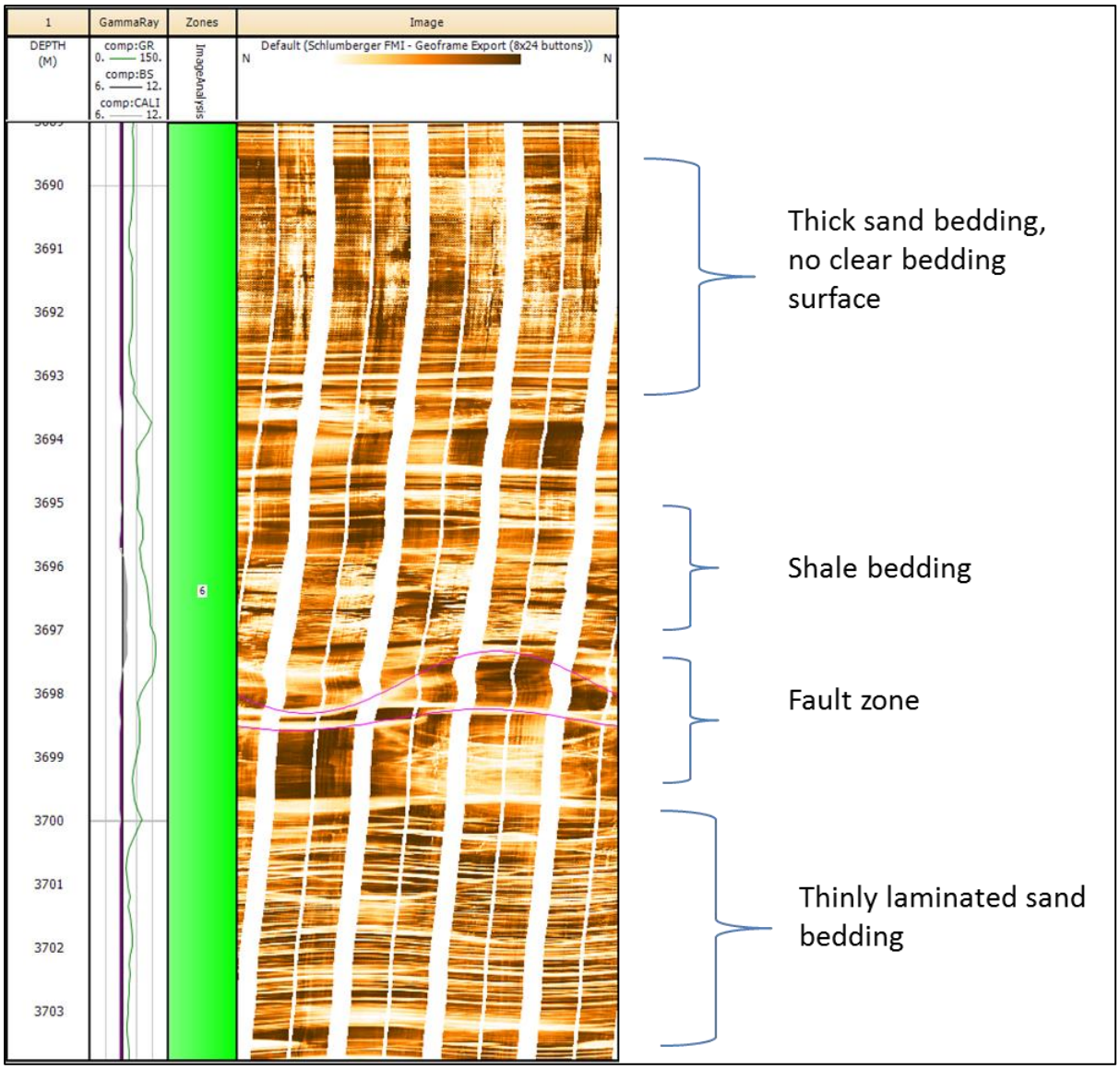

Figure 30. FMI image log of the sand beds above and below the fault zone. Thick sand bedding without bedding surface and highly laminated thin sands are visible above and below the fault respectively. (Scale 1/20)

Except a three meter sand bed right above the fault zone, which is a clear sand bed without inner layering surfaces, the rest of the zone include highly laminated thin sands. Sand beds are dipping toward NNW and the dipping magnitude is generally low, but some decreasing upward dip sequences are visible in four intervals. This can be an indication for a palaeo-flow direction toward NNW. The upper part of this interval has been interpreted as "tractional flow deposits and aggradational sand sheet" by external core sedimentary interpreter. Even though there is no clear turbidity features in the sands, the relatively low average dip magnitude and the dip direction uniformity may indicate a channelized turbidite with probably less flow energy than the deeper sands below the fault zone.

4.3 Depth interval 3738m to 3845m

This interval formed by shales and thicker scale sand bed alternation dipping toward different directions and different dip angles. Some internal sedimentary features are visible in these sands. The sand bed frequency is higher and sand beds are thicker bellow 3769.5m.
There are some deformed layers at the bottom of the zone, probably associated with the fault zone contact below this interval.

A number of thin sandy beds and thin deformed beddings within this interval can be identified. This zone is affected by some major stick and slip on FMI run, that affects the interpretation of the sandy zones visible on others logs between 3823m-3835m. As it is shown in the Figure 31, at depth 3769.5m shale bed boundary dip direction change which has been interpreted as an unconformity. Bellow this depth structural dip is toward the SE, above it is toward the SW. The top of this interval is a shale deformed zone, probably due to thick sand load of upper reservoir section.

Figure 32 illustrates dip azimuth walkout plot of this interval from the top to the bottom. Vector walkout plot allows dips to be plotted nose to tail to help find trends. In these plots, specified data, herein the azimuth is drawn in depth order with the direction of the subsequent points being determined by the plot type. An illustration of the azimuthal vectors are given at the top right corner of the plot with 5 dip azimuth trends throughout the zone. Starting from the top the dip directions are, SW-SE-NE-SE-SW. These trends define the bedding groups as well as the structural information, and depositional environment and flow directions.
Obviously the whole part of the zone has not been deposited in the low energy distal part of the turbidite lobs like the overlaid beddings.

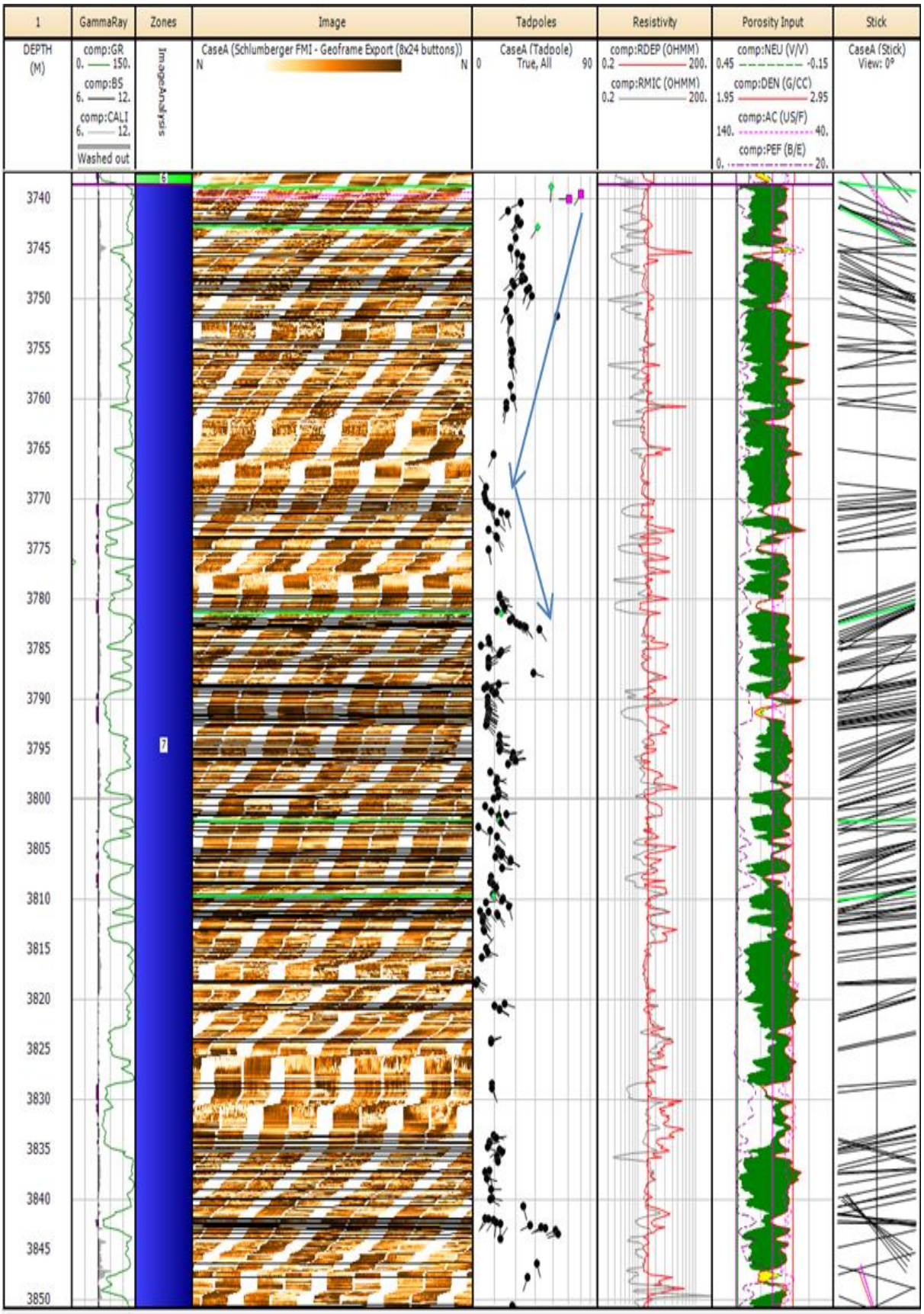

Figure 31. FMI image log of the well at the interval between 3738m-3845m together with tadpole plot and other conventional logs. (Scale 1/300)

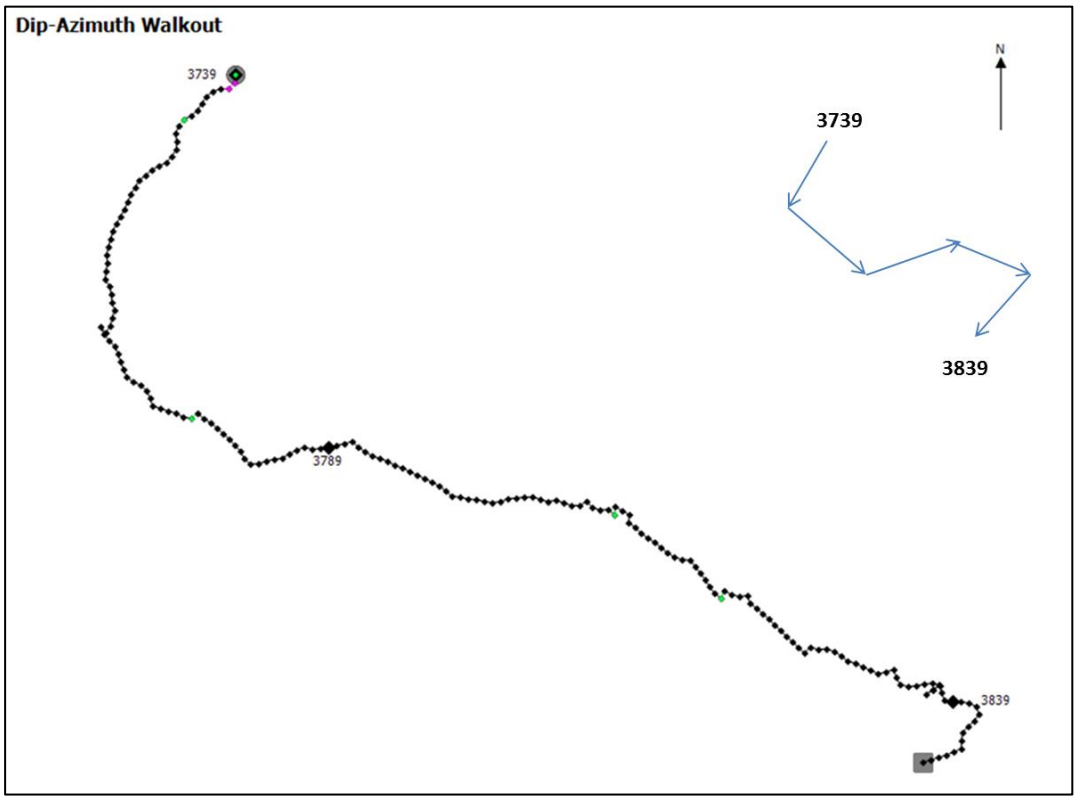

Figure 32. Dip azimuth walkout plot (vector plot) from the top to the bottom of the zone interval 3739m to 3839m. The direction to the north helps in identifying the relative azimuth of the beddings.

In general, the bottom the zone shows only a small number of sedimentary dips. The beds are mainly deformed at the bottom presumably due to the fault zone below. This causes the interpretation of the palaeo-sediment flow direction difficult. Most of the deformed beds show a directional trend toward the West and appeared as thin san beds (Figure 35, bottom interval). It might suggests those deposits are related to a syn-sedimentary deformation, possibly due to slope slide.

The zone bellow 3769.5mMD has higher frequency of sand beds, the presence of reactivated surfaces and higher angle sand dip (Figure 32). A majority of sand bed boundaries in the upper intervals show a SW trend and most of them have a low angle dipping. Based on this observation and also sedimentary features in Figure 33, it is suggested that the deposition environment for these intervals would be more turbidite outer fan with high proportion of fine grained sediment.

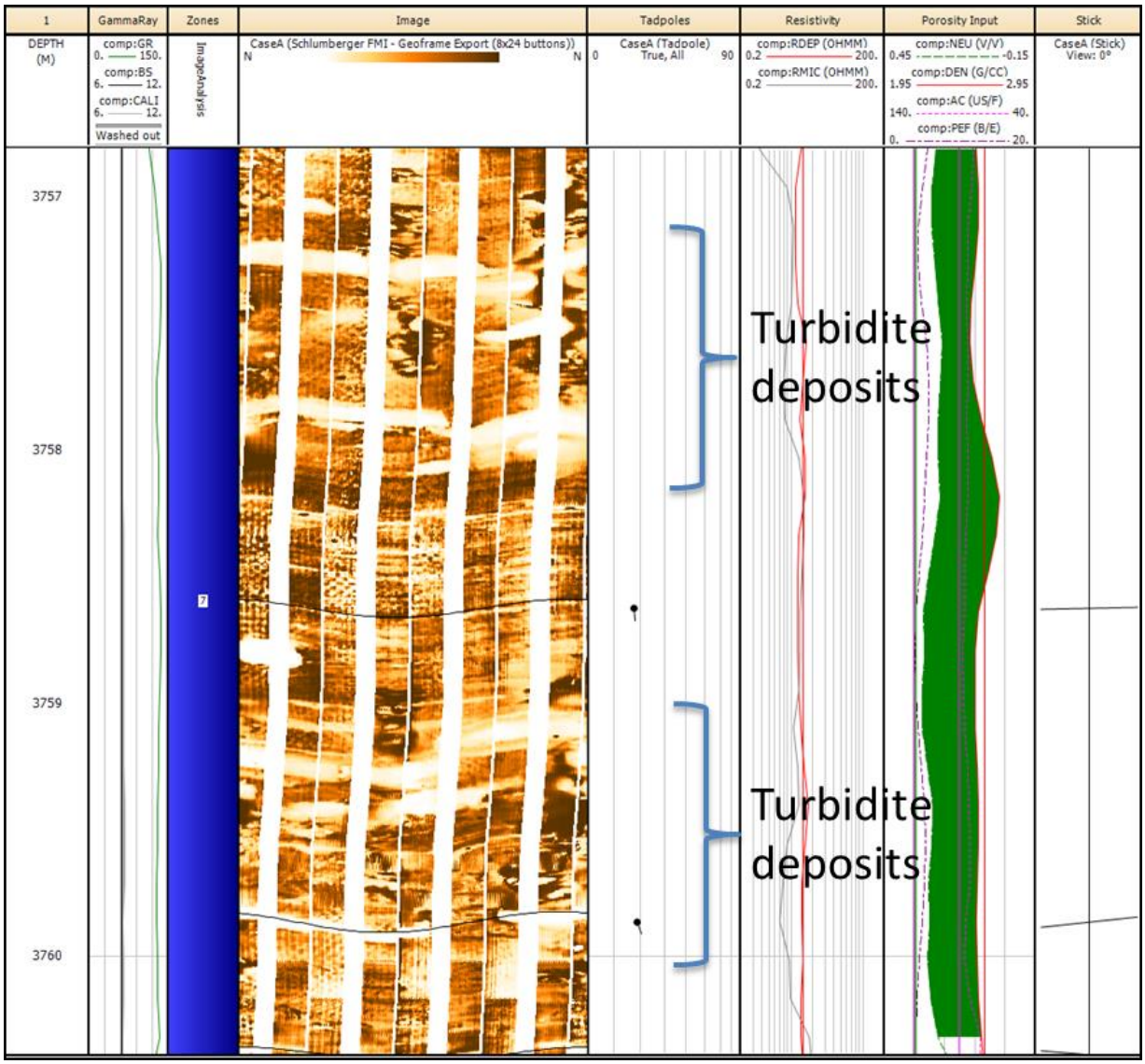

Figure 33. FMI image log showing two turbidite deposits with deformed beds at the same time. The two turbidite beds separated with one meter shale bed in between. (Scale 1/20)

Dip azimuth in most isolated sand beds in the upper intervals is consistent toward the South-West, which helps us to interpret the turbidite palaeo-flow direction toward the South-West. The zone above defined unconformity (3769.5m) shows thinner and lower frequency sand beds in comparison to the zones below unconformity. This may suggests that these intervals deposited at more distal deposition environment of the turbidite lobes very similar to the deeper intervals that defined in previous sections. It may also be possible that there was no sand deposition at this location. The palaeo-flow direction of this interval due to very few observed sand bed boundaries can't be determined.

4.4 Depth interval 3845m to 3894m

This interval is constituted with mostly shale beds with some thin cemented sandy layers. Figure 34 shows the image log of this interval together with other conventional logs. As it is seen from the image logs the log data quality is not good in some of intervals over this zone. Below the depth 3865m, the dip angle and azimuths are more consistent with a SE structural dipping direction with 10 degree dip angle. Above this interval there is package of shaly beds with slightly increasing dip angle up to 20 deg to the top of the interval but little more complex dip azimuth. Some of the shale beds have N150deg azimuth and some at the top show N200deg azimuth. The stick plot of the dips in this part of the zone clearly shows that the bedding direction at this part of the well is in two distinct directions. One possibility here is cross bedding layers.

There are two possible fault surfaces (dashed pink sinusoids) at the top of the zone with 63 deg dip angle and N272deg azimuth. Both these faults show a truncation to the adjacent beds. The faults are also associated with a fracture below (red sinusoid) and deformed beds above. This may indicate that layers above this fault have been deposited in different condition than those beneath the faults. Right above these faults deformed beds and turbidite sediment pattern is recognizable in the plot (Figure 35). FMI image log with two fault surfaces (pink colored) and one fracture below the fault (red colored). A stereonet plot of these faults together with their rose diagram is also shown in Figure 35 to illustrate the dip angle and azimuth of the faults (e.g. 63deg and N272deg respectively).

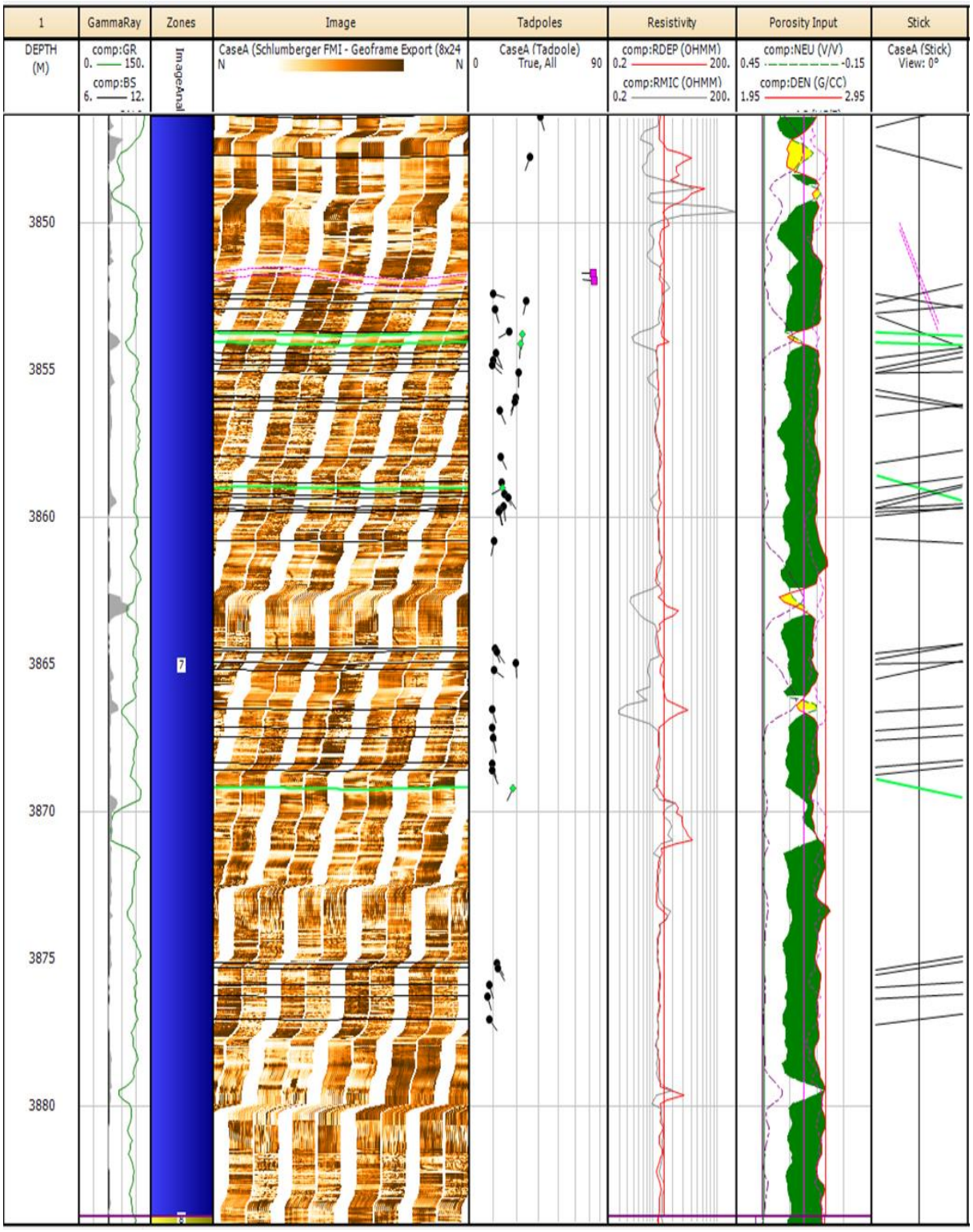

Figure 34. FMI image log of the well at the interval between 3884m-3845m together with tadpole plot and other conventional logs. . (Scale 1/100)

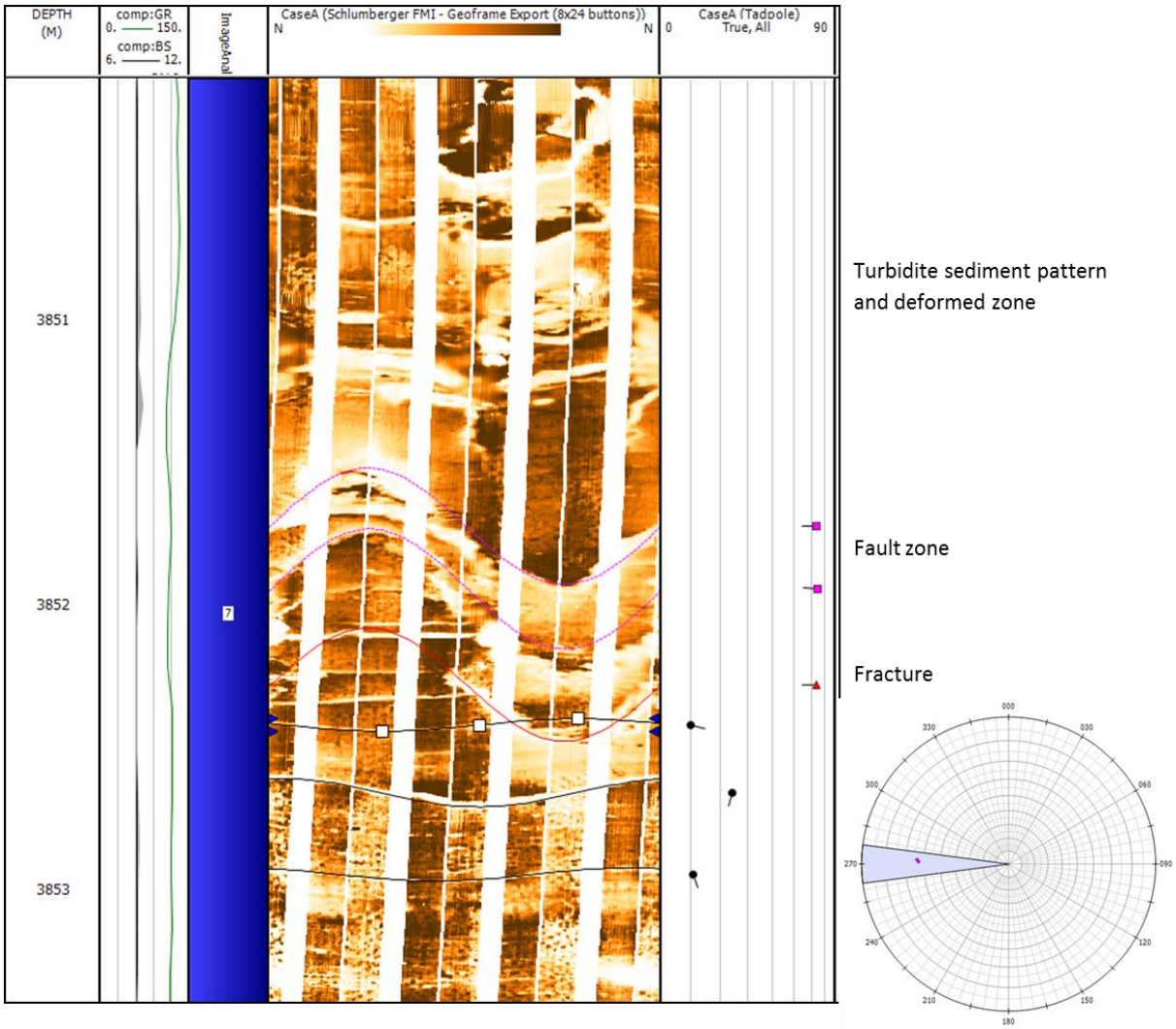

Figure 35. FMI image log with two fault surfaces (pink colored) and one fracture below the fault (red colored). Shaly beds at the bottom of the plot and turbidites layers at the top of the zone are identifiable. To the left is the stereonet plot of the faults with rose diagram of them. The dip angle and azimuth of the faults are 63deg and N272deg respectively. (Scale 1/20)

In general, too few sand beds are visible in this interval within a thick constant dipping shale layers. Conventional logs and particularly neutron-density logs confirms the thick shale bedding in this interval very similar to the previous dipper shaly beds. Quite few sedimentary environment features are visible in this interval. A deformed turbidity sediment features can be identified at 3851m depth representing similar sedimentary environment like dipper shales which deposited in the distal portion of the deep water turbidite sediments. This interval represents a scattered azimuth and slightly higher dips amplitude than the deeper shaly interval and sometimes a bit thicker.

4.5 Depth interval 3894m to 3934m

Figure 36 shows composite plot of the well for 40m interval from 3894m to 3934m depth in more shaly interval. Only two possible thin sandy beds are seen in the plot from neutron-density log crossover. The deflection of the neutron density crossover together with increase in deep resistivity curve may indicate some gas in these sands. However, the log quality from caliper/bit size curves shows that these intervals have large washout than the rest of the shaly zones and the density log measurement presumably impacted by the washout.

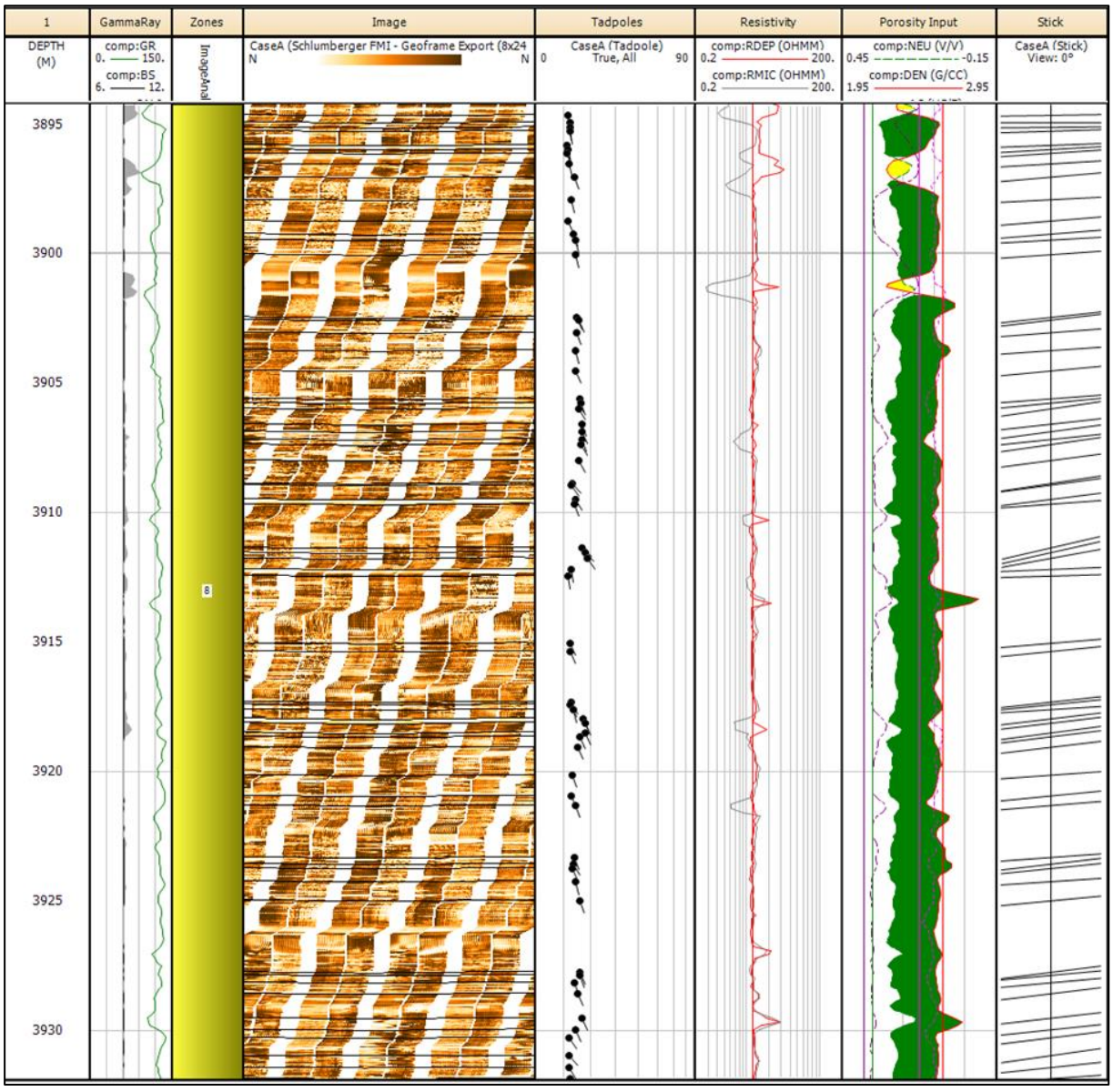

Figure 36. Image log interpretation and comparison to the other logs over the interval 3894m to 3934m. Logs from the left; depth, caliper/GR, zone, FMI log, dip/azimuth, resistivity, N/D, and stick plot of the dips. (Scale 1/100)

Decrease in the sonic log reading (e.g. faster travel time) at these intervals confirms that the rock is not very porous with gas in it. Suppose that the gassy porous sand affects the sonic log reading and the log reads very high travel time or even appears as cycle skipping. On the other hand high drop in microresistivity curve also confirms that this measurement is highly affected by drilling mud itself instead of mud filtrate in the flushed zone. Overall these sands are most probably cemented sands that washed out during the well drilling.

The sedimentary beddings visible within the beds have generally low average dip angle of 12 deg with azimuth of N170 degree. Figure 37 shows stereonet plot and scatter plot of this zone. Stereonet plot is a multi_data source dip analysis plot that plots dip data onto the surface of the reference hemisphere into the equatorial plane using map projections. Dip scatter plots are plots that allow the dip_azimuth and dip_angle to be plotted against each other. There is neither particular change in the bedding direction and azimuth nor high dip angle structures such as fault over this interval. All these observations suggest that the sedimentary deposition were in a very low energy environment.
Based on the observations from the image log features mentioned above these deep marine sediments were probably deposited in distal part of turbidites sedimentation lobes. There is unfortunately no core plugs at this interval to confirm the sedimentary environment from the core facies analysis.

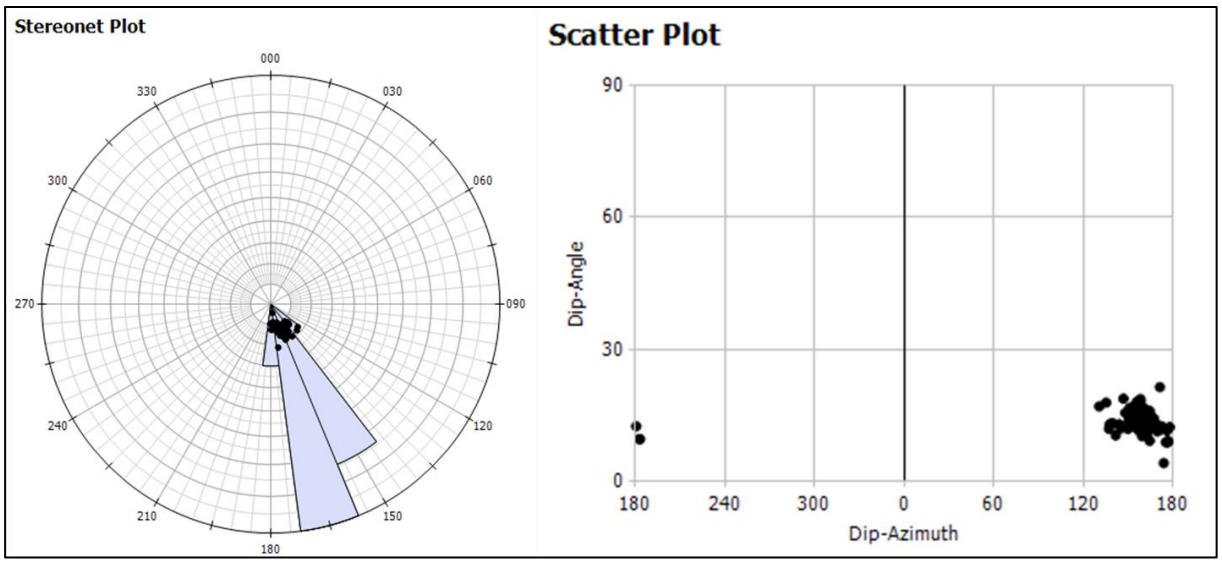

Figure 37. Stereonet plot, points displayed as poles and azimuth rose to the left and scatter plot of dip-angle against dip-azimuth.

5. Quantitative analysis of image logs for shale volume and net to gross calculation

Image log interpretation is generally implemented qualitatively for sedimentary analysis and facies modeling in the oil industry. Normally, operators do not acquire image log for quantitative use of it but for facies modeling, dip/azimuth estimation of reservoir layers and accurate placement of pressure tools. Conventional log interpretation is widely used in the oil industry to estimate reservoir petrophysical properties including shale volume, porosity, saturation, and lithology. Having gross reservoir rock volume (GRV) from seismic interpretation together with the above mentioned petrophysical properties helps in reserve volume calculation (oil in place) by the following equation:

$$OIP = GRV * (1 - Sw) * Phie \qquad \text{Equ. 2}$$

Where,
OIP: oil in place
GRV: gross rock volume
Sw: water saturation
Phie: effective porosity

Geoscientists often use certain limits (cutoff) for shale volume, porosity and water saturation to define reservoir intervals capable of hosting producible hydrocarbon. By definition, if the reservoir porosity in a certain interval is greater than the porosity cutoff (e.g., 10%) and shale volume is smaller than the shale volume cutoff (e.g., 40%) and water saturation is smaller the saturation cutoff (e.g., 50%), the zone is defined as net reservoir interval. The sum of the net interval thicknesses over the reservoir divided by the whole reservoir interval (Gross) is called net to gross ratio (NTG). Net to gross ratio as a multiplier is applied to equation 2 to estimate producible reservoir volume by following equation:

$$OIP = GRV * (1 - Sw) * Phie * NTG \qquad \text{Equ. 3}$$

This methodology often works in conventional reservoirs where the reservoir rock consists of thick sandy packages. However, as the thickness of the sandy layers get below the resolution of the logging tools e.g., thinly laminated shale-sand rocks, the measured log response is highly affected by nearby shale responses. Adjacent shale layer effect on the logging response

results in inaccurate petrophysical interpretation in thin sandy layers, hence reserves calculation. Proper solution for this problem is to use high resolution logging tools such as image logs to limit the adjacent shale layer effect on the log measurements. Overall, in thin layer formations every log response including gamma-ray log, porosity logs and resistivity logs are affected by adjacent layers to some extent. The idea in this chapter is to concentrate on the image logs to develop a method for better estimation of the net to gross ratio in thinly laminated formations.

5.1 Methodology

Sedimentary interpretation of the studied Case-A well showed turbidity channel sands and submarine fans as the dominant deposition model for the reservoir sands. Some intervals of this well show thinly laminated sand-shale response in the FMI log particularly in the interval between 3700m to 3715m. The FMI log as already mentioned measures reservoir rock conductivity through its 192 electrical buttons mounted on the logging tool. The log reading is done every 2.5mm interval by all buttons and the measurement produces an array of 192 conductivity traces for every measured point. Despite the fact the tool design is to measure formation conductivity, the measurement is not an accurate reservoir conductivity. The reason for this problem is varying voltage (EMEX current) during the log measurement which creates resistivity (conductivity) values of different amplitude than the conventional microresistivity curve (RXO). The electrical potential difference between the FMI tool pad buttons and a return electrode in the tool string (EMEX-current) is often adjusted to have a satisfactory signal in different formations. This adjustment together with variation in the current causes different resistivity amplitudes than the conventional resistivity curves.

In this part of the study Matlab Software together with IP were used for FMI data analysis. Matlab (matrix laboratory) software is a matrix-based mathematical system for numeric computation of complex engineering algorithms (Mathworks, 2012). This software allows matrix manipulations, plotting of functions and data, implementation of algorithms, creation of user interfaces, and interfacing with programs written in other languages (Wiki-definition).

An available Matlab program with related sub-functions containing image log data loading and Fourier Transform (FT) scripts received from supervisor for data handling and analysis. All FMI log data were loaded into Matlab as well as IP software. Various low pass filters

including wave numbers of K = 1, 1.5, 2, 4, 5, 8, 10, 15, 20 were applied on a single FMI trace (FCA1) of VNG FMI data and the results exported into Excel as well as IP for further analysis. As the FMI data are in conductivity unit, the FMI data converted to resistivity unit to be comparable to the micro resistivity log (RXO). As the FMI data resolution is significantly higher than the RXO log, the data point interval for RXO log changed to 2.5 mm by interpolation of data between each data point. This log was then smoothed by applying a square filter in IP. The Low pass FT-filtered FMI log with K=1 removing layers of less than one meter (1m) is called RXO.FMI_K1 and presented in Figure 38 together with raw FMI trace (RXO.FMI.raw) and RXO log. This wave number (K=1) was selected for filtering the data because applying K>1results with filtered FMI curves with much more variability than the Rxo curve.

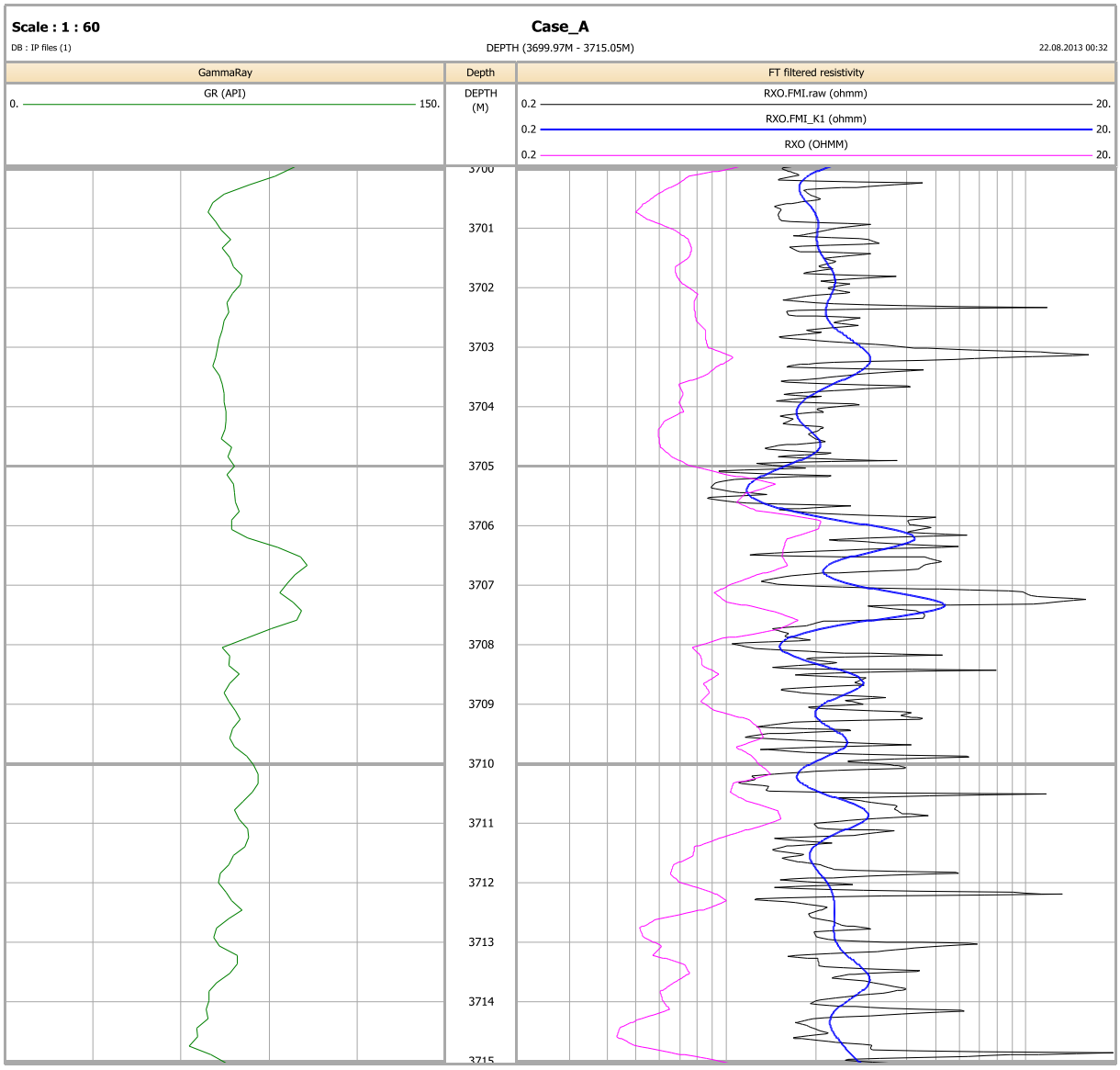

Figure 38. FT-filtered FMI trace (FCA1) resistivity log (blue curve) together with raw FMI trace (black curve) and RXO log (pink curve). Depth interval 3700 to 3715m and log plot scale 1/60.

Figure 38 illustrates a 15 meter interval of the reservoir formation from 3700m to 3715m where raw FMI log at this interval shows layers as thin as 10 centimeter up to thicker intervals of 50-60 centimeter. Applying a low pass filter Fourier Transform of K=1 (1/K=1m) removes all the thinner layers than one meter at this interval and creates a resistivity curve similar to the RXO curve from FMI trace. However, resistivity amplitudes are different between the two logs because of the EMEX current variation in the FMI log measurement as already mentioned. To be able to estimate better formation resistivity and comparable to the RXO log, the FT-filtered FMI curve (RXO.FMI_K1) and RXO curves normalized between 0 to 1 as shown in Figure 39.

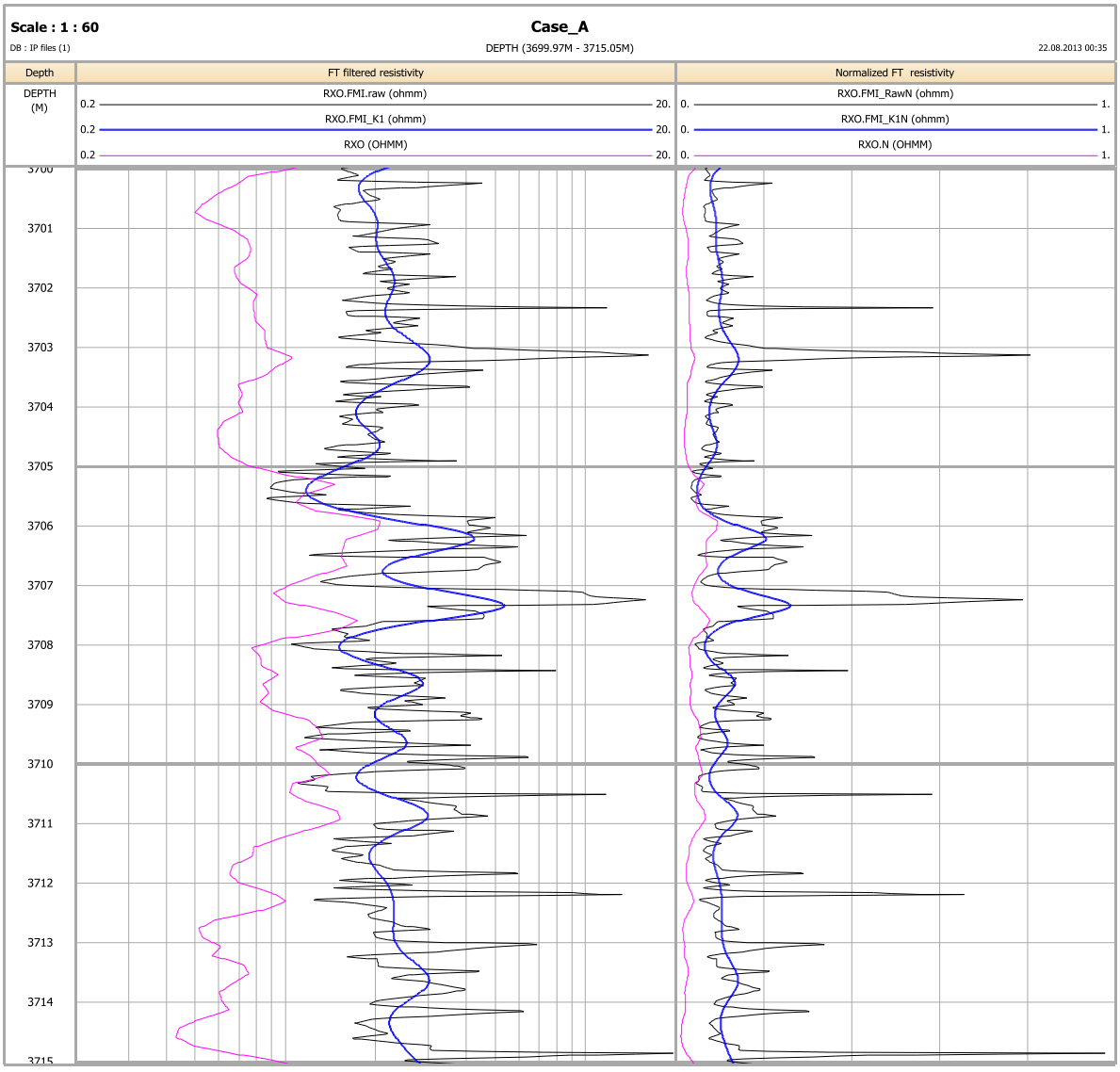

Figure 39. FT-filtered resistivity log from FMI trace (track 2) and normalized resistivities (track 3) for the depth interval 3700 to 3715m. Plot scale 1/60.

After normalization the following multiplier is applied to the raw FMI resistivity curve for every depth intervals to improve formation resistivity estimate:

Corrected FMI resistivity = [Normalized RXO/ Normalized FT-filtered FMI]*Raw FMI resistivity

Or,

$$RXO_{FMI_{Corr}} = \left[\frac{RXO.N}{RXO.FMI\_K1N}\right] * RXO.FMI.raw$$

The calculation result for the corrected FMI resistivity curve is plotted in Figure 40 below.

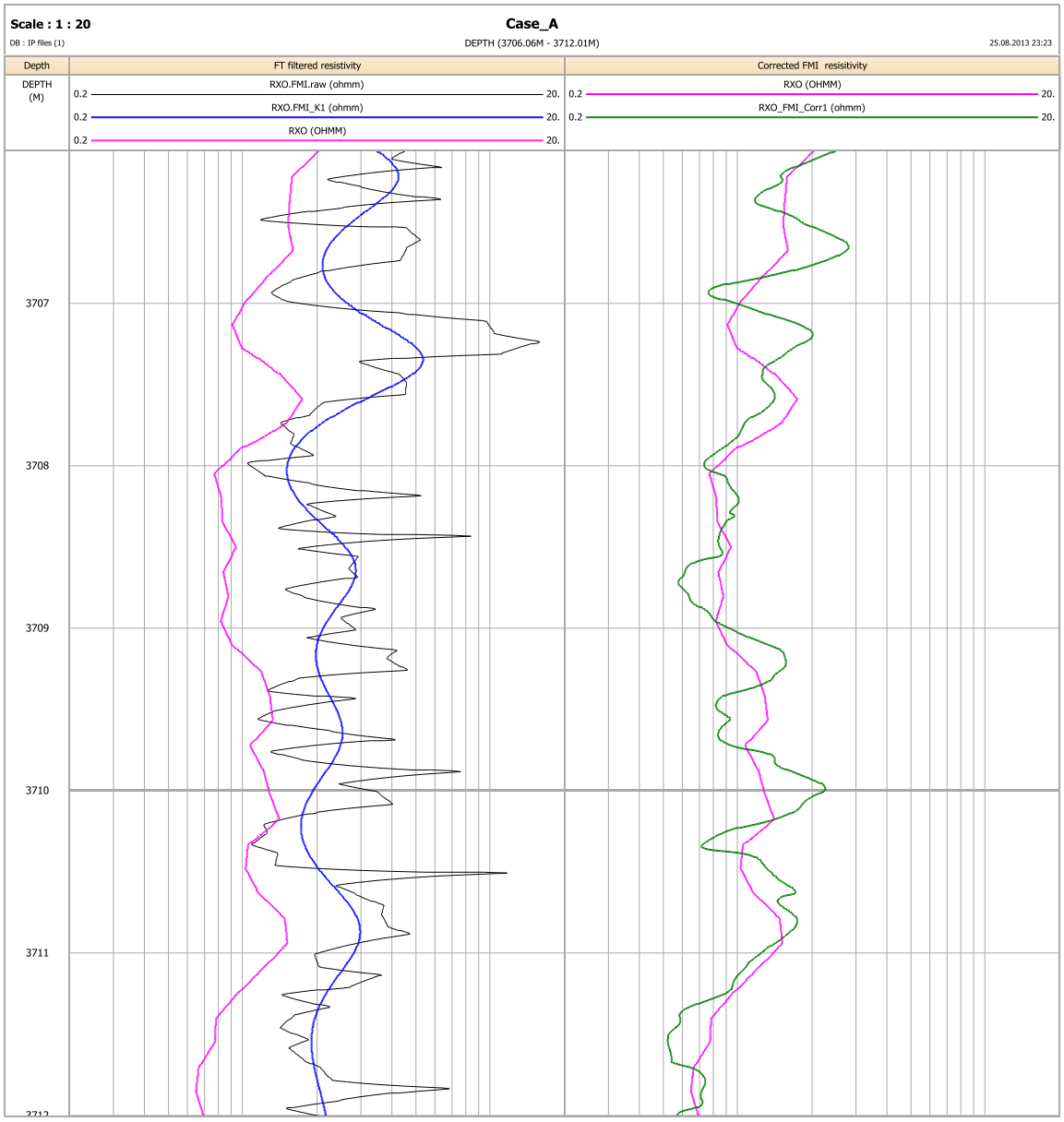

Figure 40. FT-filtered resistivity log from FMI trace (track 2) and corrected FMI resistivity log (track 3) for the depth interval 3706 to 3712m. Plot scale 1/20.

The resistivity log comparisons in track-3 of Figure 40 shows that the FMI log resistivity has been corrected properly since both curves are reading in the same range of measurements. A confirmation to accurate resistivity estimation of this methodology is that the calculated resistivity values in a thick 10m sandy interval at 3680m to 3690m has a good match with the actual resistivity curve (RXO). The comparison of the two resistivities is shown in

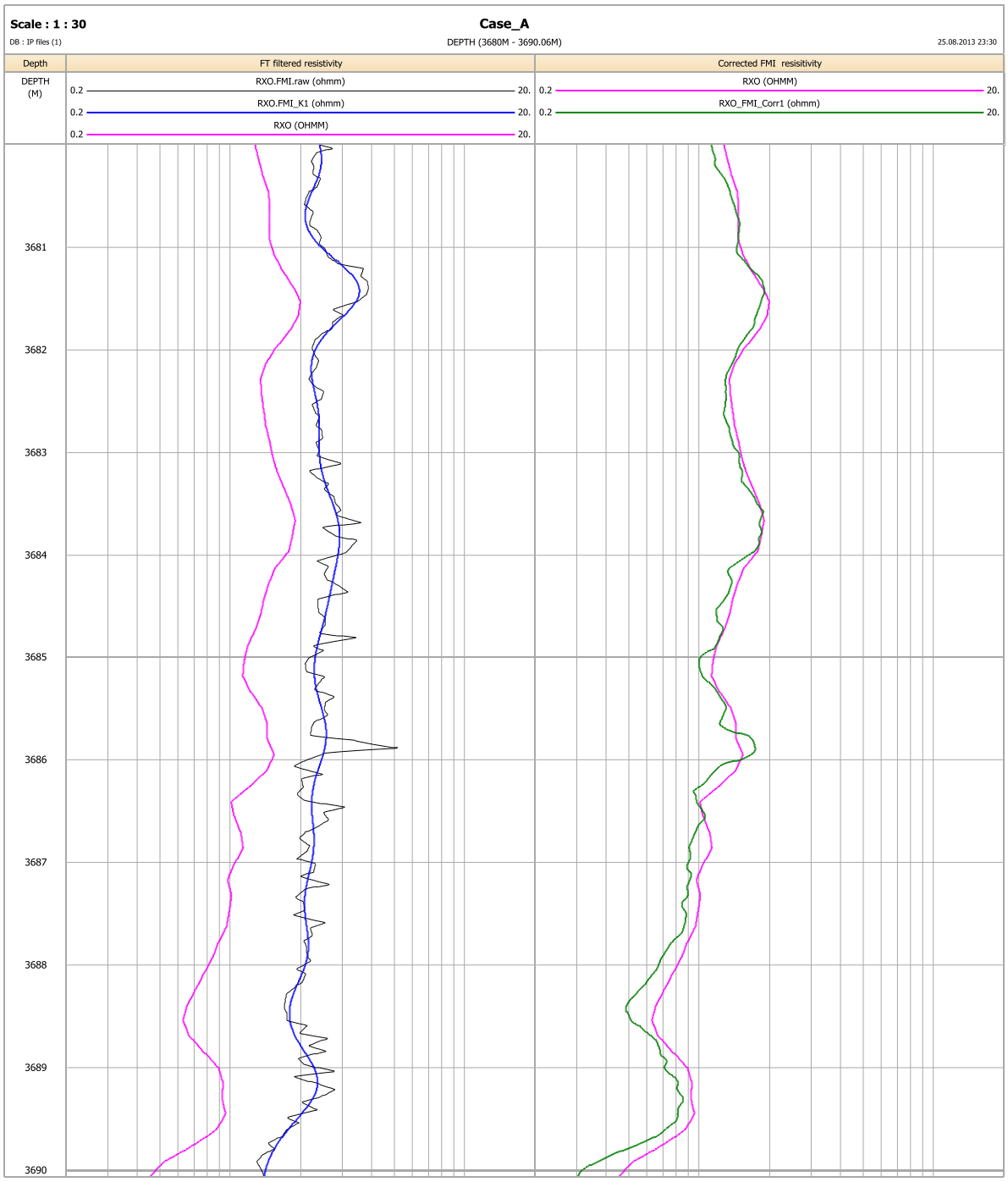

Figure 41. Comparison of the corrected FMI resistivity log with conventional RXO log (track 3) for the depth interval 3680m to 3690m. Plot scale 1/30.

The corrected FMI resistivity log in Figure 40 shows reasonable range of resistivity variation beyond the resolution of the conventional RXO log. The FMI corrected resistivity shows how the reservoir is thinly laminated in this interval.

5.2 Clay volume and net to gross (NTG) calculation

The conventional wireline and LWD logging tools with low resolution are not able to describe the thin beds. Geoscientists often get dissatisfied by the arbitrary selection of petrophysical cutoffs to define reservoir net and non-net (gross) intervals. Various definitions are available on the net and gross reservoir terminologies. Generally net sand comprises those rocks that have shale volume smaller than a defined shale volume cutoff. Net reservoir includes net sand intervals that have porosities greater than a defined porosity cutoff and net pay covers those net reservoir intervals that hold water saturation of smaller than a defined water saturation cutoff (Phillips and Wen, 2007). This part of the study I investigate clay volume of the reservoir in thinly laminated shaly sand section to define net sand intervals and net to gross ratio of the reservoir using the filtered and corrected FMI log. Net to gross ratio as already noted in Equation 3, is used in place hydrocarbon reserve calculation.

A rock that is formed of one or more of the illite, kaolinite, smectite, montmorillonite minerals is normally called clayey rock. Analysis of core data can give direct estimation of reservoir rock clay volume. However, cores are not usually available in the whole reservoir sections. Several indirect methods can be used for clay volume calculation in hydrocarbon reservoirs. Wireline/LWD logging is normally done through the whole reservoir section and analysis of these logs together with calibration to the cores can be used for clay volume calculation. Single clay indicators of Gamma Ray, Neutron, Resistivity, SP, etc. and double clay indicators of Neutron/Density, Density/Sonic, Sonic/Neutron, etc. are normally used in IP for this purpose.

Clays often appear as low resistivity rocks since the mineral lattice holds water molecules inside which helps an electrical current to pass through the rock easily. Pore sizes in clay rocks are very small such that hydrocarbon cannot migrate into clay porosity due to enormous capillarity of these micro pores. Therefore, clay rocks always keep the original water inside the micro pores. Often original water in the clay/shale rocks is saline enough to lower the resistivity reading far beyond the resistivity values in hydrocarbon bearing sands. In thinly

laminated shale-sand reservoirs, however, most of the logging tools may not be able to distinguish these low and high resistivity shale and sands due to low vertical resolution of these tools. Image log data with a very high vertical resolution (2.5mm) is one of the logging tools to differentiate thin sand and shale layers and therefore to compute a reliable reservoir hydrocarbon volume. In contrary to the low resistivity clays sometimes clay rocks can show high/very high resistivity ranges as well. Heather formation claystone in some of the North Sea reservoirs has clay resistivity of above 30 ohmm in the reservoir cap rock. These ranges of high clay resistivity cause difficulties in clay volume calculation from the use of image log resistivity logs in hydrocarbon bearing intervals as water saturated shale and hydrocarbon bearing sands are approximately at the same range of resistivities.

Herein Case-A well, the sandy layers in hydrocarbon bearing section are thick sand without thin clayey layers. The thinly laminated reservoir section lies in the water bearing zone of the well below 3700 mMD. Drilling fluid in this well is highly saline water based mud with Chlorine (CL-) concentration of 90000 ppm. The filtrate invasion affected the RXO curve such that the log read very low resistivity values in sandy sections. In contrary, clay bound water is very resistive equivalent to the salinity of 8000 ppm NaCl. This salinity contrast causes microresistivity value increase in clay/shale rock than the clean sands in the water bearing sections. This condition gives a possibility of defining baselines for shale and sand resistivities from the corrected FMI resistivity curve. The resistivity baseline of 0.6 ohmm was selected as the clean sand baselines picked from a two meter clean sand interval at 3649m to 3651m from cored interval. The shale baseline value of 3.5 ohmm was taken from a shaly interval with average GR reading of 140 API at 3766m to 3770m.

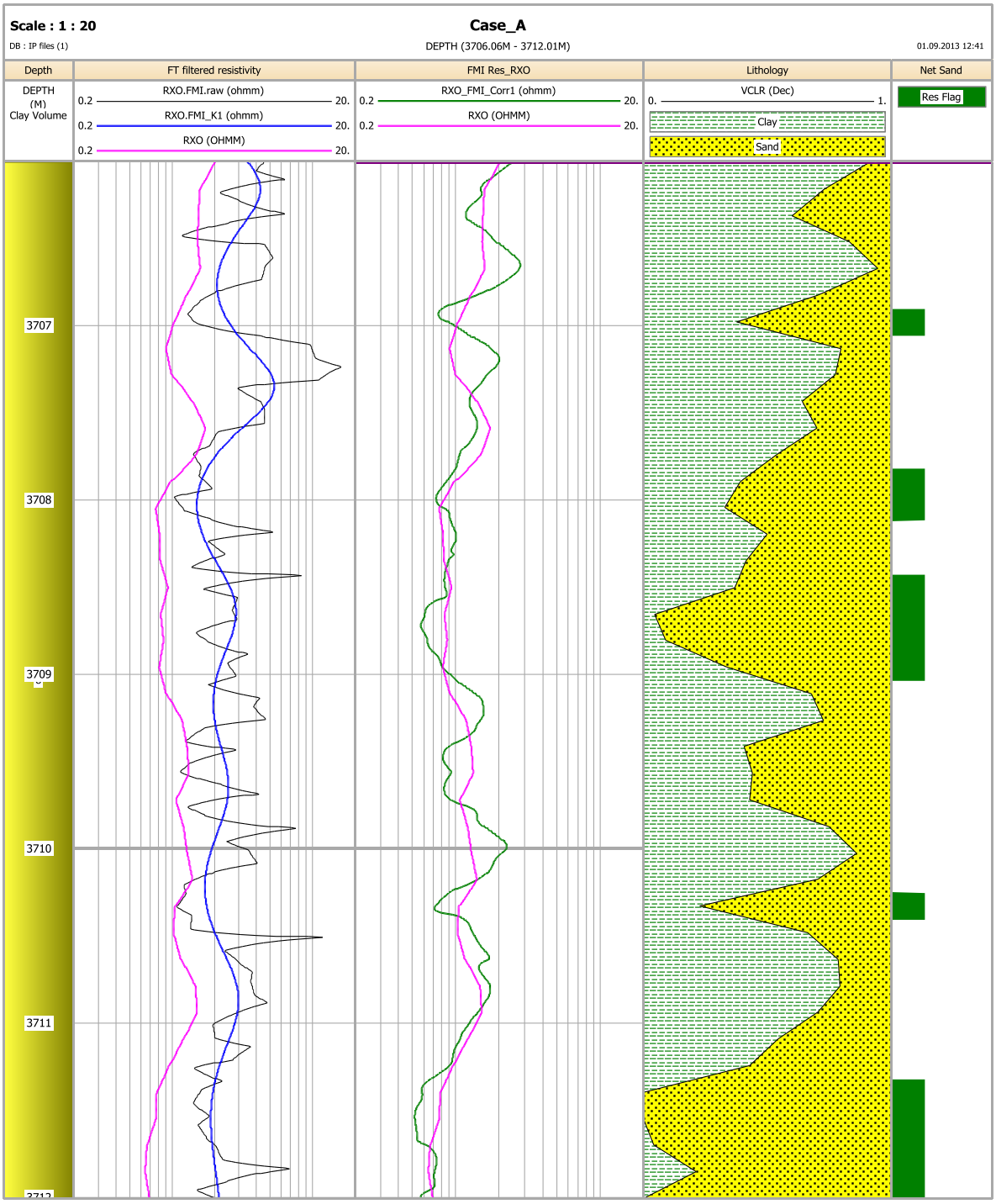
Scale : 1 : 20
Case_A
DB : IP files (1)
DEPTH (3706.06M - 3712.01M)
01.09.2013 12:41
Depth
FT filtered resistivity
FMI Res_RXO
Lithology
Net Sand
DEPTH
(M)
Clay Volume
RXO.FMI.raw (ohmm)
RXO.FMI_K1 (ohmm)
RXO (OHMM)
0.2
20.
RXO_FMI_Corr1 (ohmm)
RXO (OHMM)
VCLR (Dec)
0.
1.
Clay
Sand
Res Flag
3707
3708
3709
3710
3711
3712

Figure **42** illustrates calculated shale and sand volume from the use of corrected FMI resistivity curve. The gross thickness of the interval in

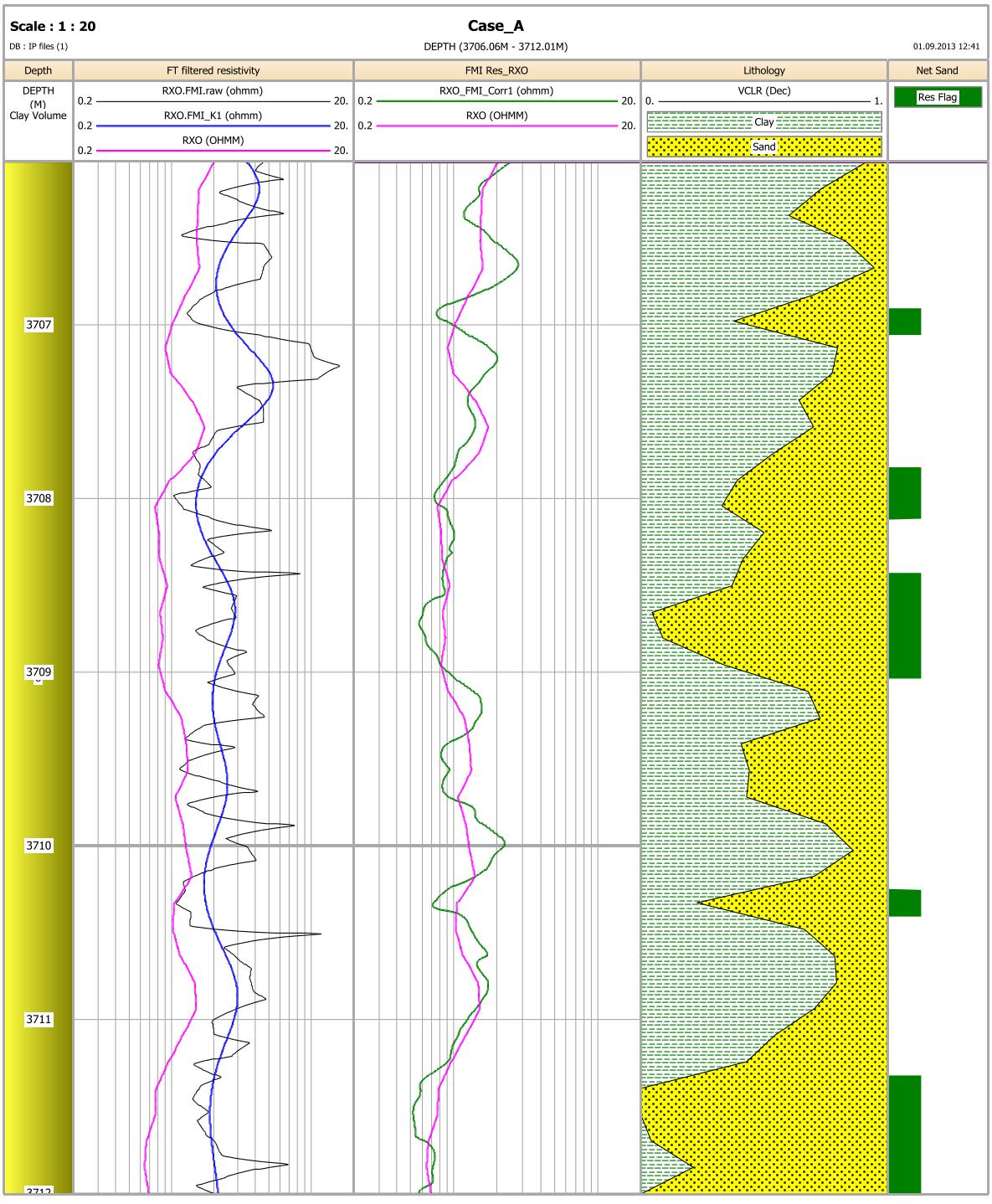

Figure **42** is 6m. Various shale volume cutoffs can be applied for net to gross calculation however, the conventional industry accepted shale volume was used in this study. A criteria of VShale<40% is defined as net sand flag and above that is defined as non-reservoir flag. According to these criterions, the net to gross of the 6m interval is calculated as 0.34 (34 %). Track 5 of the Figure 42 shows the net sand (reservoir) flag of the well in green color.

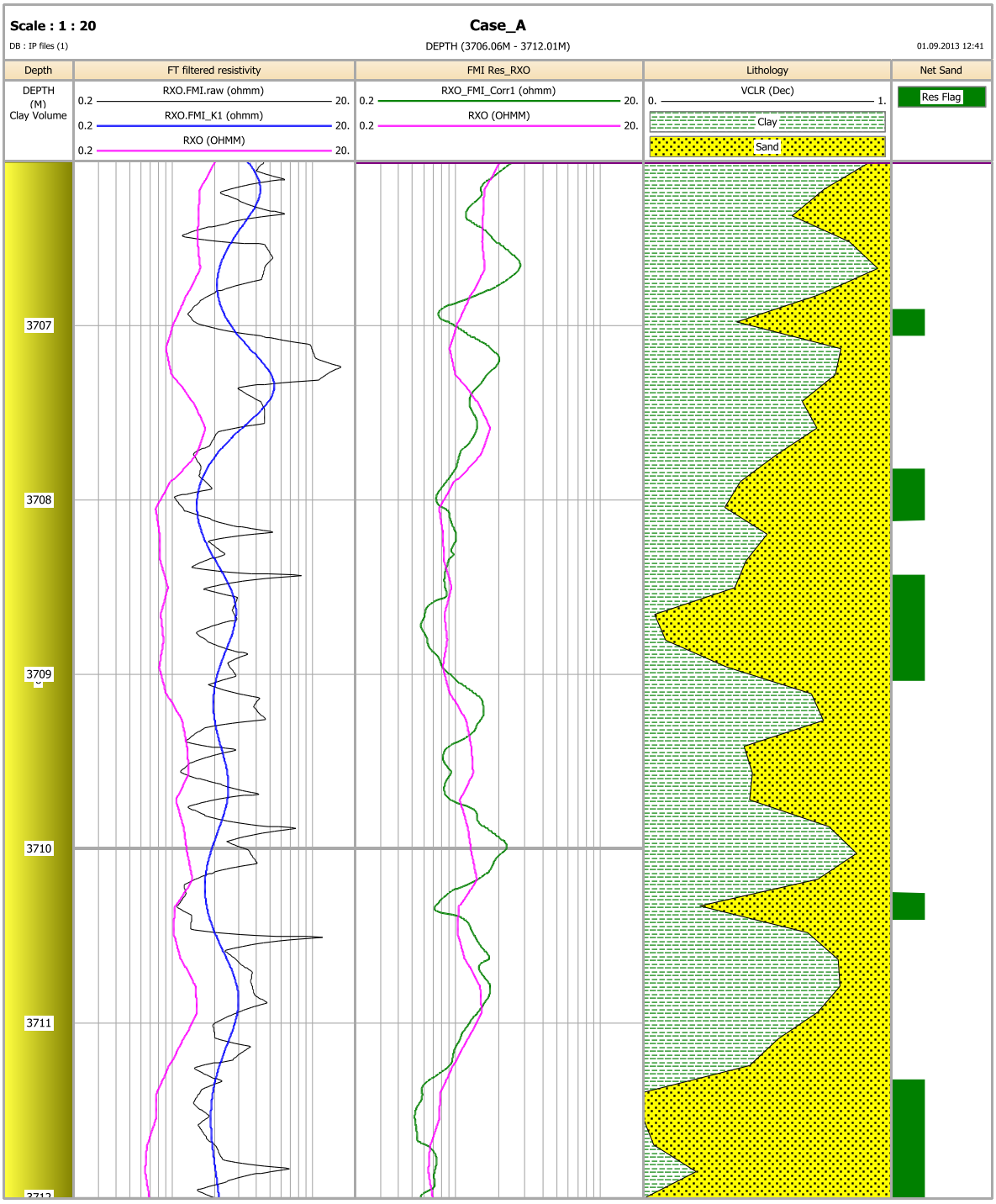

Figure 42. Comparison of the corrected FMI resistivity log with conventional RXO log (track 3) together with calculated lithology in track 4.

A comparison of the calculated clay/shale volume from the use of GR log is seen in Figure 43. The figure shows that despite to the thinly bedded shale and sand at this interval, the GR log values do not represent the true bed properties but rather an average of multiple beds. Using the same VShale > 40% cutoff, the net to gross ratio in this interval is calculated to be 0.46 (46%) which is 12% greater than the estimated value by the filtered image log data. This

indicates that the average clay volume estimated from the gamma ray log is lower than the volume of clay from FMI log. In other words, the GR log measurement in thinly laminated shale and sand interval here is more affected by sand volume than the shale. Variation in the calculated lithology from the image log confirms frequent change of lithology i.e., thinly bedded nature of the zone.

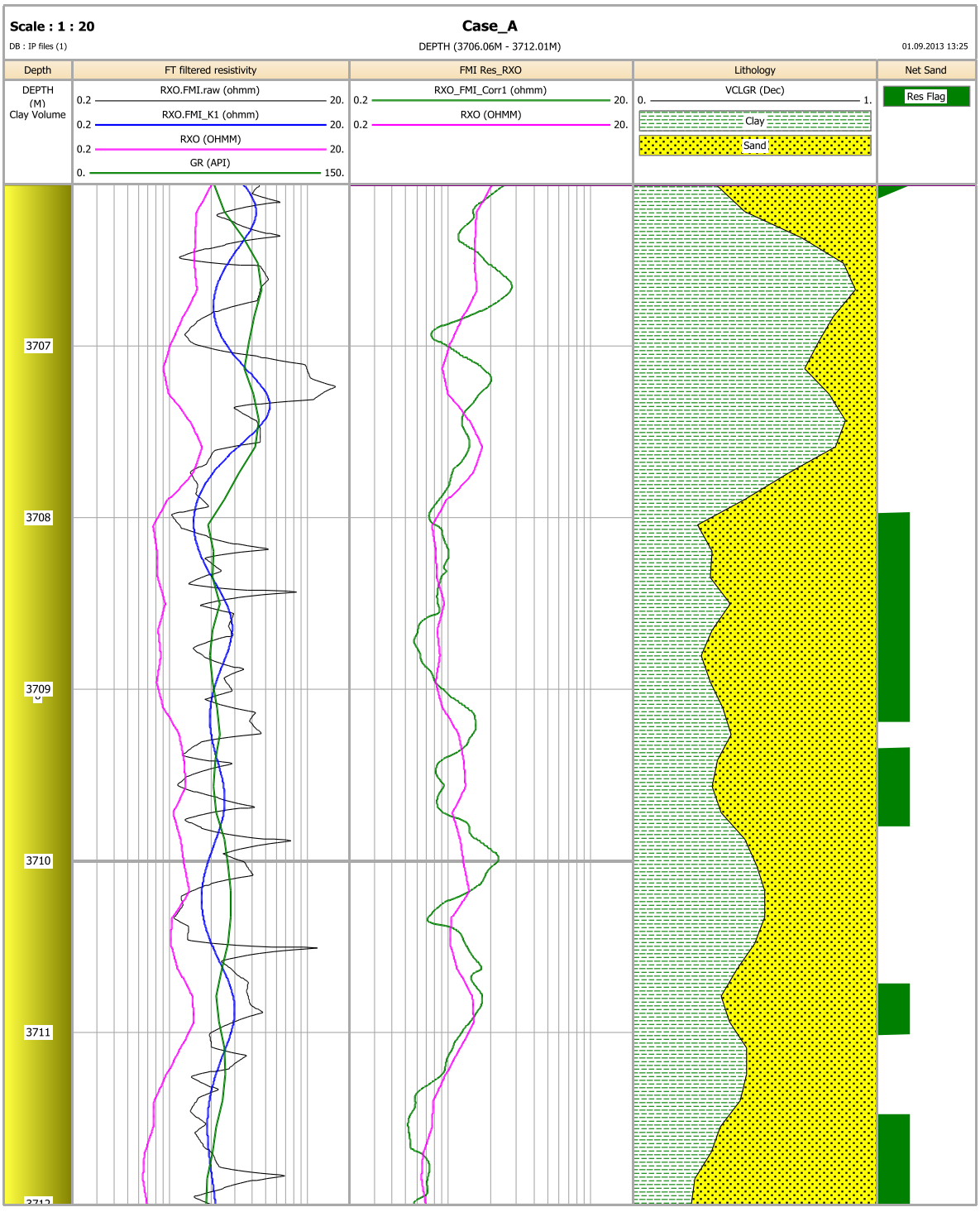

Figure 43. Clay volume calculation from GR log in the same thinly beaded shale and sand.

6. Conclusion

Borehole image log, FMI, enabled the interpretation of the sedimentary depositional environment for a case study well from offshore Norway, North Sea, operated by VNG Norge AS. Available sedimentary interpretation of the limited cores from the upper reservoir section showed turbidity channel sands and submarine fans as the dominant deposition model for the sands. Borehole image logs were used together with these data to spot the relevant core facies in the image logs. Almost all the facies types and structural features were identified in the image log. According the log interpretation the following depositional settings were defined for this well:

- The interval 3610m to 3661m has been interpreted as turbiditic channels and sheets from the overall dip direction of the bedding sets together with minor turbidity features from the image log.

- The relatively low average dip magnitude and the dip direction uniformity at the interval 3661m to 3738m indicate a channelized turbidite with probably less flow energy.

- Interval 3738m to 3845m deposited at more distal deposition environment of the turbidite lobes.

- Too few sand beds are visible in the interval 3845m to 3894m within a thick constant dipping shale layers. Very few sedimentary features are visible in this interval except deformed turbidity sediments representing distal part of turbidite sedimentation lobes.

- Deep marine sediments at the interval 3894m to 3934m deposited in the distal part of turbidite sedimentation lobes.

Following to the recognition of sedimentary environment, the reservoir shale volume and net to gross ratio was calculated for the reservoir with main focus on an interval of thinly laminated shale and sand. An image log trace out of 192 traces were selected and filtered by Fourier Transform and the resistivity values of this trace correlated with RXO curve to use for shale volume calculation due to the log high vertical resolution in spotting thin layers.

7. References

Amer, A., Glascock, M., Schwalbach, J., Khan, M., 2011, Applied Borehole Image Analysis in Complex Sedimentological and Structural Setting: A single Well Case Study, California. Annual Technical Conference and Exhibition, Society of Petroleum Engineers, Colorado, USA.

Baker Hughes, Product and Service, http://www.bakerhughes.com/products-and-services

Bouma, A. H. et al. 1985. Submarine Fans and Related Turbidite Systems. New York, NY: Springer-Verlag.

Felder, R.D., 1994, Advances in Openhole Well Logging, SPE distinguished Author Series, JPT.

Halliburton, Tools and Resources, http://www.halliburton.com/en-US/tools-resources.

Lagraba P. J., Hansen, M., Spalburg, and M. Helmy, 2010, Borehole image tool design, value of information, and tool selection, in M. Po¨ppelreiter, C. Garcý´a-Carballido, and M. Kraaijveld, eds., Dipmeter and borehole image log technology: AAPGMemoir 92, p. 15–38.

Lucchi F. R., Muttim, E., 1972, Turbidites of the northern Apennines: Introduction to facies analysis, International Geology Review, v.20, p. 125-166.

Middleton, G. V. & Hampton, M. A., 1973. Sediment gravity flows: Mechanics of flow and deposition, in Turbidites and Deep-water Sedimentation, eds. G. V. Middleton & A. H. Bouma, Los Angeles, CA: Society of Economic Paleontologists and Mineralogists, 1-38.

Mathworks. 2012. Matlab - the language of technical computing.

Phillips, P., and Wen, R., 2007, Improving net-to-gross reservoir estimation with small-scale geological modeling, Adapted from oral presentation at AAPG Annual Convention, Long Beach, California, April 1-4.

Pickering, K. T. 1982. The shape of deep-water siliciclastic systems: A discussion. Geo-Marine Letters 2, 41-46 (1982).

Rider, M. H., and Kenedy, M., 2011, The geological interpretation of well logs, Sutherland, Rider-French Consulting Ltd.

Saadallah, A., Enhanced reservoir characterization based on borehole images and dipmeter data. Personal notes.

Schlumberger, Services and Products, http://www.slb.com/services.aspx

Slatt, R. M., 2006, Startigraphic reservoir characterization for petroleum geologists, geophysicists and engineers, Handbook of Petroleum Exploration and Production, Elsevier V6.

Tehrani, M.A., Sawdon, C.A., and Levey, S.J.M., 2001, Electrically conductive oil based mud, Chemistry in the oil industry VII, RSC Publishing, 84-95, pp125.

8. Appendix I

Figure 44. STAR Imager Service, Baker Hughes

Figure 45. Earth Imager Service, Baker Hughes

Figure 46. Circumferential Borehole Imaging Log Service, Baker Hughes

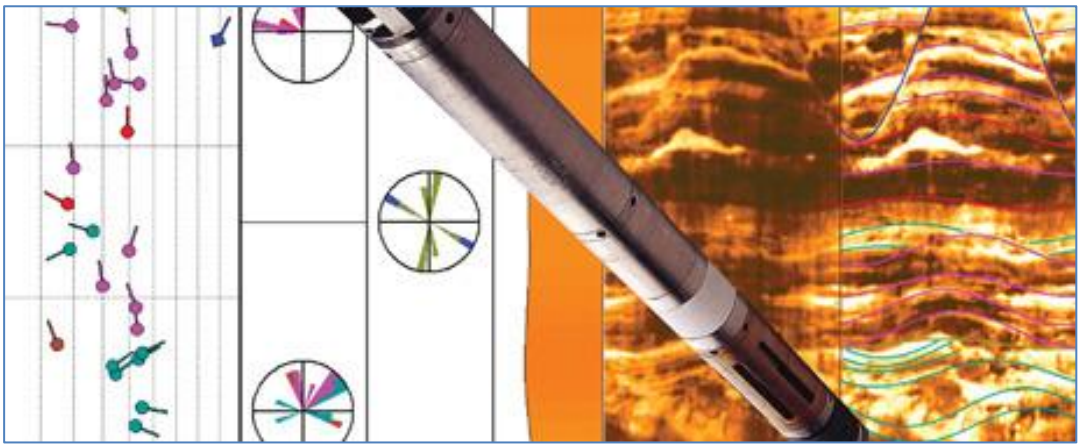

Figure 47. Ultrasonic Xplorer Imaging Service, Baker Hughes

Figure 48. Geo Xplorer Imaging Service, Baker Hughes

Figure 49. UBI rotating transducer, Schlumberger

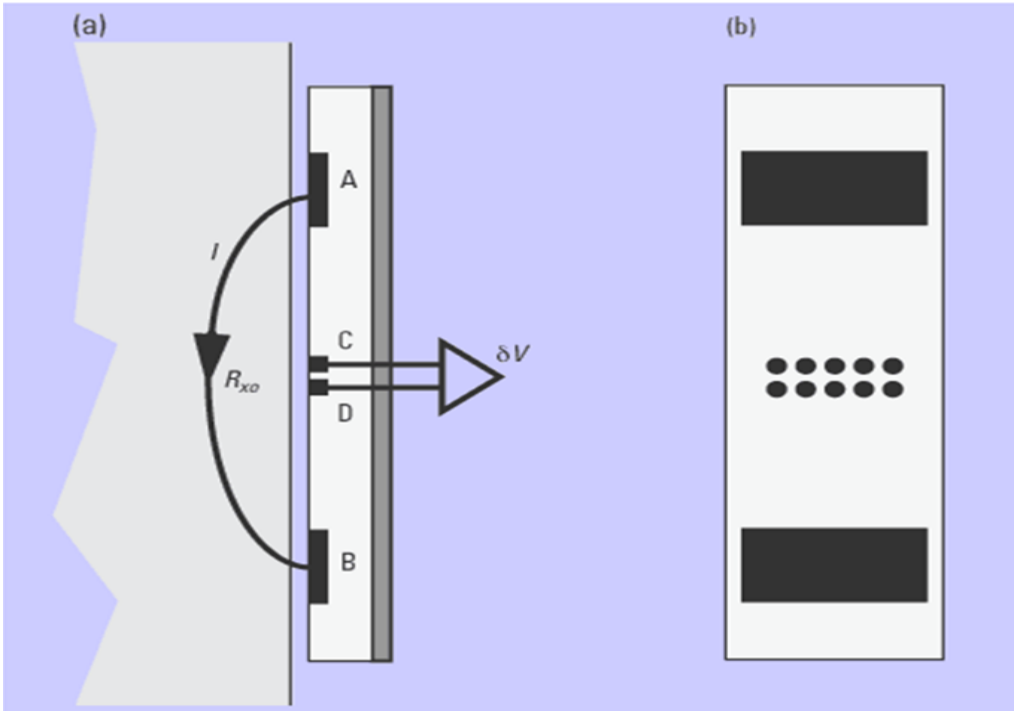

Figure 50. Oil-Based MicroImager (OBMI, Schlumberger) measures 5 pairs of potential differences in each of pads which are then converted to resistivity.

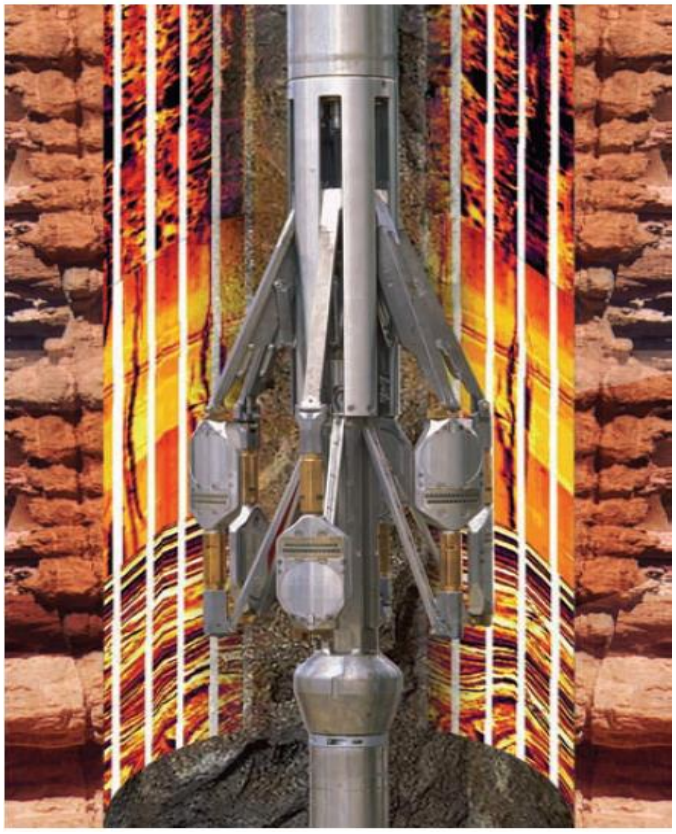

Figure 51. Electrical Micro Imaging (EMI) Log Service, Halliburton

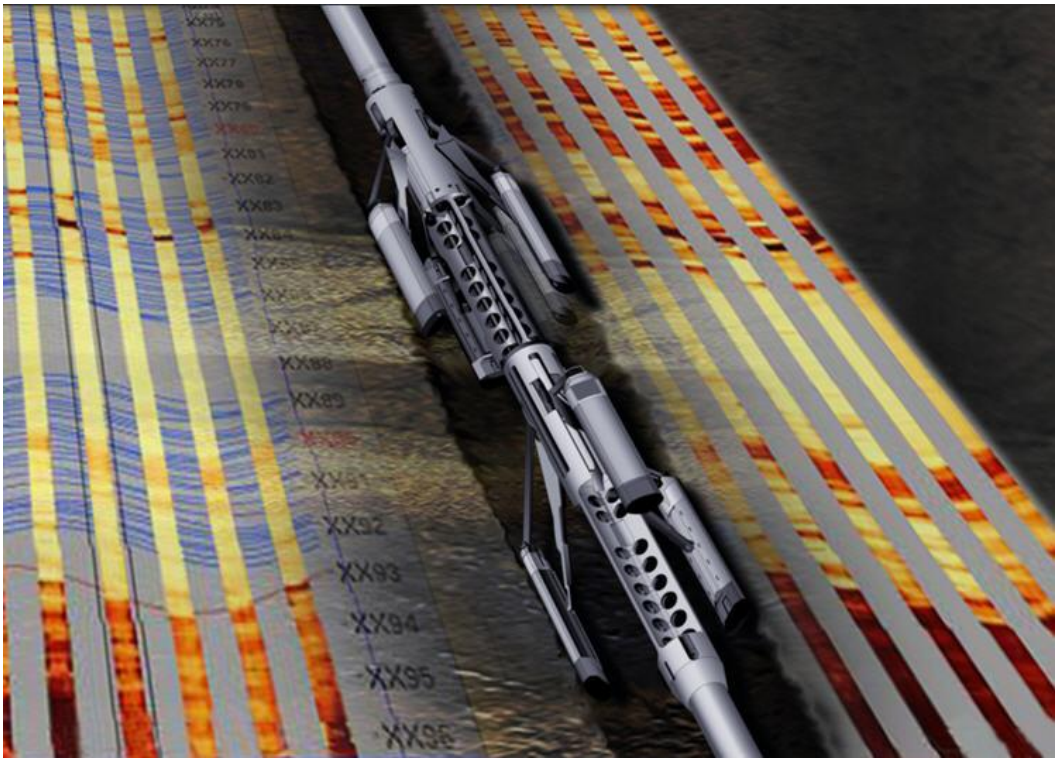

Figure 52. Oil Based Mud Imaging (OMRISM) Log Service, Halliburton